Chapter 2

PHYSICS
(4 TeV AND 500 GeV)

Contents

2.1 Abstract

We discuss the capabilities of future muon colliders to resolve important particle physics questions. A collider with c.m. energy $\sqrt{s} = 100$ to 500 GeV offers the unique opportunity

to produce Higgs bosons in the s-channel and thereby measure the Higgs masses, total widths and several partial widths to high precision. At this same machine, $t\bar{t}$ and W^+W^- threshold studies would yield superior precision in the determination of m_t and m_W. A multi-TeV $\mu^+\mu^-$ collider would open up the realm of physics above the 1 TeV scale, allowing, for example, copious production of supersymmetric particles up to the highest anticipated masses or a detailed study of the strongly-interacting scenario of electroweak symmetry breaking.

Techniques and strategies for discovering and measuring the properties of Higgs bosons via s-channel production at a $\mu^+\mu^-$ collider, and the associated requirements for the machine and detector, are discussed in detail. The unique feature of s-channel production is that, with good energy resolution, the mass, total width and partial widths of a Higgs boson can be directly measured with remarkable accuracy in most cases. For the expected machine parameters and luminosity the Standard Model (SM) Higgs boson h_{SM}, with mass $\lesssim 2m_W$, the light h^0 of the minimal supersymmetric Standard Model (MSSM), and the heavier MSSM Higgs bosons (the CP-odd A^0 and the CP-even H^0) can all be studied in the s-channel, with the heavier states accessible up to the maximal $\sqrt{s}$ over a large fraction of the MSSM parameter space. In addition, it may be possible to discover the A^0 and H^0 by running the collider at full energy and observing excess events in the bremsstrahlung tail at lower energy. The integrated luminosity, beam resolution and machine/detector features required to distinguish between the h_{SM} and h^0 are delineated.

2.2 Particle Physics Opportunities at $\mu^+\mu^-$ Colliders

2.2.1 Introduction

There is increasing interest recently in the possible construction of a $\mu^+\mu^-$ collider[1, 2, 3, 4]. The expectation is that a muon collider with energy and integrated luminosity comparable to or superior to those attainable at e^+e^- colliders can be achieved[5, 6, 7]. An initial survey of the physics potential of muon colliders has been carried out[8]. In this report we summarize some of the progress on the physics issues that has been made in the last year; a more comprehensive report is in preparation[9].

One of the primary arguments for an e^+e^- collider is the complementarity with physics studies at the LHC. The physics potential of a muon collider is comparable to that of an electron collider with the same energy and luminosity. However, electron colliders are at a technologically more advanced stage and will likely be built before muon colliders. Hence a very relevant issue is what can be done at a muon collider that cannot be done at an electron collider.

The advantages of a muon collider can be summarized briefly as follows:

- The muon is significantly heavier than the electron, and therefore couplings to Higgs bosons are enhanced making possible their study in the s-channel production process.
- The limitation on luminosity from beam-beam interactions that arises at an e^+e^- collider is not relevant for muon beam energies below about 100 TeV; very small/flat beams are unnecessary. Instead, large luminosity is achieved for $\sim 3\,\mu$m size beams by storing multiple bunches in the final storage ring and having a large number of turns of storage per cycle. Radiative losses in the storage ring are small due to the large muon mass. Thus, extending the energy reach of these colliders well beyond the 1 TeV range is possible.
- The muon collider can be designed to have finer energy resolution than an e^+e^- machine.
- At a muon collider, $\mu^+\mu^+$ and $\mu^-\mu^-$ collisions are likely to be as easily achieved as $\mu^+\mu^-$ collisions.

There are two slight drawbacks of a muon collider. The first is that substantial polarization of the beams can probably not be achieved without sacrificing luminosity. The second drawback is that the $\gamma\gamma$ and $\mu\gamma$ options are probably not feasible. At future linear e^+e^- colliders, the possibility exists to backscatter laser photons off the electron and/or positron beams. The resulting back-scattered photons are highly collimated and could serve as a photon beam, thus converting the e^+e^- collider to a $e\gamma$ or $\gamma\gamma$ collider. The collisions from the back-scattered photons have center-of-mass energies that range up almost to that of the parent e^+e^- collider. Including this option at a $\mu^+\mu^-$ collider is problematic from kinematic considerations. The highest photon energy ω attainable from a lepton with energy E is

$$\frac{\omega_{\rm max}}{E} = \frac{x}{x+1}\,, \tag{2.1}$$

where

$$x = \frac{4E\omega_0}{m_\mu^2 c^4}\,. \tag{2.2}$$

For a muon collider $x \ll 1$ unless a laser photon energy ω_0 of the order of keV is possible, which seems unlikely.

A proposed schematic design for a muon collider is shown in Fig. 1.1 in chapter 1. Protons produce π's in a fixed target which subsequently decay giving μ's. The muons must be collected, cooled and subsequently accelerated to high energies. Since the muon is so

much heavier than the electron, synchrotron radiation is much less so that circular storage rings are feasible even at TeV energies.

The monochromaticity of the beams will prove critically important for some of the physics that can be done at a $\mu^+\mu^-$ collider. The energy profile of the beam is expected to be roughly Gaussian in shape, and the rms deviation R is expected to naturally lie in the range $R = 0.04\%$ to 0.08%[10]. Additional cooling could further sharpen the beam energy resolution to $R = 0.01\%$.

Two possible $\mu^+\mu^-$ machines have been discussed as design targets and are being actively studied [2, 3, 4]:

(i) A first muon collider (FMC) with low c. m. energy ($\sqrt{s}$) between 100 and 500 GeV and $\mathcal{L} \sim 2 \times 10^{33}\,\mathrm{cm}^{-2}\,\mathrm{s}^{-1}$ delivering an annual integrated integrated luminosity $L \sim 20\ \mathrm{fb}^{-1}$.

(ii) A next muon collider (NMC) with high $\sqrt{s} \gtrsim 4$ TeV and $\mathcal{L} \sim 10^{35}\,\mathrm{cm}^{-2}\,\mathrm{s}^{-1}$ giving $L \sim 1000\ \mathrm{fb}^{-1}$ yearly.

2.2.2 *s*-Channel Higgs Physics

The simplest Higgs sector is that of the Standard Model (SM) with one Higgs boson. However, the naturalness and hierarchy problems that arise in the SM and the failure of grand unification of couplings in the SM suggest that a single Higgs boson is probably not the whole story of electroweak symmetry breaking. Therefore, it is crucially important to understand and delineate experimentally various alternative possibilities.

Supersymmetry is an especially attractive candidate theory in that it solves the naturalness and hierarchy problems (for a sufficiently low scale of supersymmetry breaking) and in that scalar bosons, including Higgs bosons, are on the same footing as fermions as part of the particle spectrum. The minimal supersymmetric model (MSSM) is the simplest SUSY extension of the SM. In the MSSM, every SM particle has a superpartner. In addition, the minimal model contains exactly two Higgs doublets. At least two Higgs doublet fields are required in order that both up and down type quarks be given masses without breaking supersymmetry (and also to avoid anomalies in the theory). Exactly two doublets allows unification of the SU(3), SU(2) and U(1) coupling constants. (Extra Higgs singlet fields are allowed by unification, but are presumed absent in the MSSM.) For two Higgs doublets and

no Higgs singlets, the Higgs spectrum comprises 5 physical Higgs bosons

$$h^0, H^0, A^0, H^+, H^- \ . \tag{2.3}$$

The quartic couplings in the MSSM Higgs potential are related to the electroweak gauge couplings g and g' and the tree-level Higgs mass formulas imply an upper bound on the mass of the lightest Higgs boson, $m_h \leq M_Z$. At one loop, the radiative correction to the mass of the lightest Higgs state depends on the top and stop masses

$$\delta m_{h^0}^2 \simeq \frac{3g^2}{8\pi^2 m_W^2} m_t^4 \ln\left(\frac{m_{\tilde{t}_1} m_{\tilde{t}_2}}{m_t^2}\right) \ . \tag{2.4}$$

Two-loop corrections are also significant. The resulting iron-clad upper bounds on the possible mass of the lightest Higgs boson are

$$m_{h^0} \lesssim 130 \text{ GeV} \qquad \text{MSSM}, \tag{2.5}$$

$$m_{h^0} \lesssim 150 \text{ GeV} \qquad \text{any SUSY GUT}, \tag{2.6}$$

$$m_{h^0} \lesssim 200 \text{ GeV} \qquad \text{any model with GUT and desert.} \tag{2.7}$$

In the largest part of parameter space, e.g. $m_{A^0} > 150$ GeV in the MSSM, the lightest Higgs boson has fairly SM-like couplings.

The first discovery of a light Higgs boson is likely to occur at the LHC which might be operating for several years before a next-generation lepton collider is built. Following its discovery, interest will focus on measurements of its mass, total width, and partial widths. A first question then is what could be accomplished at the Large Hadron Collider (LHC) or the Next Linear Collider (NLC) in this regard.

At the LHC, a SM-like Higgs can be discovered either through gluon fusion, followed by $\gamma\gamma$ or 4ℓ decay,

$$gg \to h \to \gamma\gamma \ , \tag{2.8}$$

$$gg \to h \to ZZ^\star \to 4l \ , \tag{2.9}$$

or through associated production

$$gg \to t\bar{t}h \quad \hookrightarrow \gamma\gamma \ , \tag{2.10}$$

$$q\overline{q} \to Wh \quad \hookrightarrow \gamma\gamma \ . \tag{2.11}$$

The LHC collaborations report that the Higgs boson is detectable in the mass range $50 \lesssim m_h \lesssim 150$ GeV via its $\gamma\gamma$ decay mode. The mass resolution is expected to be $\lesssim 1\%$. At the NLC the Higgs boson is produced in the Bjorken process

$$e^+e^- \to Z^\star \to Zh \tag{2.12}$$

and the h can be studied through its dominant $b\bar{b}$ decay. At the NLC (which may be available prior to a $\mu^+\mu^-$ collider) the mass resolution is strongly dependent on the detector performance and signal statistics:

$$\Delta m_h \simeq R_{\rm event}({\rm GeV})/\sqrt{N}\ , \tag{2.13}$$

where $R_{\rm event}$ is the single event resolution and N is the number of signal events. The single event resolution is about 4 GeV for an SLD-type detector[11], but improved performance as typified by the "super"-LC detector would make this resolution about 0.3 GeV[12, 13]. The uncertainty in the Higgs boson mass for various integrated luminosities is shown in Fig. 2.1. For a Higgs boson with Standard Model couplings this gives a Higgs mass determination of

$$\Delta m_{h_{SM}} \simeq 400\ {\rm MeV} \left(\frac{10\ {\rm fb}^{-1}}{L}\right)^{1/2}\ , \tag{2.14}$$

for the SLD-type detector. Precision measurements of the Higgs total width and partial widths will be necessary to distinguish between the predictions of the SM Higgs boson h_{SM} and the MSSM Higgs boson h^0. Can the total and partial widths be measured at other machines? This is a complicated question since each machine contributes different pieces to the puzzle. The bottom line[14] is that the LHC, NLC, and $\gamma\gamma$ colliders each measure interesting couplings and/or branching ratios, but their ability to detect deviations due to the differences between the h^0 and h_{SM} is limited to $m_{A^0} \lesssim 300$ GeV. Further, a model-independent study of all couplings and widths requires all three machines with consequent error propagation problems.

The s-channel process $\mu^+\mu^- \to b\overline{b}$ shown in Fig. 2.2 is uniquely suited to several critical precision Higgs boson measurements [15, 16]. Detecting and studying the Higgs boson in the s-channel would require that the machine energy be adjusted to correspond to the Higgs mass. Since the storage ring is only a modest fraction of the overall muon collider cost[17], a special-purpose ring could be built to optimize the luminosity near the Higgs peak.

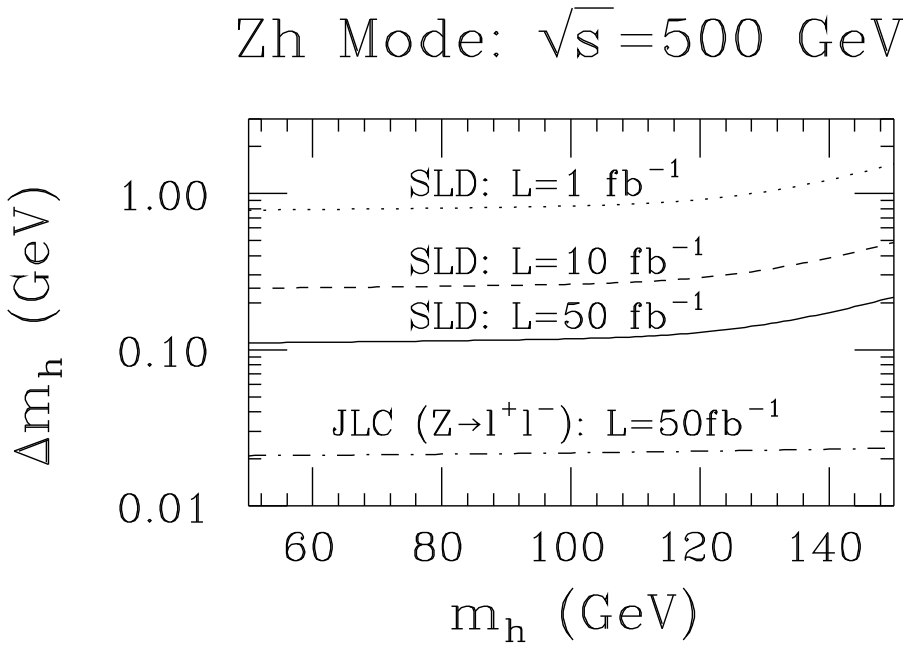

Figure 2.1: The uncertainty $\pm\Delta m_h$ in the determination of m_h for a SM-like Higgs boson using Zh production and a ± 4 GeV ("SLD") or ± 0.3 GeV ("JLC") single event mass resolution for m_h.

The s-channel Higgs phenomenology is set by the $\sqrt{s}$ rms Gaussian spread denoted by $\sigma_{\sqrt{s}}$. A convenient formula for $\sigma_{\sqrt{s}}$ is

$$\sigma_{\sqrt{s}} = (7 \text{ MeV}) \left(\frac{R}{0.01\%}\right) \left(\frac{\sqrt{s}}{100 \text{ GeV}}\right) . \tag{2.15}$$

A crucial consideration is how this natural spread in the muon collider beam energy compares to the width of the Higgs bosons, given in Fig. 2.3. In particular, a direct scan measurement of the Higgs width requires a beam spread comparable to the width. The narrowest Higgs boson widths are those of a light SM Higgs boson with mass $\lesssim 100$ GeV. In the limit where the heavier MSSM Higgs bosons become very massive, the lightest supersymmetric Higgs typically has a mass of order 100 GeV and has couplings that are sufficiently SM-like that its width approaches that of a light h_{SM} of the same mass. In either case, the discriminating power of a muon collider with a very sharp energy resolution would be essential for a direct width measurement.

A quantitative examination of Fig. 2.3 shows that for typical muon beam resolution

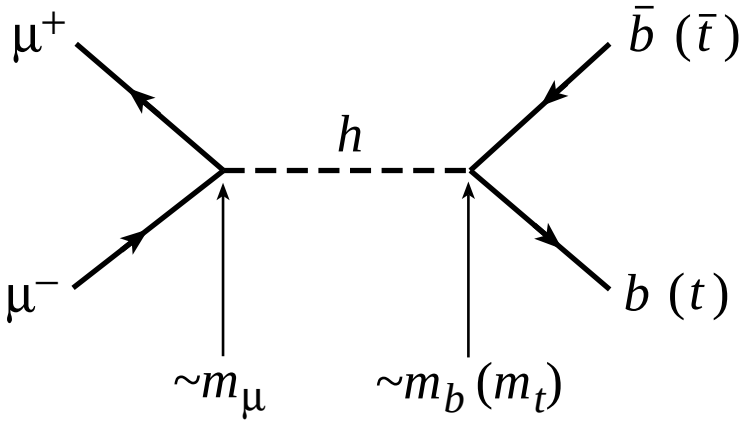

Figure 2.2: Feynman diagram for s-channel production of a Higgs boson.

$(R = 0.06\%)$

$$\sigma_{\sqrt{s}} \gg \Gamma_{h_{SM}} \text{ , for } m_{h_{SM}} \sim 100 \text{ GeV} , \tag{2.16}$$

$$\sigma_{\sqrt{s}} \sim \Gamma_{h^0} \text{ , for } m_{h^0} \text{ not near } m_{h^0}^{\max} , \tag{2.17}$$

$$\sigma_{\sqrt{s}} \lesssim \Gamma_{H^0}, \Gamma_{A^0} \text{ , at moderate } \tan\beta , \tag{2.18}$$

$$\text{for } m_{H^0,A^0} \sim 400 \text{ GeV} ,$$

$$\ll \Gamma_{H^0}, \Gamma_{A^0} \text{ , at large } \tan\beta , \tag{2.19}$$

$$\text{for } m_{H^0,A^0} \sim 400 \text{ GeV} .$$

To be sensitive to the $\Gamma_{h_{SM}}$ case, a resolution $R \sim 0.01\%$ is mandatory. This is an important conclusion given that such a small resolution requires early consideration in the machine design.

The s-channel Higgs resonance cross section is

$$\sigma_h = \frac{4\pi\Gamma(h \to \mu\mu)\,\Gamma(h \to X)}{(\hat{s} - m_h^2)^2 + m_h^2[\Gamma_h^{\text{tot}}]^2} , \tag{2.20}$$

where $\hat{s} = (p_{\mu^+} + p_{\mu^-})^2$ is the c. m. energy squared of the event, X denotes a final state and Γ_h^{tot} is the total width. The effective cross section is obtained by convoluting this resonance form with the Gaussian distribution of width $\sigma_{\sqrt{s}}$ centered at $\sqrt{s}$. When the Higgs width is much smaller than $\sigma_{\sqrt{s}}$, the effective signal cross section result for $\sqrt{s} = m_h$, denoted by $\overline{\sigma}_h$,

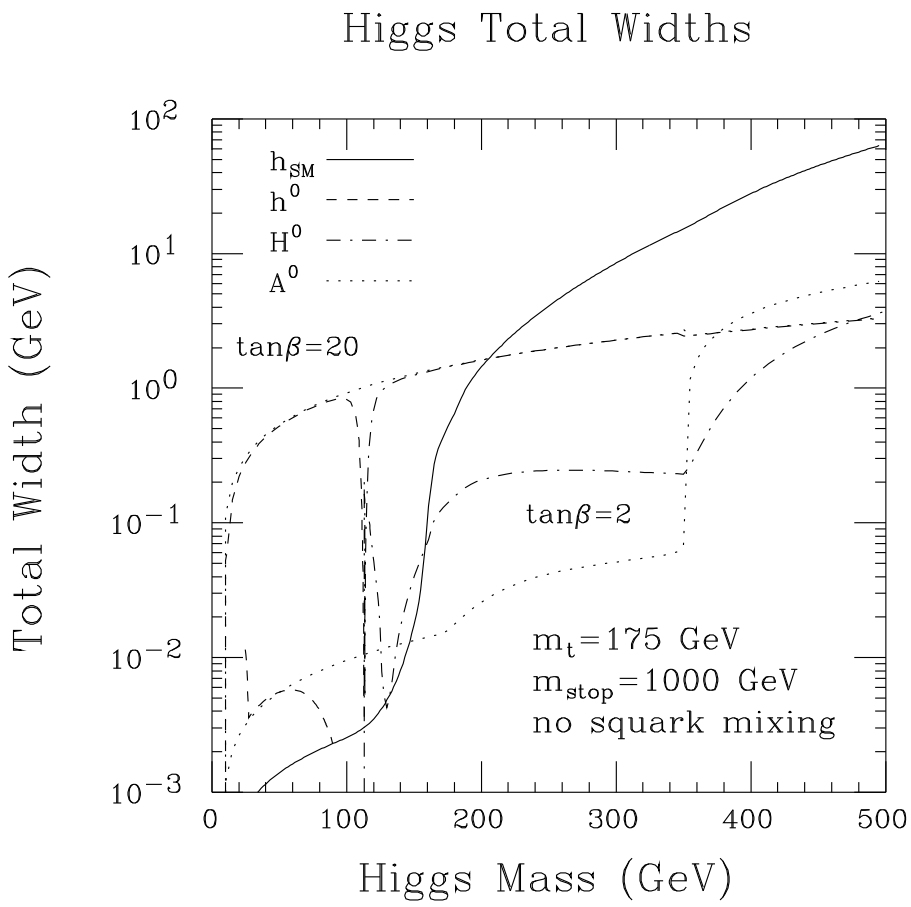

Figure 2.3: Total width vs mass of the SM and MSSM Higgs bosons for $m_t = 175$ GeV. In the case of the MSSM, we have plotted results for $\tan\beta = 2$ and 20, taking $m_{\tilde{t}} = 1$ TeV and including two-loop corrections following Refs. [18, 19] neglecting squark mixing; SUSY decay channels are assumed to be absent.

is

$$\overline{\sigma}_h = \frac{2\pi^2 \Gamma(h \to \mu\mu)\, BF(h \to X)}{m_h^2} \times \frac{1}{\sigma_{\sqrt{s}}\sqrt{2\pi}} \,. \tag{2.21}$$

In the other extreme, where the Higgs width is much broader than $\sigma_{\sqrt{s}}$, at $\sqrt{s} = m_h$ we obtain

$$\overline{\sigma}_h = \frac{4\pi BF(h \to \mu\mu) BF(h \to X)}{m_h^2} \,. \tag{2.22}$$

Figure 2.4 illustrates the result of this convolution as a function of $\sqrt{s}$ for $\sqrt{s}$ near m_h in the three situations: $\Gamma_h^{\rm tot} \ll \sigma_{\sqrt{s}}$, $\Gamma_h^{\rm tot} \sim \sigma_{\sqrt{s}}$ and $\Gamma_h^{\rm tot} \gg \sigma_{\sqrt{s}}$. We observe that small R greatly

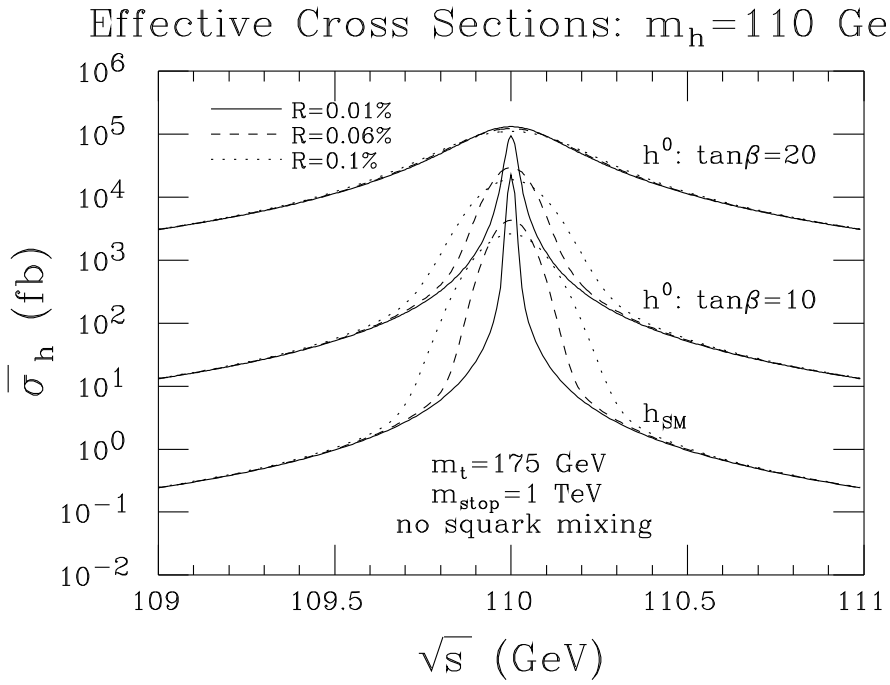

Figure 2.4: The effective cross section, $\overline{\sigma}_h$, obtained after convoluting σ_h with the Gaussian distributions for $R = 0.01\%$, $R = 0.06\%$, and $R = 0.1\%$, is plotted as a function of $\sqrt{s}$ taking $m_h = 110$ GeV.

enhances the peak cross section for $\sqrt{s} = m_h$ when $\Gamma_h^{\rm tot} \ll \sigma_{\sqrt{s}}$, as well as providing an opportunity to directly measure $\Gamma_h^{\rm tot}$.

As an illustration, suppose $m_h \sim 110$ GeV and h is detected in $e^+e^- \to Zh$ or $\mu^+\mu^- \to Zh$ with mass uncertainty $\delta m_h \sim \pm 0.8$ GeV (obtained with luminosity $L \sim 1$ fb^{-1}). For a standard model Higgs of this mass, the width is about 3.1 MeV. How many scan points and how much luminosity are required to zero in on $m_{h_{SM}}$ to within one rms spread $\sigma_{\sqrt{s}}$? For $R = 0.01\%$ ($R = 0.06\%$), $\sigma_{\sqrt{s}} \sim 7.7$ MeV (~ 45 MeV) and the number of scan points required to cover the 1.6 GeV mass zone at intervals of $\sigma_{\sqrt{s}}$ will be 230 (34), respectively. The luminosity required to observe (or exclude) the Higgs at each point is $L \gtrsim 0.01$ fb^{-1} ($L \gtrsim 0.3$ fb^{-1}) for $R = 0.01\%$ ($R = 0.06\%$). Thus, the total luminosity required to zero in on the Higgs will be ~ 2.3 fb^{-1} (~ 10.2 fb^{-1}) in the two cases.

More generally, the L required at each scan point decreases as (roughly) $R^{1.7}$, whereas the number of scan points only grows like $1/R$, implying that the total L required for the scan decreases as $\sim R^{0.7}$. Thus, the $\mu^+\mu^-$ collider should be constructed with the smallest

possible R value with the proviso that the number of $\sqrt{s}$ settings can be correspondingly increased for the required scan. It must be possible to quickly and precisely adjust the energy of the $\mu^+\mu^-$ collider to do the scan.

To measure the width of a SM-like Higgs boson, one would first determine m_h to within $d\sigma_{\sqrt{s}}$ with $d \lesssim 0.3$ and then measure the cross section accurately at the wings of the excitation peak, see Fig. 2.4. The two independent measurements of $\sigma_{\rm wings}/\sigma_{\rm peak}$ give improved precision for the Higgs mass and determine the Higgs width. It is advantageous to put more luminosity on the wings than the peak. Thus, to extract the total width we propose the following procedure[16]. First, conduct a rough scan to determine m_h to a precision $\sigma_{\sqrt{s}}d$, with $d \lesssim 0.3$. Then perform three measurements. At $\sqrt{s}_1 = m_h + \sigma_{\sqrt{s}}d$ expend a luminosity L_1 and measure the total rate $N_1 = S_1 + B_1$. Then perform measurements at

$$\sqrt{s}_2 = \sqrt{s}_1 - n_{\sigma_{\sqrt{s}}}\sigma_{\sqrt{s}} \tag{2.23}$$

and one at

$$\sqrt{s}_3 = \sqrt{s}_1 + n_{\sigma_{\sqrt{s}}}\sigma_{\sqrt{s}} \tag{2.24}$$

yielding $N_2 = S_2 + B_2$ and $N_3 = S_3 + B_3$ events, respectively, with luminosities of $L_2 = \rho_2 L_1$ and $L_3 = \rho_3 L_1$. The backgrounds can be determined from measurements farther from the resonance or from theoretical predictions. Next evaluate the ratios $r_2 = (S_2/\rho_2)/S_1$ and $r_3 = (S_3/\rho_3)/S_1$, for which the partial decay rates in the numerator in Eq. (2.55) cancel out. Since the excitation curve has a specific shape given by convoluting the denominator in Eq. (2.55) with the Gaussian distribution, these measured ratios determine the mass and total width of the Higgs boson. We find that the choices $n_{\sigma_{\sqrt{s}}} \simeq 2$ and $\rho_2 = \rho_3 \simeq 2.5$ are roughly optimal when $\sigma_{\sqrt{s}} \gtrsim \Gamma_h^{\rm tot}$. For these choices and $R = 0.01\%$, a total luminosity $L = L_1 + L_2 + L_3$ of 2 fb^{-1} (200 fb^{-1}) would be required to measure $\Gamma_h^{\rm tot}$ with an accuracy of $\pm 30\%$ for $m_h = 110$ GeV ($m_h = m_Z$). An accuracy of $\pm 10\%$ for $\Gamma_h^{\rm tot}$ could be achieved for reasonable luminosities provided m_h is not near m_Z.

It must be stressed that the ability to precisely determine the energy of the machine when the three measurements are taken is crucial for the success of the three-point technique. A mis-determination of the *spacing* of the measurements in Eqs. (2.66) and (2.67) by just 3% would result in an error in $\Gamma_{h_{SM}}^{\rm tot}$ of 30%. This does not present a problem provided some polarization of the beam can be achieved so that the precession of the spin of the muon as it circulates in the final storage ring can be measured. Given this and the rotation rate, the

energy can be determined to the nearly 1 part in a million accuracy required. This energy calibration capability must be incorporated in the machine design from the beginning.

The other quantity that can be measured with great precision at a $\mu^+\mu^-$ collider for a SM-like Higgs with $m_h \lesssim 130$ GeV is $G(b\bar{b}) \equiv \Gamma(h \to \mu^+\mu^-)BF(h \to b\bar{b})$. For $L = 50$ fb^{-1} and $R = 0.01\%, 0.06\%$, $G(b\bar{b})$ can be measured with an accuracy of $\pm 0.4\%, \pm 2\%$ ($\pm 3\%, \pm 15\%$) at $m_h = 110$ GeV ($m_h = m_Z$). By combining this measurement with the $\pm \sim 7\%$ determination of $BF(h \to b\bar{b})$ that could be made in the Zh production mode, a roughly $\pm 8 - 10\%$ determination of $\Gamma(h \to \mu^+\mu^-)$ becomes possible. ($R = 0.01\%$ is required if $m_h \sim m_Z$.)

Suppose we find a light Higgs h and measure its mass, total width and partial widths. The critical questions that then arise are:

- Can we determine if the particle is a SM Higgs or a supersymmetric Higgs?
- If the particle is a supersymmetric Higgs boson, say in the MSSM, can we then predict masses of the heavier Higgs bosons H^0, A^0, and $H^\pm$ in order to discover them in subsequent measurements?

In the context of the MSSM, the answers to these questions can be delineated.

Enhancements of $\Gamma_h^{\rm tot}$ of order 30% relative to the prediction for the SM h_{SM} are the norm (even neglecting possible SUSY decays) for $m_{A^0} \lesssim 400$ GeV. A 10% measurement of $\Gamma_h^{\rm tot}$ would thus be relatively likely to reveal a 3σ statistical enhancement. However, using the deviation to determine the value of m_{A^0} is model-dependent. For example, if $m_h = 110$ GeV and there is no stop mixing, then the percentage deviation would fairly uniquely fix m_{A^0}, whereas if $m_h = 110$ GeV and there is maximal stop mixing, as defined in Ref. [14], then the measured deviation would only imply a relation between $\tan\beta$ and m_{A^0}.

$\Gamma_h^{\rm tot}$ could be combined with branching ratios to yield a more definitive determination of m_{A^0}. For instance, we can compute $\Gamma(h \to b\bar{b}) = \Gamma_h^{\rm tot} BF(h \to b\bar{b})$ using $BF(h \to b\bar{b})$ as measured in Zh production. It turns out that the percentage deviation of this partial width for the h^0 from the h_{SM} prediction is rather independent of $\tan\beta$ and gives a mixing-independent determination of m_{A^0}, which, after including systematic uncertainties in our knowledge of m_b, would discriminate between a value of $m_{A^0} \leq 300$ GeV vs. $m_{A^0} = \infty$ at the $\geq 3\sigma$ statistical level.

Returning to $\Gamma(h \to \mu^+\mu^-)$, deviations at the $\gtrsim 3\sigma$ statistical level in the prediction for this partial width for the h^0 as compared to the h_{SM} are predicted out to $m_{A^0} \gtrsim 400$ GeV. Further, the percentage of deviation from the SM prediction would provide a relatively

accurate determination of m_{A^0} for $m_{A^0} \lesssim 400$ GeV. For example, if $m_h = 110$ GeV, $\Gamma(h^0 \to \mu^+\mu^-)$ changes by 20% (a $\gtrsim 2\sigma$ effect) as m_{A^0} is changed from 300 GeV to 365 GeV.

Deviations for other quantities, e.g. $BF(h \to b\bar{b})$, depend upon the details of the stop squark masses and mixings, the presence of SUSY decay modes, and so forth, much as described in the case of $\Gamma_h^{\rm tot}$. Only partial widths provide a mixing-independent determination of m_{A^0}. The $\mu^+\mu^-$ collider provides, as described, as least two particularly unique opportunities for determining two very important partial widths, $\Gamma(h \to b\bar{b})$ and $\Gamma(h \to \mu^+\mu^-)$, thereby allowing a test of the predicted proportionality of these partial widths to fermion mass independent of the lepton/quark nature of the fermion.

Thus, if $m_{A^0} \lesssim 400$ GeV, we may gain some knowledge of m_{A^0} through precision measurements of the h^0's partial widths. This would greatly facilitate direct observation of the A^0 and H^0 via s-channel production at a $\mu^+\mu^-$ collider with $\sqrt{s} \lesssim 500$ GeV. As discussed in more detail shortly, even without such pre-knowledge of m_{A^0}, discovery of the A^0, H^0 Higgs bosons would be possible in the s-channel at a $\mu^+\mu^-$ collider provided that $\tan\beta \gtrsim 3-4$. With pre-knowledge of m_{A^0}, detection becomes possible for $\tan\beta$ values not far above 1, provided $R \sim 0.01\%$ (crucial since the A^0 and H^0 become relatively narrow for low $\tan\beta$ values).

Other colliders offer various mechanisms to directly search for the A^0, H^0, but also have limitations:

- The LHC has a discovery hole and "h^0-only" regions at moderate $\tan\beta$, $m_{A^0} \gtrsim$ 200 GeV.

- At the NLC one can use the mode $e^+e^- \to Z^\star \to H^0A^0$ (the mode h^0A^0 is suppressed for large m_{A^0}), but it is limited to $m_{H^0} \sim m_{A^0} \lesssim \sqrt{s}/2$.

- A $\gamma\gamma$ collider could probe heavy Higgs up to masses of $m_{H^0} \sim m_{A^0} \sim 0.8\sqrt{s}$, but this would quite likely require $L \sim 100$ fb^{-1}, especially if the Higgs bosons are at the upper end of the $\gamma\gamma$ collider energy spectrum[20].

Most GUT models predict $m_{A^0} \gtrsim 200$ GeV, and perhaps as large as a TeV[21]. For large $m_{A^0} \sim m_{H^0}$, s-channel searches can be made at a $\mu^+\mu^-$ collider up to $\sim \sqrt{s}$, whereas the $Z^\star \to H^0A^0$ mode at an e^+e^- collider fails for $m_{A^0} \sim m_{H^0} \gtrsim \sqrt{s}/2$. In particular, at a muon collider with $\sqrt{s} \sim 500$ GeV, scan detection of the A^0, H^0 is possible in the mass range from 200 to 500 GeV in s-channel production, provided $\tan\beta \gtrsim 3-4$, whereas an e^+e^- collider

of the same energy can only probe $m_{H^0} \sim m_{A^0} \lesssim 220$ GeV. That the signals become viable when $\tan\beta > 1$ (as favored by GUT models) is due to the fact that the couplings of A^0 and (once $m_{A^0} \gtrsim 150$ GeV) H^0 to $b\overline{b}$ and, especially to $\mu^+\mu^-$, are proportional to $\tan\beta$, and thus increasingly enhanced as $\tan\beta$ rises.

Although the $\mu^+\mu^-$ collider cannot discover the H^0, A^0 in the $\tan\beta \lesssim 3$ region, this is a range in which the LHC *could* find the heavy Higgs bosons in a number of modes. That the LHC and the NMC are complementary in this respect is a very crucial point. Together, discovery of the A^0, H^0 is essentially guaranteed.

If the H^0, A^0 are observed at the $\mu^+\mu^-$ collider, measurement of their widths will typically be straightforward. For moderate $\tan\beta$ the A^0 and H^0 resonance peaks do not overlap and $R \lesssim 0.06\%$ will be adequate, since for such R values $\Gamma_{H^0,A^0} \gtrsim \sigma_{\sqrt{s}}$. However, if $\tan\beta$ is large, then for most of the $m_{A^0} \gtrsim 200$ GeV parameter range the A^0 and H^0 are sufficiently degenerate that there is significant overlap of the A^0 and H^0 resonance peaks. In this case, $R \sim 0.01\%$ resolution would be necessary for observing the double-peaked structure and separating the A^0 and H^0 resonances.

A $\sqrt{s} \sim 500$ GeV muon collider still might not have sufficient energy to discover heavy supersymmetric Higgs bosons. Further, distinguishing the MSSM from the SM by detecting small deviations of the h^0 properties from those predicted for the h_{SM} becomes quite difficult for $m_{A^0} \gtrsim 400$ GeV. However, construction of a higher energy machine, say $\sqrt{s} = 4$ TeV, would allow discovery of A^0, H^0 in the $b\overline{b}$ or $t\overline{t}$ channels (see the discussion in Section 2.2.5).

We close this section with brief comments on the effects of bremsstrahlung and beam polarization. Soft photon radiation must be included when determining the resolution in energy and the peak luminosity achievable at an e^+e^- or $\mu^+\mu^-$ collider. This radiation is substantially reduced at a $\mu^+\mu^-$ collider due to the increased mass of the muon compared to the electron. In Fig. 2.5 we show the luminosity distribution before and after including the soft photon radiation. These bremsstrahlung effects are calculated in Ref. [16]. A long tail extends down to low values of the energy.

For a SM-like Higgs boson with width smaller than $\sigma_{\sqrt{s}}$, the primary effect of bremsstrahlung is a reduction in the peak luminosity. The ratio of the luminosity peak height after and before including the bremsstrahlung is shown in Fig. 2.6. The conclusions above regarding s-channel Higgs detection are those obtained with inclusion of bremsstrahlung effects. The low-energy bremsstrahlung tail provides a self-scan over the range of energies below the design energy, and thus can be used to detect s-channel resonances. The full

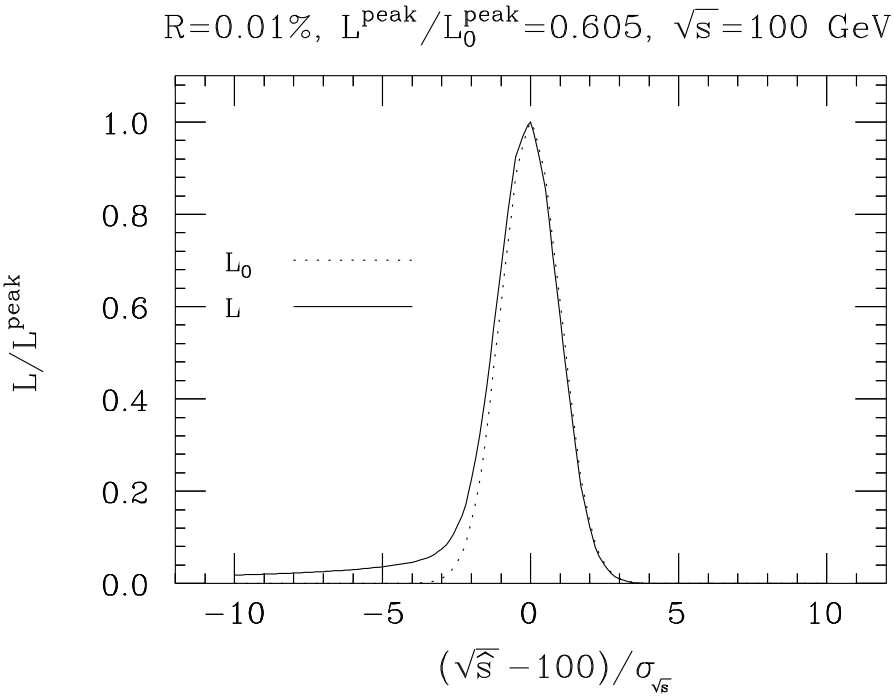

Figure 2.5: $d\mathcal{L}/d\sqrt{\hat{s}}$ relative to its peak value at $\sqrt{\hat{s}} = \sqrt{s}$ is plotted before and after soft-photon radiation. We have taken $\sqrt{s} = 100$ GeV and $R = 0.01\%$. The ratio of peak height after including soft-photon radiation to that before is 0.605.

luminosity distribution for the tail is shown in Fig. 2.7. Observation of A^0, H^0 peaks in the $b\bar{b}$ mass distribution $m_{b\bar{b}}$ created by this bremsstrahlung tail may be possible. The region of the $(m_{A^0}, \tan\beta)$ parameter space plane for which a peak is observable depends strongly on the $b\bar{b}$ invariant mass resolution. For an excellent $m_{b\bar{b}}$ mass resolution of order ± 5 GeV and integrated luminosity of $L = 50$ fb^{-1} at $\sqrt{s} = 500$ GeV, the A^0, H^0 peak(s) are observable for $\tan\beta \gtrsim 5$ at $m_{A^0} \gtrsim 400$ GeV (but only for very large $\tan\beta$ values in the $m_{A^0} \sim m_Z$ region due to the large s-channel Z contribution to the $b\bar{b}$ background).

In the s-channel Higgs studies, polarization of the muon beams could present a significant advantage over the unpolarized case, since signal and background come predominantly from different polarization states. Polarization P of both beams would enhance the significance of a Higgs signal provided the factor by which the luminosity is reduced is not larger than $(1 + P^2)^2/(1 - P^2)$. For example, a reduction in luminosity by a factor of 10 could be compensated by a polarization $P = 0.84$, leaving the significance of the signal unchanged[22].

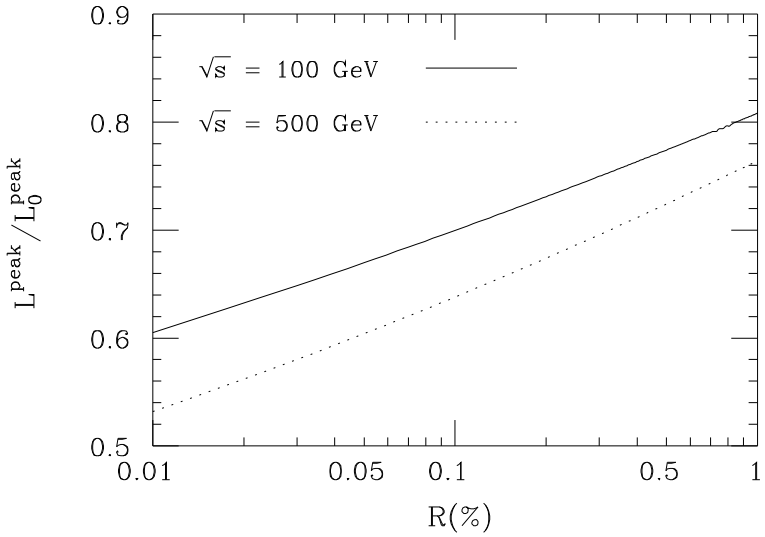

Figure 2.6: $\frac{d\mathcal{L}}{d\sqrt{\hat{s}}}/\frac{d\mathcal{L}_0}{d\sqrt{\hat{s}}}\Big|_{\sqrt{\hat{s}}=\sqrt{s}}$ as a function of R for $\sqrt{s} = 100$ and 500 GeV.

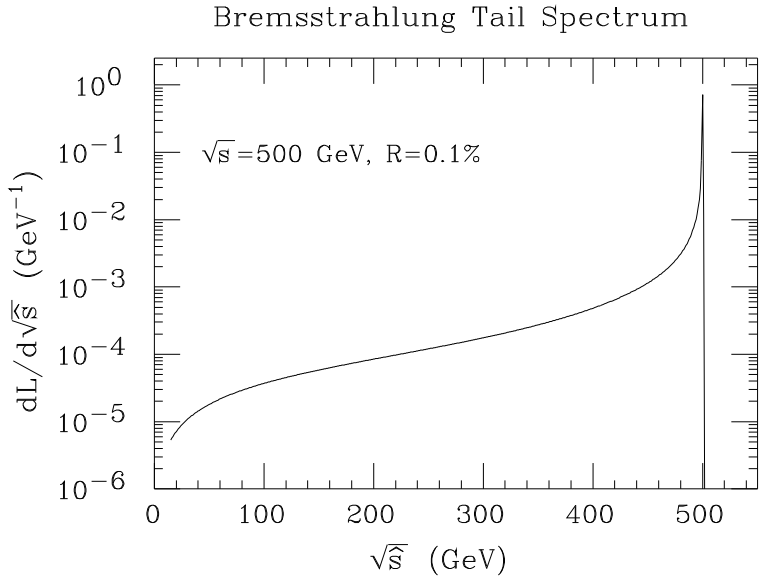

Figure 2.7: $\frac{d\mathcal{L}}{d\sqrt{\hat{s}}}$ as a function of $\sqrt{\hat{s}}$ for $R = 0.1\%$ and $\sqrt{s} =$ 500 GeV. The integral under the curve is normalized to 1.

Furthermore, *transverse* polarization of the muon beams could prove useful for studying CP-violation in the Higgs sector. Muons are produced naturally polarized from π and K decays.

An important consideration for the future design of muon colliders is the extent to which polarization can be maintained through the cooling and acceleration processes.

2.2.3 Precision Threshold Studies

Good beam energy resolution is crucial for the determination of the Higgs width. Another area of physics where the naturally good resolution of a $\mu^+\mu^-$ collider would prove valuable is studies of the $t\bar{t}$ and W^+W^- thresholds, similar to those proposed for the NLC and LEP II. The $t\bar{t}$ threshold shape determines m_t, Γ_t and the strong coupling α_s, while the W^+W^- threshold shape determines m_W and possibly also Γ_W. At a $\mu^+\mu^-$ collider, even a conservative natural beam resolution $R \sim 0.1\%$ would allow substantially increased precision in the measurement of most of these quantities as compared to other machines. Not only is such monochromaticity already greatly superior to e^+e^- collider designs, where typically $R \sim 1\%$, but also at a $\mu^+\mu^-$ collider there is no significant beamstrahlung and the amount of initial state radiation (ISR) is greatly reduced. ISR and, especially, beam smearing cause significant loss of precision in the measurement of the top quark and W masses at e^+e^- colliders.

To illustrate, consider threshold production of the top quark, which has been extensively studied for e^+e^- colliders[24]. Figure 2.8 shows the effects of including beam smearing and ISR for the threshold production of top quarks using a Gaussian beam spread of 1% for the e^+e^- collider[25]. Also shown are our corresponding results for the $\mu^+\mu^-$ collider with $R = 0.1\%$, see [25]. The threshold peak is no longer washed out in the $\mu^+\mu^-$ case. The precision with which one could measure m_t, α_s and Γ_t at various facilities is shown in Table 2.1. Improvements in the determination of m_W should also be possible[23].

The value of such improvements in precision can be substantial. Consider precision electroweak corrections, for example. The prediction for the SM or SM-like Higgs mass m_h depends on m_W and m_t through the one-loop equation

$$m_W^2 = m_Z^2 \left[1 - \frac{\pi\alpha}{\sqrt{2}G_\mu m_W^2(1-\delta r)}\right]^{1/2}, \tag{2.25}$$

where δr depends quadratically on m_t and logarithmically on m_h. Current expectations for LEP II and the Tevatron imply precisions of order

$$\Delta m_W = 40 \text{ MeV}, \tag{2.26}$$

$$\Delta m_t = 4 \text{ GeV}. \tag{2.27}$$

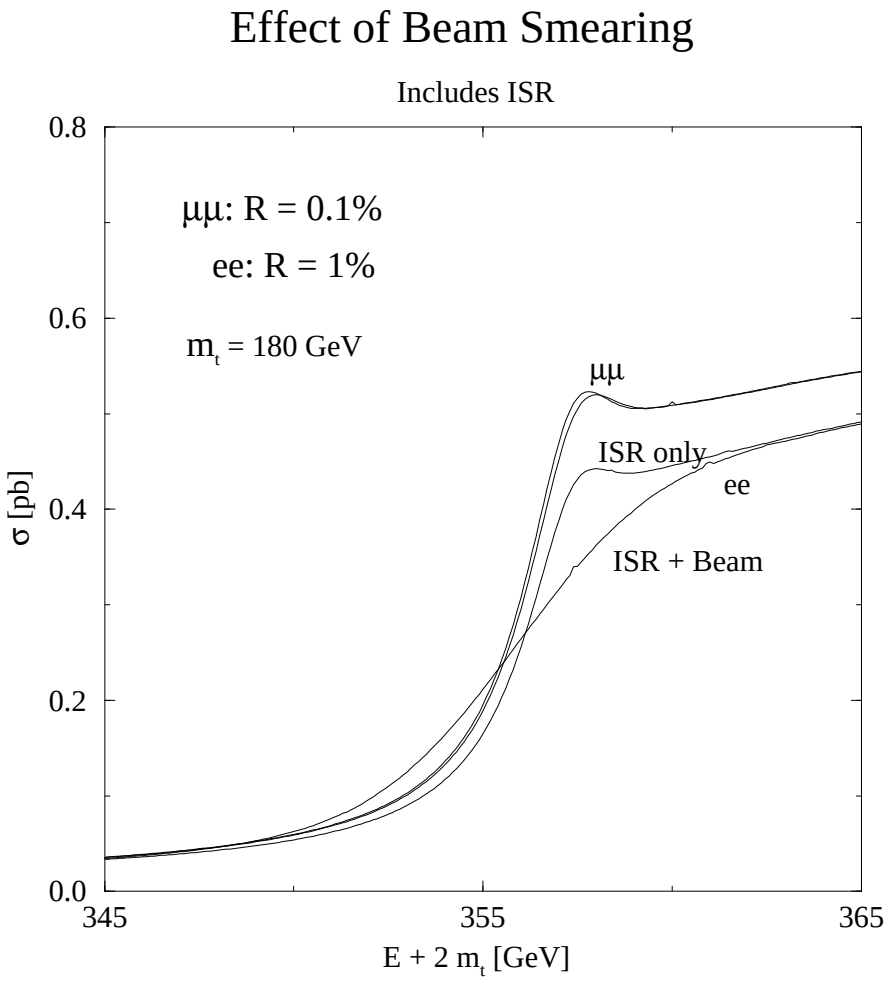

Figure 2.8: The threshold curves are shown for $\mu^+\mu^-$ and e^+e^- machines including ISR and with and without beam smearing. Beam smearing has only a small effect at a muon collider, whereas at an electron collider the threshold region is significantly smeared. The strong coupling is taken to be $\alpha_s(m_Z) = 0.12$.

For the uncertainties of Eq. (2.27) and the current central values of $m_W = 80.4$ GeV and $m_t = 180$ GeV, the Higgs mass would be constrained to the 1σ range

$$50 < m_h < 200 \text{ GeV} . \tag{2.28}$$

In electroweak precision analysis, an error of $\Delta m_W = 40$ MeV is equivalent to an error of $\Delta m_t = 6$ GeV, so increased precision for m_W would be of greatest immediate interest given

Table 2.1: Measurements of the standard model parameters: top mass m_t, strong coupling α_s, and top quark width Γ_t.

	Tevatron ($1000\ pb^{-1}$) ($10\ fb^{-1}$)	LHC ($20\ pb^{-1}$)	NLC ($10\ fb^{-1}$)	FMC ($10\ fb^{-1}$)
Δm_t(GeV)	4 1	2	0.52[a]	0.3
$\Delta\alpha_s$			0.009	0.008
$\Delta\Gamma_t/\Gamma_t$	0.3[b]		0.2	better

[a] See Ref.[26]
[b] See Ref.[27]

the $\Delta m_t = 4$ GeV error quoted above. In order to make full use of the $\Delta m_t \lesssim 0.5$ GeV precision possible at a $\mu^+\mu^-$ collider would require $\Delta m_W \lesssim 4$ MeV. We are currently studying the possibility that the latter can be achieved at a $\mu^+\mu^-$ collider.

Such precisions, combined with the essentially exact determination of m_h possible at a $\mu^+\mu^-$ collider, would allow a consistency test for precision electroweak measurements at a hitherto unimagined level of accuracy. If significant inconsistency is found, new physics could be revealed. For example, inconsistency could arise if the light h is not that of the SM but rather the h^0 of the MSSM and there is a contribution to precision electroweak quantities arising from the H^0 of the MSSM having a non-negligible WW, ZZ coupling. The contributions of stop and chargino states to loops would be another example.

A precise determination of the top quark mass m_t could well be important in its own right. One scenario is that the low-energy spectrum of particles (SUSY or not) has been measured and there is a desert up to the GUT scale. We would then want to extrapolate the low-energy parameters up to the grand unified scale to test in a detailed way the physics at that scale. Then the top quark mass (and the Yukawa coupling) would be crucially important since this parameter determines to a large extent the evolution of all the other Yukawas, including flavor mixings. These considerations become especially important if the top quark Yukawa coupling is determined by an infrared quasi-fixed point for which very small changes in the top quark mass translate into very large changes in the renormalized values of many other parameters in the theory.

2.2.4 CP Violation and FCNC in the Higgs Sector

A nonstandard Higgs sector could have sizable CP-violating effects as well as new flavor changing neutral current (FCNC) effects that could be probed with a $\mu^+\mu^-$ collider. A general two Higgs doublet model has been studied in Refs. [28, 29, 30]. There one would either (i) measure correlations in the final state, or (ii) transversely polarize the muon beams to observe an asymmetry in the production rate as a function of spin orientation. For the second option, the ability to achieve transverse polarization with the necessary luminosity is a crucial consideration.

New FCNC effects could be studied as well[31]. For example a Higgs in the s-channel could exhibit the decay $\mu^+\mu^- \to H^0 \to t\overline{c}$. This decay would have to compete against the $WW^\star$ decays.

2.2.5 Exotic Higgs Bosons/Scalars

In general, a muon collider can probe any type of scalar that has significant fermionic couplings. Interesting new physics could be revealed. To give one example, consider the possibility that a doubly-charged Higgs boson with lepton-number-violating coupling $\Delta^{--} \to \ell^-\ell^-$ exists, as required in left-right symmetric models where the neutrino mass is generated by the see-saw mechanism through a vacuum expectation value of a neutral Higgs triplet field. Such a Δ^{--} could be produced in $\ell^-\ell^-$ collisions. This scenario was studied in Ref. [32] for an e^-e^- collider, but a $\mu^-\mu^-$ collider would be even better due to the much finer energy resolution (which enhances cross sections) and the fact that the $\Delta^{--} \to \mu^-\mu^-$ coupling should be larger than the $\Delta^{--} \to e^-e^-$ coupling.

Most likely, a Δ^{--} in the $\lesssim 500$ GeV region would already be observed at the LHC by the time the muon collider begins operation. In some scenarios, it would even be observed to decay to $\mu^-\mu^-$ so that the required s-channel coupling would be known to be non-zero. However, the magnitude of the coupling would not be determined; for this we would need the $\mu^-\mu^-$ collider. In the likely limit where $\Gamma_{\Delta^{--}} \ll \sigma_{\sqrt{s}}$, the number of Δ^{--} events for $L = 50$ fb^{-1} is given by

$$N(\Delta^{--}) = 6 \times 10^{11} \left(\frac{c_{\mu\mu}}{10^{-5}}\right) \left(\frac{0.01\%}{R(\%)}\right) , \tag{2.29}$$

where the standard Majorana-like coupling-squared is parameterized as

$$|h_{\mu\mu}|^2 = c_{\mu\mu} m^2_{\Delta^{--}}(\text{ GeV}) . \tag{2.30}$$

Current limits on the coupling correspond to $c_{\mu\mu} \lesssim 5 \times 10^{-5}$. Assuming that 30 to 300 events would provide a distinct signal (the larger number probably required if the dominant Δ^{--} decay channel is into $\mu^-\mu^-$, for which there is a significant $\mu^-\mu^- \to \mu^-\mu^-$ background), the muon collider would probe some 11 to 10 orders of magnitude more deeply in the coupling-squared than presently possible. This is a level of sensitivity that would almost certainly be adequate for observing a Δ^{--} that is associated with the triplet Higgs boson fields that give rise to see-saw neutrino mass generation in the left-right symmetric models.

2.2.6 Physics at a 2⊗2 TeV $\mu^+\mu^-$ Collider

Bremsstrahlung radiation scales like m^{-4}, so a circular storage ring can be used for muons at high energies. A high energy lepton collider with center-of-mass energy of 4 TeV would provide new physics reach beyond that contemplated at the LHC or NLC (with $\sqrt{s} \lesssim 1.5$ TeV). We concentrate primarily on the following scenarios for physics at these energies: (1) heavy supersymmetric (SUSY) particles, (2) strong scattering of longitudinal gauge bosons (generically denoted W_L) in the electroweak symmetry breaking (EWSB) sector, and (3) heavy vector resonance production, like a Z'.

SUSY Factory

Low-energy supersymmetry is a theoretically attractive extension of the Standard Model. Not only does it solve the naturalness problem, but also the physics remains essentially perturbative up to the grand unification scale, and gravity can be included by making the supersymmetry local. Since the SUSY-breaking scale and, hence, sparticle masses are required by naturalness to be no larger than $1 - 2$ TeV, a high energy $\mu^+\mu^-$ collider with $\sqrt{s} = 4$ TeV is guaranteed to be a SUSY factory if SUSY is nature's choice. Indeed, it may be the only machine that would guarantee our ability to study the full spectrum of SUSY particles. The LHC has sufficient energy to produce supersymmetric particles but disentangling the spectrum and measuring the masses will be a challenge due to the complex cascade decays and QCD backgrounds. The NLC would be a cleaner environment than the LHC to study the supersymmetric particle decays, but the problem here may be insufficient energy to completely explore the full particle spectrum.

Most supersymmetric models have a symmetry known as an R-parity that requires that supersymmetric particles be created or destroyed in pairs. This means that the energy

required to find and study heavy scalars is more than twice their mass. (If R-parity is violated, then sparticles can also be produced singly; the single sparticle production rate would depend on the magnitude of the violation, which is model- and generation-dependent.) Further, a p-wave suppression is operative for the production of scalars (in this case the superpartners to the ordinary quarks and leptons), and energies well above the kinematic threshold might be required to produce the scalar pairs at an observable rate, as illustrated in Fig. 2.9. In addition, a large lever arm for exploring the different threshold behavior of spin-0 and spin-1/2 SUSY sparticles could prove useful in mass determinations.

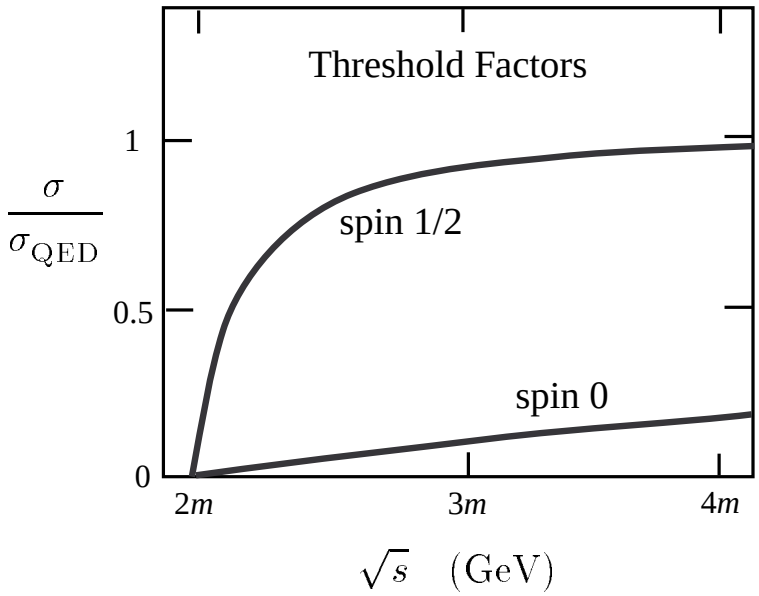

Figure 2.9: Comparison of kinematic suppression for fermion pairs and squark pair production at e^+e^- or $\mu^+\mu^-$ colliders.

To be more specific, it is useful to constrain the parameter space by employing a supergravity (SUGRA) model. Such models are particularly attractive in that the breaking of the electroweak symmetry is accomplished radiatively by the large top quark Yukawa coupling driving one of the Higgs doublet masses negative through renormalization group evolution. The simplest SUGRA models contain the following parameters:

- a universal scalar mass m_0;
- a universal gaugino mass $m_{1/2}$;

- the ratio of the electroweak scale Higgs v's, $\tan\beta = v_2/v_1$;
- a universal trilinear term A_0;
- the sign of the Higgs mixing: sign(μ).

The parameters above are constrained by various means. Experimental bounds on the superpartner masses put a lower bound on $m_{1/2}$. Naturalness considerations yield upper bounds on both $m_{1/2}$ and m_0, which, in turn, imply upper limits on the superparticle masses. If one supposes that the LSP is the cold dark matter of the universe, then there is an upper limit on m_0 so that the annihilation channels for the LSP are not suppressed by the heavy scalar masses. The A_0 parameter is limited by the requirement of an acceptable vacuum state; $1 \lesssim \tan\beta \lesssim 50 - 60$ is required for perturbativity of the Yukawa couplings. A representative choice of parameters that is consistent with all these constraints, but at the same time illustrates the power of a $\mu^+\mu^-$ collider is:

$$\begin{aligned} m_0 = 2m_{1/2} = 500 \text{ GeV} , \\ \tan\beta = 2, \quad A_0 = 0, \quad \mu < 0 . \end{aligned} \tag{2.31}$$

By adopting a large ratio of $m_0/m_{1/2} = 2$ the scalars become heavy (with the exception of the lightest Higgs boson) compared to the gauginos. The particle and sparticle masses obtained from renormalization group evolution are:

$$m_{h^0} = 88 \text{ GeV}, \quad m_{A^0} = 921 \text{ GeV} , \tag{2.32}$$

$$m_{H^\pm} = m_{H^0} = 924 \text{ GeV} , \tag{2.33}$$

$$m_{\tilde{q}_L} \simeq 752 \text{ GeV}, \quad m_{\tilde{q}_R} \simeq 735 \text{ GeV} , \tag{2.34}$$

$$m_{\tilde{b}_1} = 643 \text{ GeV}, \quad m_{\tilde{b}_2} = 735 \text{ GeV} , \tag{2.35}$$

$$m_{\tilde{t}_1} = 510 \text{ GeV}, \quad m_{\tilde{t}_2} = 666 \text{ GeV} , \tag{2.36}$$

$$m_{\tilde{\nu}} \sim m_{\tilde{\ell}} \sim 510 - 530 \text{ GeV} , \tag{2.37}$$

$$m_{\tilde{\chi}^0_{1,2,3,4}} = 107, 217, 605, 613 \text{ GeV} , \tag{2.38}$$

$$m_{\tilde{\chi}^+_{1,2}} = 217, 612 \text{ GeV} . \tag{2.39}$$

Thus, the choice of GUT parameters, Eq. (2.31), leads, as desired, to a scenario such that pair production of heavy scalars is only accessible at a high energy machine like the NMC.

First, we consider the pair production of the heavy Higgs bosons

$$\mu^+\mu^- \;\to\; Z \to H^0 A^0 \,, \tag{2.40}$$

$$\mu^+\mu^- \;\to\; \gamma, Z \to H^+ H^- \,. \tag{2.41}$$

The cross sections are shown in Fig. 2.10 versus $\sqrt{s}$. A $\mu^+\mu^-$ collider with $\sqrt{s} \gtrsim 2$ TeV is needed and well above the threshold the cross section is $\mathcal{O}(1$ fb). In the scenario of Eq. (2.31), the decays of these heavy Higgs bosons are predominantly into top quark modes ($t\bar{t}$ for the neutral Higgs and $t\bar{b}$ for the charged Higgs), with branching fractions near 90%. Observation of the H^0, A^0, and $H^\pm$ would be straightforward even for a pessimistic luminosity of $L = 100$ fb^{-1}. Backgrounds would be negligible once the requirement of roughly equal masses for two back-to-back particles is imposed.

In other scenarios the decays may be more complex and include multiple decay modes into supersymmetric particles, in which case the overall event rate might prove crucial to establishing a signal. In some scenarios investigated in Ref. [33] complex decays are important, but the $\mu^+\mu^-$ collider has sufficient production rate that one or more of the modes

$$(H^0 \to b\bar{b}) + (A^0 \to b\bar{b}) \,, \tag{2.42}$$

$$(H^0 \to h^0 h^0 \to b\bar{b}b\bar{b}) + (A^0 \to X) \,, \tag{2.43}$$

$$(H^0 \to t\bar{t}) + (A^0 \to t\bar{t}) \,, \tag{2.44}$$

are still visible above the backgrounds for $L \gtrsim 500$ fb^{-1}. Despite the significant dilution of the signal by the additional SUSY decay modes (which is most important at low $\tan\beta$), one can observe a signal of $\gtrsim 50$ events in one channel or another.

The high energy $\mu^+\mu^-$ collider will yield a large number of the light SM-like h^0 via $\mu^+\mu^- \to Z^\star \to Zh^0$ and WW fusion, $\mu^+\mu^- \to \nu\bar{\nu}h^0$. In contrast to a machine running at FMC energies ($\sqrt{s} \sim 500$ GeV), where the cross sections for these two processes are comparable, at higher energies, $\sqrt{s} \gtrsim 1$ TeV, the WW fusion process dominates as shown in Fig. 2.10.

Any assessment of the physics signals in the pair production of the supersymmetric partners of the quarks and leptons is model-dependent. However, as illustrated by the specific SUGRA scenario masses of Eq. (2.39), squarks are expected to be somewhat heavier than the sleptons due to their QCD interactions which affect the running of their associated 'soft' masses away from the universal mass m_0 in the evolution from the GUT scale to low

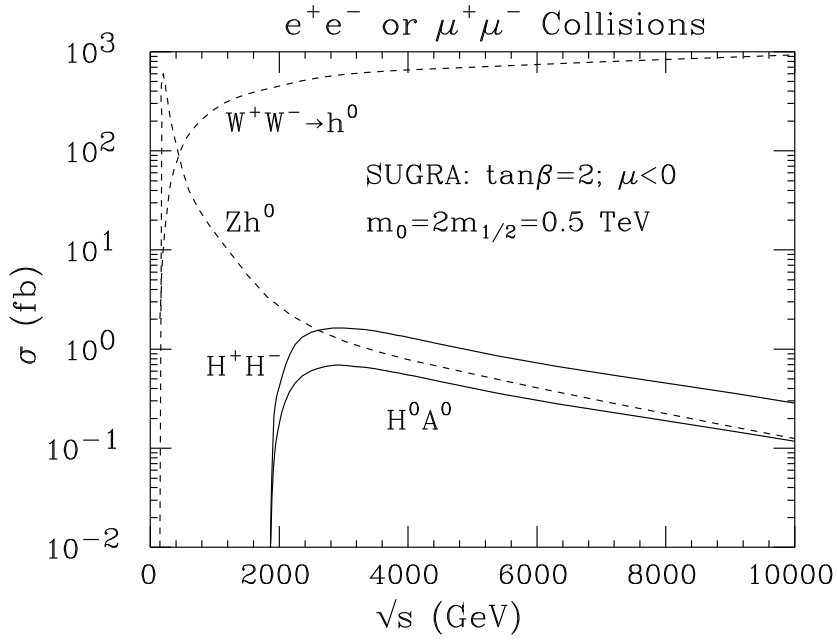

Figure 2.10: Pair production of heavy Higgs bosons at a high energy lepton collider. For comparison, cross sections for the lightest Higgs boson production via the Bjorken process $\mu^+\mu^- \to Z^\star \to Zh^0$ and via the WW fusion are also presented.

energies. Except for the LSP, the lightest superpartner of each type decays to a gaugino (or gluino) and an ordinary fermion, and the gaugino will decay if it is not the LSP. Since the particles are generally too short-lived to be observed, we must infer everything about their production from their decay products.

We illustrate the production cross sections for several important sparticle pairs in Fig. 2.11 for the SUGRA model of Eq. (2.31). For a collider with $\sqrt{s} \sim 4$ TeV, cross sections of ~ 2–30 fb are expected.

The final states of interest are determined by the dominant decay modes, which in this model are $\widetilde{e}_R \to e\widetilde{\chi}_1^0$ $(BF = 0.999)$, $\widetilde{\chi}_1^+ \to W^+\widetilde{\chi}_1^0$ $(BF = 0.999)$, $\widetilde{d}_L \to \widetilde{\chi}_1^- u, \widetilde{\chi}_2^0 d, \widetilde{g}d$ $(BF = 0.52, 0.27, 0.20)$, and $\widetilde{t}_1 \to \widetilde{\chi}_1^+ t$. Thus, for example, with a luminosity of $L = 200$ fb^{-1} at $\sqrt{s} = 4$ TeV, $\widetilde{d}_L$ pair production would result in $200 \times 2 \times (0.52)^2 = 100$ events containing two u-quark jets, two energetic leptons (not necessarily of the same type), and substantial missing energy. The SM background should be small, and the signal would be clearly visible.

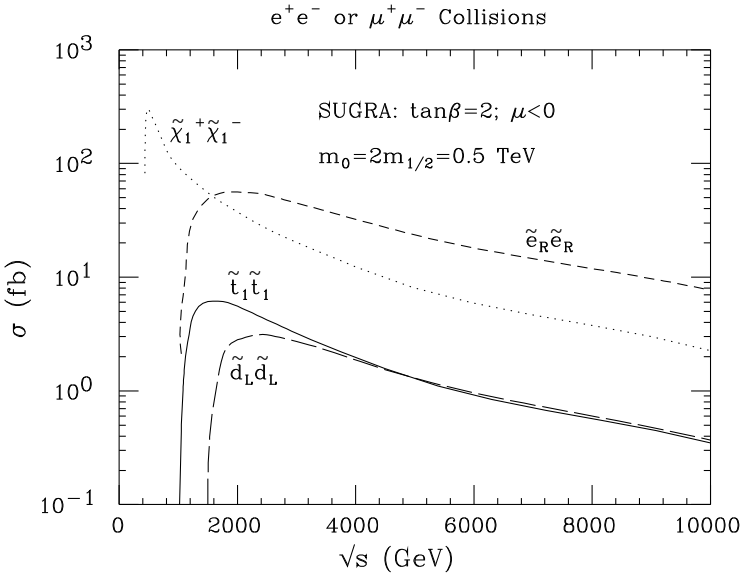

Figure 2.11: The production cross sections for SUSY particles in a supergravity model with heavy scalars.

The energy spectra of the quark jets would allow a determination of $m_{\widetilde{d}_L} - m_{\widetilde{\chi}_1^+}$ while the lepton energy spectra would fix $m_{\widetilde{\chi}_1^+} - m_{\widetilde{\chi}_1^0}$. If the machine energy can be varied, then the turn-on of such events would fix the $\widetilde{d}_L$ mass. The $\widetilde{\chi}_1^+$ and $\widetilde{\chi}_1^0$ masses would presumably already be known from studying the $\ell^+\ell^-$+missing-energy signal from $\widetilde{\chi}_1^+\widetilde{\chi}_1^-$ pair production, best performed at much lower energies. Thus, cross checks on the gaugino masses are possible, while at the same time two determinations of the $\widetilde{d}_L$ mass become available (one from threshold location and the other via the quark jet spectra combined with a known mass for the $\widetilde{\chi}_1^+$).

This example illustrates the power of a $\mu^+\mu^-$ collider, especially one whose energy can be varied over a broad range. Maintaining high luminosity over a broad energy range may require the construction of several (relatively inexpensive) final storage rings.

The $W_LW_L \to W_LW_L$ probe of EWSB

A compelling motivation for building any new machine is to discover the mechanism behind EWSB. This may involve directly producing the Higgs particle of the Standard Model or supersymmetric particles. Alternatively it could be that no light Higgs bosons exist; then

general arguments based on partial wave unitarity require that the interactions of the longitudinal gauge bosons (W and Z) become strong and nonperturbative. The energy scale where this happens is about 1–2 TeV, implying that a collider needs to probe vector boson scattering at energies at least this high. The LHC energy and the currently envisioned NLC energies (up to ~ 1.5 TeV) are marginally able to do this. In contrast, a 4 TeV muon collider is in the optimal energy range for a study of strong vector boson scattering. The construction of a multi-TeV e^+e^- collider is also a possibility[35].)

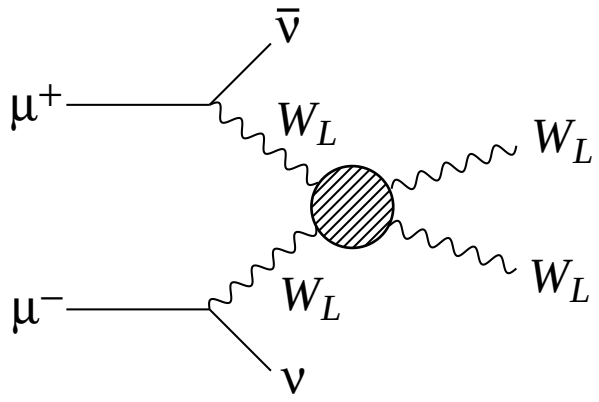

Figure 2.12: Symbolic diagram for strong WW scattering.

Strong electroweak scattering (SEWS) effects can be estimated by using the Standard Model with a heavy Higgs as a prototype of the strong scattering sector. The SM with a light Higgs is an appropriate definition of the electroweak background since only transversely polarized W's contribute to vector boson scattering when the Higgs has a small mass. For a 1 TeV SM Higgs boson, the signal is thus defined as

$$\Delta\sigma = \sigma(m_{h_{SM}} = 1 \text{ TeV}) - \sigma(m_{h_{SM}} = 10 \text{ GeV}) \; . \tag{2.45}$$

Results for $\Delta\sigma$ are shown in Table 2.2 for $\sqrt{s} = 1.5$ TeV (possibly the upper limit for a first e^+e^- collider) and 4 TeV. The strong scattering signal is relatively small at energies of order 1 TeV, but grows substantially as multi-TeV energies are reached. Thus, the highest energies in $\sqrt{s}$ that can be reached at a muon collider could be critically important.

Many other models for the strongly interacting gauge sector have been constructed in addition to the SM, including[36]:

Table 2.2: Strong electroweak scattering signals in $W^+W^- \to W^+W^-$ and $W^+W^- \to ZZ$ at future lepton colliders.

$\sqrt{s}$	$\Delta\sigma(W^+W^-)$	$\Delta\sigma(ZZ)$
1.5 TeV	8 fb	6 fb
4 TeV	80 fb	50 fb

- a ("Scalar") model in which there is a scalar Higgs resonance with $M_S = 1$ TeV but non-SM width of $\Gamma_S = 350$ GeV;
- a ("Vector") model in which there is no scalar resonance, but rather a vector resonance with $M_V = 1$ TeV and $\Gamma_V = 35$ GeV;
- a model, denoted by "LET" or "$m_{h_{SM}} = \infty$", in which the SM Higgs is taken to have infinite mass and the partial waves simply follow the behavior predicted by the low-energy theorems;
- a model (denoted by "LET-K") in which the LET behavior is unitarized via K-matrix techniques.

To differentiate among models, a complete study of the physics of strongly interacting gauge bosons would be required. In particular, all the following vector-boson scattering channels must be studied:

$$W^+W^- \to W^+W^-, ZZ\ , \tag{2.46}$$
$$W^\pm Z \to W^\pm Z\ , \tag{2.47}$$
$$W^\pm W^\pm \to W^\pm W^\pm\ . \tag{2.48}$$

Partial exploration of the three isospin channels can be made at the LHC. The signal and background for gold-plated (purely leptonic) events is shown in Table 2.3 for the LHC operating at 14 TeV with $L = 100$ fb^{-1}, for several of the above models. These channels have also been studied for a 1.5 TeV NLC[37], and, again, event rates are at a level that first signals of the strongly interacting vector boson sector would emerge, but the ability to discriminate between models and actually study these strong interactions would be limited.

For a $\mu^+\mu^-$ collider operating at 4 TeV the statistical significances markedly improve. Table 2.4 summarizes the total signal S and background B event numbers, summing over

Table 2.3: Total numbers of $W_LW_L \to$ 4-lepton signal S and background B events calculated for the LHC[36], assuming $L = 100$ fb^{-1}.

	Bkgd	Scalar	Vector	LET-K
$ZZ(4\ell)$	1	5	1.5	1.5
$(2\ell 2\nu)$	2	17	5	4.5
W^+W^-	12	18	6	5
W^+Z	22	2	70	3
$W^\pm W^\pm$	4	7	12	13

Table 2.4: Total numbers of $W^+W^-, ZZ \to$ 4-jet signal S and background B events calculated for a 4 TeV $\mu^+\mu^-$ collider with integrated luminosity 200 fb^{-1}. Events are summed over the mass range $0.5 < M_{WW} < 1.5$ TeV except for the W^+W^- channel with a narrow vector resonance for which $0.9 < M_{WW} < 1.1$ TeV. The statistical significance $S/\sqrt{B}$ is also given. The hadronic branching fractions of WW decays and the $W^\pm/Z$ identification/misidentification are included.

channels	SM $m_{h_{SM}} = 1$ TeV	Scalar $M_S = 1$ TeV	Vector $M_V = 1$ TeV	SM $m_{h_{SM}} = \infty$
$S(\mu^+\mu^- \to \bar{\nu}\nu W^+W^-)$	1900	1400	370	230
B(backgrounds)	1100	1100	110	1100
$S/\sqrt{B}$	57	42	35	6.9
$S(\mu^+\mu^- \to \bar{\nu}\nu ZZ)$	970	700	220	350
B(backgrounds)	160	160	160	160
$S/\sqrt{B}$	77	55	17	28

diboson invariant mass bins, together with the statistical significance $S/\sqrt{B}$ for different models of the strongly-interacting physics. A broad Higgs-like scalar will enhance both W^+W^- and ZZ channels with $\sigma(W^+W^-) > \sigma(ZZ)$; a ρ-like vector resonance will manifest itself through W^+W^- but not ZZ; while the $m_{h_{SM}} = \infty$ (LET) amplitude will enhance ZZ more than W^+W^-. The $m_{h_{SM}} = \infty$ signal for W^+W^- is visible, although still far from robust; the ratio S/B can be enhanced by making a higher mass cut (*e.g.* $M_{WW} > 0.7$ TeV), but the significance $S/\sqrt{B}$ is not improved.

Signals and the irreducible electroweak background for the W^+W^- and ZZ modes are shown in Fig. 2.13. The complementarity of these two modes is clear from the figure.

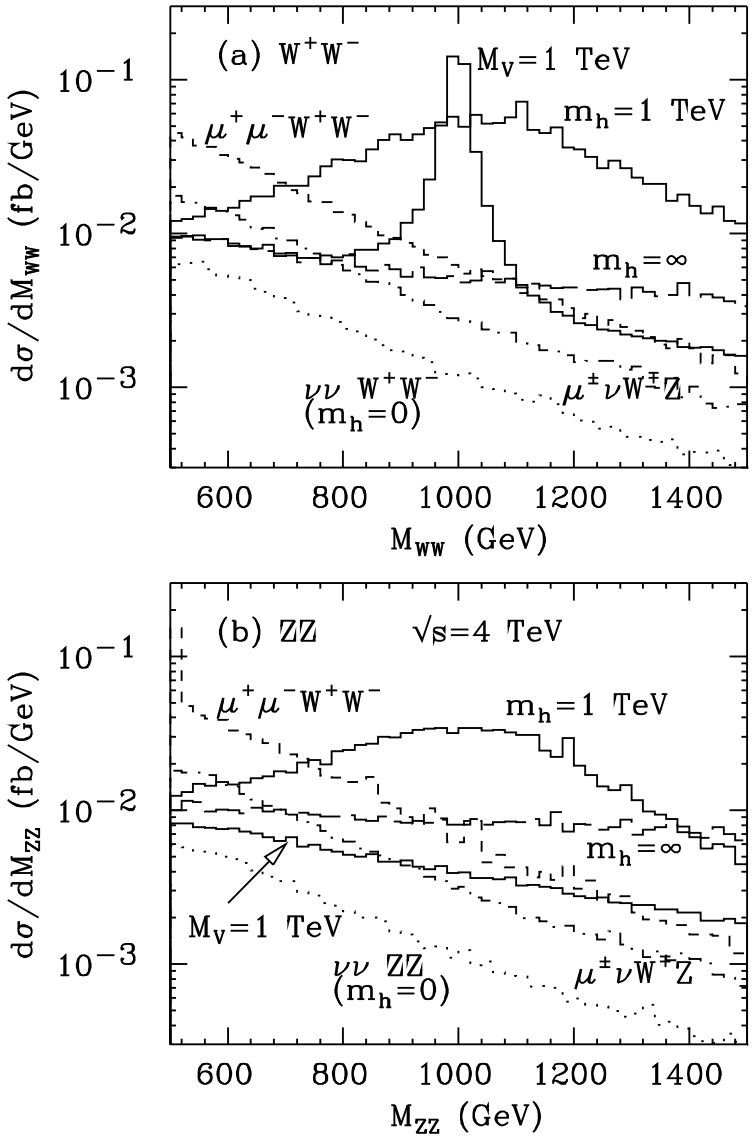

Figure 2.13: Histograms for the signals and backgrounds in strong vector boson scattering in the (a) W^+W^- and (b) ZZ final states. The background is given by the strictly electroweak $m_{h_{SM}} = 0$ limit of the Standard Model. The three signals shown are (I) a vector resonance with $M_V = 1$ TeV, $\Gamma_V = 35$ GeV, (II) the SM Higgs with $m_{h_{SM}} = 1$ TeV, and (III) the SM with $m_{h_{SM}} = \infty$ (LET model). In the figure the shorthand notation h is used for h_{SM}.

However, to make use of this complementarity it is crucial to be able to distinguish final state W and Z bosons using the dijet invariant masses. This is possible provided there is sufficient jet energy resolution, as discussed in Ref. [37].

Finally, we note that event numbers in the 1 TeV SM Higgs and Vector resonance cases, and possibly even in the $m_{h_{SM}} = \infty$ (LET) case, are such that not only could a substantial overall signal be observed, but also at high L the shape of the excess, due to strong interactions, in the distribution in vector boson pair mass could be measured over a broad interval in the 1 TeV range. For instance, from Fig. 2.13a in the case of $m_{h_{SM}} = \infty$, a 100 GeV interval from 1.4 TeV to 1.5 TeV would contain $L \times 100$ GeV $\times (4 \times 10^{-3}$ fb/ GeV$) = 400$ signal events for $L = 1000$ fb^{-1}, thereby allowing a 5% measurement of the $m_{W^+W^-}$ signal distribution in this bin. The level of accuracy in this one bin alone would distinguish this model from the Vector or $m_{h_{SM}} = 1$ TeV models. The difference between the three different distributions plotted in Fig. 2.13 could be tracked in both channels. The ability to measure the distributions with reasonable precision would allow detailed insight into the dynamics of the strongly interacting electroweak sector when the collider achieves energies substantially above 1 TeV. Thus, if some signals for a strongly interacting sector emerge at the LHC, a $\sqrt{s} = 3 - 4$ TeV $\mu^+\mu^-$ (or e^+e^-, if possible) collider will be essential.

Exotic Heavy States

The very high energy of a 4 TeV collider would open up the possibility of directly producing many new particles outside of the Standard Model. Some exotic heavy particles that could be discovered and studied at a muon collider are (1) sequential fermions, $Q\overline{Q}$, $L\overline{L}$[38], (2) lepto-quarks, (3) vector-like fermions[39], and (4) new gauge bosons like a Z' or W_R[40].

A new vector resonance such as a Z' or a technirho, $\rho_{\rm TC}$, is a particularly interesting possibility. The collider could be designed to sit on the resonance $\sqrt{s} \sim M_V$ in which case it would function as a Z' or $\rho_{\rm TC}$ factory as illustrated in Fig. 2.14. Alternatively, if the mass of the resonance is not known a priori, then the collider operating at an energy above the resonance mass could discover it via the bremsstrahlung tail shown in Fig. 2.7. Figure 2.15 shows the differential cross section in the reconstructed final state mass M_V for a muon collider operating at 4 TeV for two cases where the vector resonance has mass 1.5 TeV and 2 TeV. Dramatic and unmistakable signals would appear even for integrated luminosity as low as $L \gtrsim 50 - 100$ fb^{-1}.

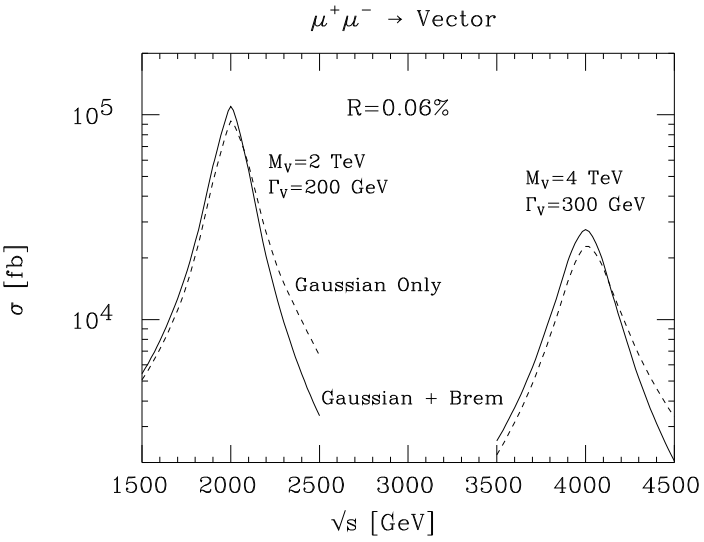

Figure 2.14: High event rates are possible if the muon collider energy is set equal to the vector resonance (Z' or $\rho_{\rm TC}$) mass. Two examples are shown here with $R = 0.06\%$.

2.2.7 Conclusions

A muon collider is very likely to add substantially to our knowledge of physics in the coming decades. A machine with energy in the range $\sqrt{s} = 100$–500 GeV is comparable to the NLC and provides valuable additional features. The most notable of these is the possibility of creating a Higgs boson in the s-channel and measuring its mass and decay widths directly and precisely. Even if a light Higgs does not exist, studies of the $t\bar{t}$ and W^+W^- thresholds at such a low-energy machine would yield higher precision in determining m_t and m_W than possible at other colliders. A $\mu^+\mu^-$ collider with energy as high as $\sqrt{s} \sim 4$ TeV appears to be entirely feasible and is ideally suited for studying a strongly-interacting symmetry breaking sector, since the center-of-mass energy is well above the energy range at which vector boson interactions must become strong. Many other types of exotic physics beyond the Standard Model could be probed at such a high machine energy. For example, if supersymmetry exists, a 4 TeV $\mu^+\mu^-$ collider would be a factory for sparticle pair production. Observation of a heavy Z' in the bremsstrahlung luminosity tail would be straightforward and the machine energy could later be reset to provide a Z' factory. All the issues presented in this paper will be discussed in greater detail in a forthcoming review article[9].

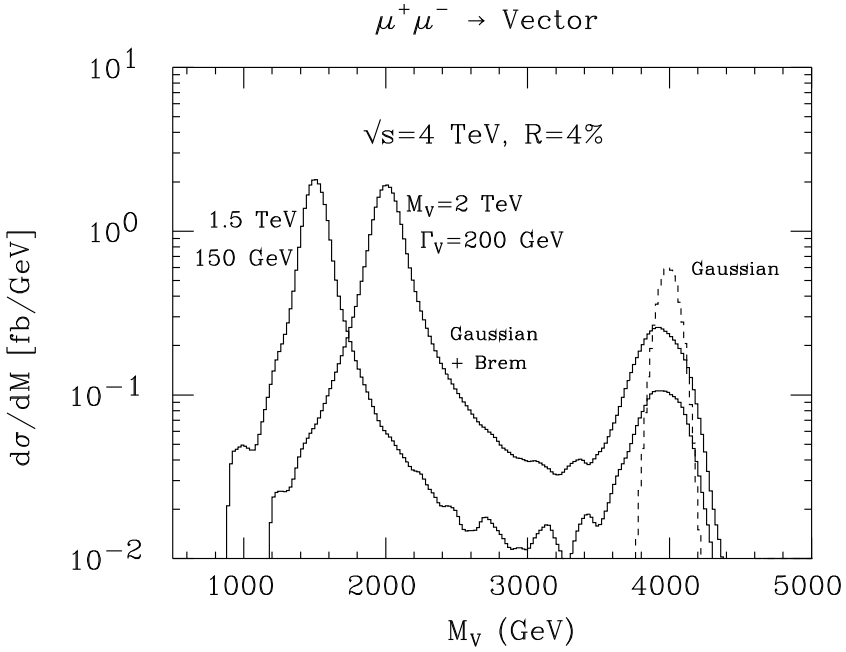

Figure 2.15: A heavy vector resonance can be visible in the bremsstrahlung tail of a high energy collider. Here a $\mu^+\mu^-$ collider operating at 4 TeV is shown for $M_V = 1.5$ TeV and 2 TeV.

2.3 Higgs Boson Physics in the s-Channel at $\mu^+\mu^-$ Colliders

2.3.1 Introduction

Despite the extraordinary success of the Standard Model (SM) in describing particle physics up to the highest energy available today, the mechanism responsible for electroweak symmetry-breaking (EWSB) has yet to be determined. In particular, the Higgs bosons predicted in the minimal Standard Model and the theoretically attractive Supersymmetric (SUSY) Grand Unified Theory (GUT) extensions thereof have yet to be observed. If EWSB does indeed derive from non-zero vacuum expectation values for elementary scalar Higgs fields, then one of the primary goals of constructing future colliders must be to *completely* delineate the associated Higgs boson sector. In particular, it will be crucial to discover all of the physical Higgs bosons and determine their masses, widths and couplings.

The remainder of the introduction is divided into two subsections. In the first, we briefly review crucial properties of the Standard Model and MSSM Higgs bosons. In the second, we outline basic features and parameters of the proposed $\mu^+\mu^-$ colliders, and give a first description of how they relate to our ability to discover and study the SM and MSSM Higgs bosons in s-channel $\mu^+\mu^-$ collisions.

Higgs Bosons in the SM and the MSSM

The EWSB mechanism in the Standard Model is phenomenologically characterized by a single Higgs boson (h_{SM}) in the physical particle spectrum. The mass of the h_{SM} is undetermined by the theory, but its couplings to fermions and vector bosons are completely determined, being given by $gm_f/(2m_W)$, gm_W and $gm_Z/\cos\theta_W$ for a fermion f, the W and the Z, respectively. Although the SM Higgs sector is very simple, it leads to problems associated with naturalness and mass hierarchies which suggest that the SM is simply an effective low-energy theory. Recent summaries of the phenomenology of the SM Higgs sector can be found in Refs. [41, 42].

The most attractive extensions of the SM that solve the naturalness and hierarchy problems are those based on supersymmetry. The Higgs sector of a supersymmetric model must contain at least two Higgs doublet fields in order to give masses to both up and down quarks and to be free of anomalies. If it contains two, and only two, Higgs doublet fields, then the strong and electroweak coupling constants all unify reasonably well at a GUT scale of order 10^{16} GeV. Thus, the minimal supersymmetric Standard Model, defined as having exactly two Higgs doublets, is especially attractive. The resulting spectrum of physical Higgs fields includes three neutral Higgs bosons, the CP-even h^0 and H^0 and the CP-odd A^0. At tree-level the entire Higgs sector is completely determined by choosing values for the parameters $\tan\beta = v_2/v_1$ (where v_2 and v_1 are the vacuum expectation values of the neutral members of the Higgs doublets responsible for up-type and down-type fermion masses, respectively) and m_{A^0} (the mass of the CP-odd A^0). For a summary, see Refs. [41, 42].

In the MSSM there is a theoretical upper bound on the mass of the lightest state h^0 [43, 44] which is approached at large m_{A^0} and large $\tan\beta$. After including two-loop/RGE-improved radiative corrections [45, 46] the bound depends upon the top quark (t) and top squark ($\tilde{t}$) masses and upon parameters associated with squark mixing. Assuming $m_t = 175$ GeV and

$m_{\tilde{t}} \lesssim 1$ TeV, the maximal mass is

$$m_{h^0}^{\max} \sim 113 \text{ to } 130 \text{ GeV}\,, \tag{2.49}$$

depending upon the amount of squark mixing. The 113 GeV value is obtained in the absence of squark mixing. Figure 2.16 illustrates the mass of the h^0 versus the parameter $\tan\beta$ for $m_{A^0} = 100$, 200 and 1000 GeV. Mass contours for the MSSM Higgs bosons are illustrated in Fig. 2.17 in the conventional $m_{A^0}, \tan\beta$ parameter plane. Both these figures include two-loop/RGE-improved radiative corrections to the Higgs masses computed for $m_t = 175$ GeV, $m_{\tilde{t}} = 1$ TeV and neglecting squark mixing.

The Higgs sector of the MSSM can be extended to include extra singlet fields without affecting any of its attractive features. A general supersymmetric model bound of

$$m_{h^0} \lesssim 130 \sim 150 \text{ GeV} \tag{2.50}$$

applies for such non-minimal extensions of the MSSM, assuming a perturbative renormalization group (RGE) evolved grand unified theory (GUT) framework.

The couplings of the MSSM Higgs bosons to fermions and vector bosons are generally proportional to the couplings of the SM Higgs boson, with the constant of proportionality being determined by the angle β (from $\tan\beta$) and the mixing angle α between the neutral Higgs states (α is determined by m_{A^0}, $\tan\beta$, m_t, $m_{\tilde{t}}$, and the amount of stop mixing). Those couplings of interest in this report are [47]

	$\mu^+\mu^-, b\overline{b}$	$t\overline{t}$	ZZ, W^+W^-	ZA^0
h^0	$-\sin\alpha/\cos\beta$	$\cos\alpha/\sin\beta$	$\sin(\beta-\alpha)$	$\cos(\beta-\alpha)$
H^0	$\cos\alpha/\cos\beta$	$\sin\alpha/\sin\beta$	$\cos(\beta-\alpha)$	$-\sin(\beta-\alpha)$
A^0	$-i\gamma_5\tan\beta$	$-i\gamma_5/\tan\beta$	0	0

(2.51)

times the Standard-Model factor of $gm_f/(2m_W)$ in the case of fermions (where m_f is the relevant fermion mass), or $gm_W, gm_Z/\cos\theta_W$ in the case of the W, Z, and $g(p_A - p_h)^\mu/2\cos\theta_W$ in the case of ZA^0, where $p_A(p_h)$ is the outgoing momentum of $A^0(h^0, H^0)$.

An important illustrative limit is $m_{A^0} \gtrsim 2m_Z$, since this is typical of SUSY GUT models [48]. In this limit, $\alpha \approx \beta - \pi/2$, $m_{A^0} \sim m_{H^0}$, m_{h^0} approaches its upper limit for the given

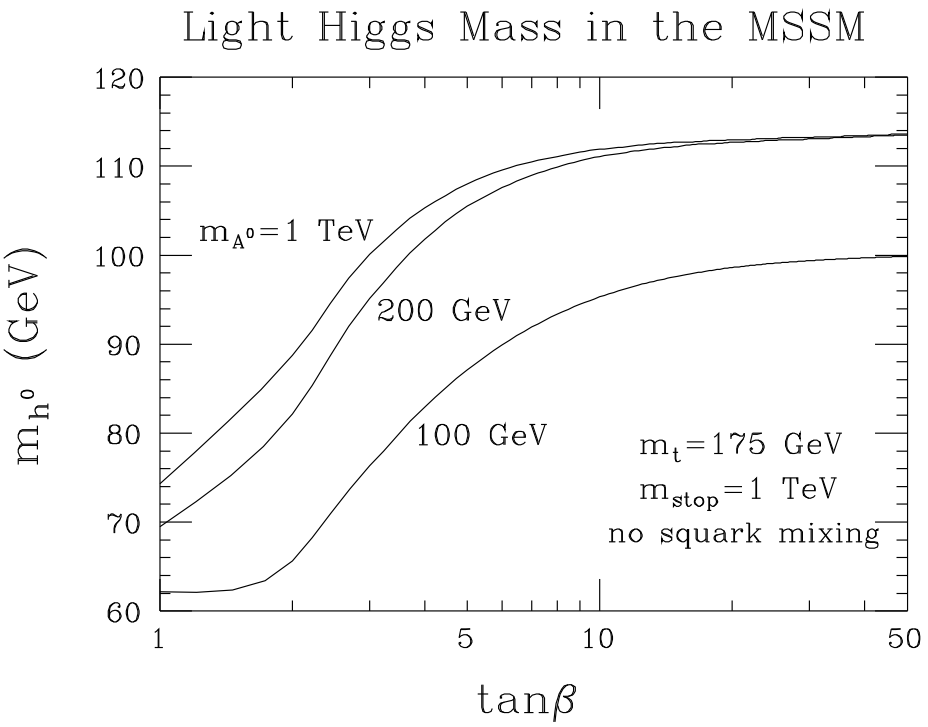

Figure 2.16: m_{h^0} vs $\tan\beta$ for $m_{A^0} = 100$, 200 and 1000 GeV. Two-loop/RGE-improved radiative corrections are included, see Refs. [45, 46], taking $m_t = 175$ GeV, $m_{\tilde{t}} = 1$ TeV and neglecting squark mixing.

value of $\tan\beta$, and the coupling factors of the Higgs bosons are approximately

$$\begin{array}{cccccc} & \mu^+\mu^-, b\bar{b} & & t\bar{t} & ZZ, W^+W^- & ZA^0 \\ h^0 & 1 & & 1 & 1 & 0 \\ H^0 & \tan\beta & & -1/\tan\beta & 0 & -1 \\ A^0 & -i\gamma_5 \tan\beta & & -i\gamma_5/\tan\beta & 0 & 0 \end{array} \tag{2.52}$$

times the Standard-Model factors as given below Eq. (2.51). Thus at large m_{A^0} it is the h^0 which is SM-like, while the H^0, A^0 have similar fermion couplings and small, zero (respectively) tree-level WW, ZZ couplings. Note that the H^0 and A^0 couplings to $\mu^+\mu^-$ and $b\bar{b}$ are enhanced in the (preferred) $\tan\beta > 1$ portion of parameter space.

For $m_{A^0} \lesssim m_Z$, the roles of the h^0 and H^0 are reversed: in this mass range the H^0 becomes roughly SM-like, while the h^0 has couplings (up to a possible overall sign) roughly like those given for H^0 in Eq. (2.52). (See Refs. [42, 49, 41] for details; Ref. [41] gives

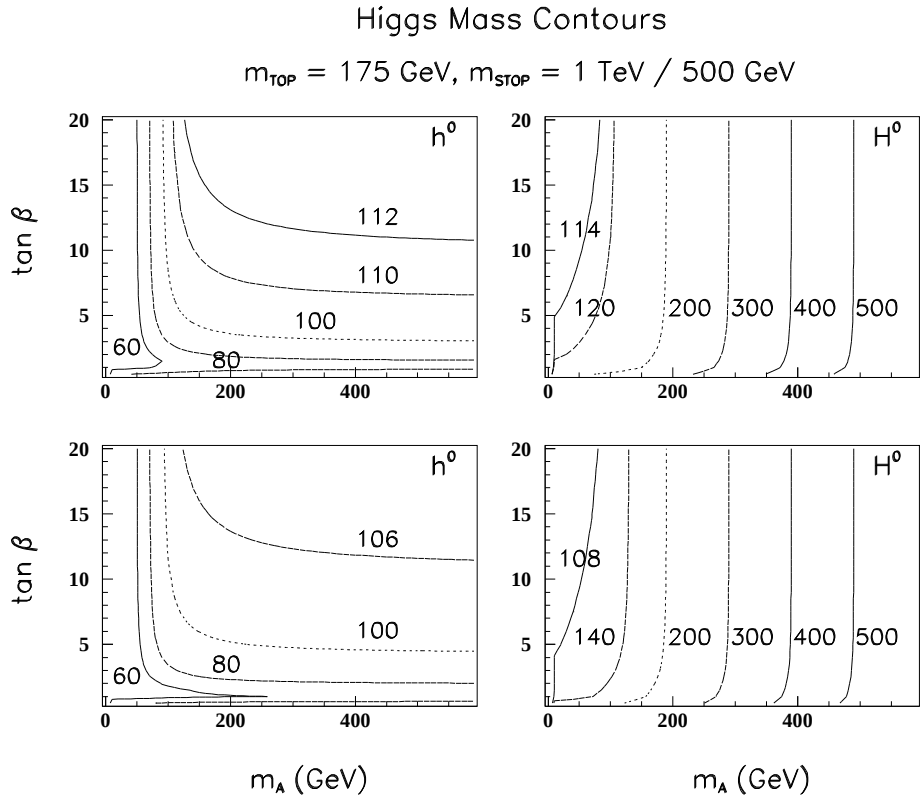

Figure 2.17: Contours for the h^0 and H^0 masses in $(m_{A^0}, \tan\beta)$ parameter space. Results include two-loop/RGE-improved radiative corrections computed for $m_t = 175$ GeV, with $m_{\tilde{t}} = 1$ TeV (upper plots) and $m_{\tilde{t}} = 500$ GeV (lower plots), neglecting squark mixing.

the corrections that imply that the simple rules are only roughly correct after including radiative corrections.) It is also useful to recall [47, 49] that the ZA^0H^0 (ZA^0h^0) coupling is maximal (~ 0) at large m_{A^0}, while at small m_{A^0} the reverse is true. The following discussions emphasize the case of large m_{A^0}.

The Higgs boson widths are crucial parameters for the searches and studies. In particular, we shall see that the width compared to the resolution in $\sqrt{s}$ of the machine is a crucial issue. Widths for the Standard Model Higgs h_{SM} and the three neutral Higgs bosons h^0, H^0, A^0 of the MSSM are illustrated in Fig. 2.3; for the MSSM Higgs bosons, results at $\tan\beta = 2$ and 20 are shown. As a function of $\tan\beta$, the total width of h^0 is plotted in Fig. 2.3.1 for $m_{h^0} = 100$, 110 and 120 GeV. We note that for masses below ~ 130 GeV, both the h_{SM} and a SM-like h^0 have very small widths (in the few MeV range); we will discover

that these widths are often smaller than the expected resolution in $\sqrt{s}$. At high $\tan\beta$ and large $m_{A^0} \sim m_{H^0}$, the $\mu^+\mu^-$, $\tau^+\tau^-$ and $b\bar{b}$ couplings of the H^0 and A^0 are greatly enhanced (being proportional to $\tan\beta$). Consequently, $\Gamma^{\rm tot}_{H^0}$ and $\Gamma^{\rm tot}_{A^0}$ are generally large compared to the expected $\sqrt{s}$ resolution.

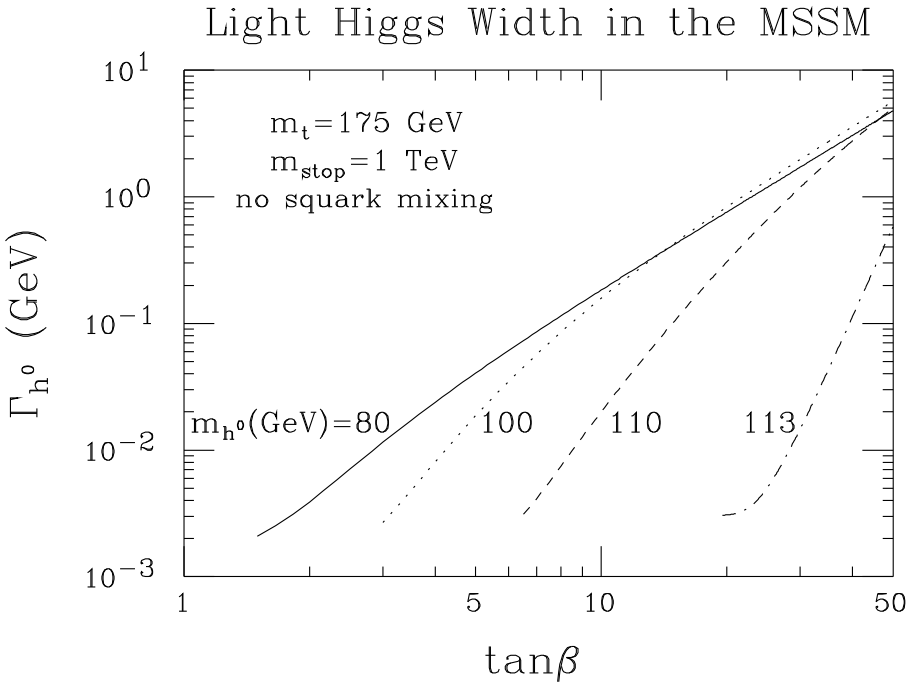

Figure 2.18: $\Gamma^{\rm tot}_{h^0}$ vs $\tan\beta$ for $m_{h^0} = 80$, 100, 110 and 113 GeV, assuming $m_t = 175$ GeV. Two-loop/RGE-improved radiative corrections to Higgs masses, mixing angles and self-couplings have been included, taking $m_{\tilde{t}} = 1$ TeV and neglecting squark mixing. SUSY decay channels are assumed to be absent.

Figure 2.3.1 illustrates the h_{SM} branching fractions for the $\mu^+\mu^-$, $b\bar{b}$, $WW^{(\star)}$ and $ZZ^{(\star)}$ decay modes. For an h_{SM} with $m_{h_{SM}} \lesssim 130$ GeV, the $b\bar{b}$ branching fraction is of order 0.8–0.9, implying that this will be the most useful discovery channel. Once the $WW^{(\star)}$ and $ZZ^{(\star)}$ modes turn on ($m_{h_{SM}} \gtrsim 2m_W$), the h_{SM} becomes broad and the branching fraction $BF(h_{SM} \to \mu^+\mu^-)$, which governs s-channel production, declines precipitously. Branching fractions for the h^0 of the MSSM are similar to those of h_{SM} for $m_{h_{SM}} = m_{h^0}$ when m_{A^0} is large. At high $\tan\beta$ and large $m_{A^0} \sim m_{H^0}$, the enhancement of the $\mu^+\mu^-$, $\tau^+\tau^-$ and $b\bar{b}$ couplings implies that the $b\bar{b}$, $\tau^+\tau^-$ and $\mu^+\mu^-$ branching fractions of the H^0 and A^0 are

the only important ones, and are not unlike those of a light h_{SM}, with relative magnitudes determined by $m_b^2 : m_\tau^2 : m_\mu^2$.

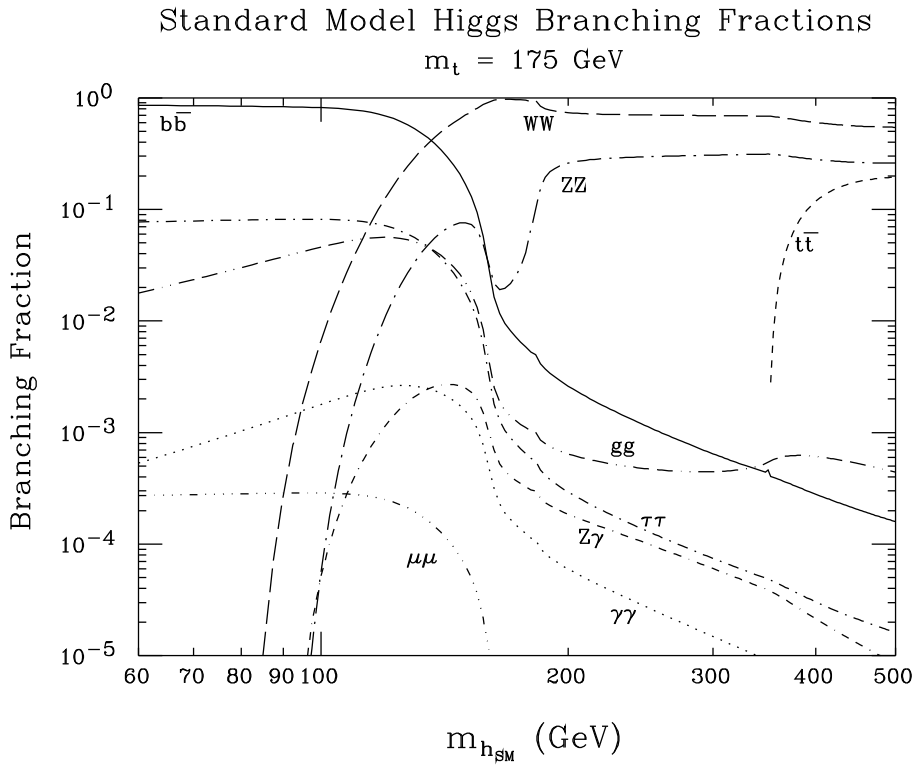

Figure 2.19: Branching fractions for the Standard Model h_{SM}.

Finally, it is relevant to note that in non-minimal extensions of the MSSM, parameter choices are possible such that the lightest Higgs boson to which the bound of Eq. (2.50) applies has very weak coupling to ZZ. This has been demonstrated [50] in the case of the minimal non-minimal supersymmetric model (MNMSSM), which contains one extra singlet Higgs representation, yielding three neutral Higgs bosons in all. However, for parameter choices such that the lightest Higgs decouples from ZZ, there is a strong upper bound on the mass of the least massive Higgs boson *with significant ZZ coupling*. The proof of this fact in the MNMSSM case relies on the observation that as the lighter Higgs bosons decouple from ZZ, the upper bound on the next heaviest Higgs boson moves down. This result may generalize to the case of more singlets.

s-Channel Higgs Boson Physics at $\mu^+\mu^-$ Colliders

The ability of a new accelerator to fully explore EWSB physics weighs heavily in its justification. Recently, there has been much interest in the possibility of constructing a $\mu^+\mu^-$ collider [51, 52, 53, 54], and a survey of the physics opportunities at such a collider has been made [55]. It is currently anticipated that a $\mu^+\mu^-$ collider can, at a minimum, achieve the same integrated luminosities and energies as an e^+e^- collider [56, 57, 58]. Further, with adequate detector segmentation the extra backgrounds resulting from muon decays can be tamed [59]. It then follows that a $\mu^+\mu^-$ collider can essentially explore all the same physics that is accessible at an e^+e^- collider of the same energy. In particular, all the established techniques for probing EWSB at e^+e^- colliders are applicable at a $\mu^+\mu^-$ collider. In addition, should one or more Higgs boson(s) (generically denoted by h) with substantial $\mu^+\mu^-$ coupling(s) exist, a $\mu^+\mu^-$ collider opens up the particularly interesting possibility of direct s-channel $\mu^+\mu^- \to h$ production. The SM Higgs boson, h_{SM}, is a prototypic example. Direct s-channel h_{SM} production is greatly enhanced at a $\mu^+\mu^-$ collider compared to an e^+e^- collider because its coupling to the incoming $\mu^+\mu^-$ is proportional to the lepton mass. Quantitative studies of s-channel Higgs production have been presented in Refs. [55, 60]. With the machine energy set to the Higgs mass ($\sqrt{s} = m_h$) the $\mu^+\mu^- \to h_{SM}$ rate is sufficiently large to allow detection of the h_{SM}, provided that $m_{h_{SM}} \lesssim 2m_W$ (the so-called intermediate Higgs mass region). In addition, *all* the Higgs bosons of the minimal supersymmetric model (MSSM) are produced in sufficient abundance in s-channel $\mu^+\mu^-$ collisions to allow their detection for most of the model parameter space.

In the present report, we expand on these results and provide the documentation underlying the discussion of Ref. [60] on precision studies of both the SM h_{SM} and the MSSM Higgs bosons. We find that the basic properties of the h_{SM} can be determined with remarkable accuracy in $\mu^+\mu^-$ s-channel production, and that the properties of MSSM Higgs bosons can be detailed over a larger fraction of model parameter space than at any other proposed accelerator. One particularly important conclusion is that s-channel Higgs production at a $\mu^+\mu^-$ collider of appropriate design has greater potential for distinguishing between a light SM h_{SM} and the SM-like h^0 of the MSSM than other processes/machines. The techniques and strategies for attaining the above results, and the associated requirements for the machine and detector, are discussed at length.

Two possible $\mu^+\mu^-$ machines are being actively studied [52, 53, 54]:

- A first muon collider (FMC, for short) with low c. m. energy ($\sqrt{s}$) between 100 and 500 GeV and $\mathcal{L} \sim 2 \times 10^{33}\,\mathrm{cm}^{-2}\,\mathrm{s}^{-1}$ delivering an annual integrated integrated luminosity $L \sim 20$ fb^{-1}.

- A next muon collider (NMC) with high $\sqrt{s} \gtrsim 4$ TeV and $\mathcal{L} \sim 10^{35}\,\mathrm{cm}^{-2}\,\mathrm{s}^{-1}$ giving $L \sim 1000$ fb^{-1} yearly; the extent to which such a machine could be run at high luminosity for $\sqrt{s}$ values starting at 500 GeV remains to be determined.

One of our goals will be to quantify the amount of integrated luminosity that is required to detect and study the various Higgs bosons via s-channel production as the Higgs mass is varied. For s-channel study of a SM-like Higgs boson, only the lower energy machine is relevant because a SM-like Higgs can only be detected in s-channel collisions if it has mass $\lesssim 2m_W$, given the anticipated luminosity. However, higher $\sqrt{s}$ will be important if the MSSM is the correct theory. The expected luminosity will allow detection and study of the heavier MSSM Higgs bosons (the CP-odd A^0 and the CP-even H^0) via s-channel production at the FMC for m_{A^0}, m_{H^0} up to the maximal $\sqrt{s}$. If the NMC can be run with high luminosity at $\sqrt{s}$ values starting at the maximal FMC energy (~ 500 GeV) and above, then the ability to discover the A^0 and H^0 via s-channel production would extend to correspondingly higher masses.

For s-channel Higgs studies, it will be important to deliver the maximum possible luminosity at c.m. energies where Higgs bosons are either expected or observed. Fortunately, this should be possible for the proposed FMC designs due to the fact that the final muon storage ring(s) would comprise a modest fraction of the overall cost [61]. (The most costly component of a muon collider is the muon source — decays of pions produced by proton collisions.) It is thus envisioned that multiple storage rings could eventually be tailor-made for c.m. energies spanning the desired range. This approach could presumably also be used to allow the high energy NMC to run with high luminosity at $\sqrt{s}$ values starting at ~ 500 GeV, where the FMC leaves off.

A crucial machine parameter for s-channel studies of Higgs bosons is the energy resolution of the colliding beams. A Gaussian shape for the energy spectrum of each beam is expected to be a good approximation, with an rms deviation, R, most naturally in the range [62]

$$R = 0.04\% \text{ to } 0.08\%$$

which could be decreased to as low as

$$R = 0.01\%$$

via additional cooling. Excellent energy resolution is mandatory to detect and study a Higgs boson with a very narrow width, which is the case for the h_{SM} with $m_{h_{SM}} \lesssim 2m_W$ and the lightest MSSM Higgs boson. The large value of the muon mass compared to the electron mass makes possible the required energy resolution in three ways:

i) it is possible (albeit, probably expensive) to achieve $R = 0.01\%$;

ii) bremsstrahlung smearing, while non-negligible, leaves a large portion of the narrow central Gaussian beam energy peak intact.

iii) designs with small beamstrahlung are naturally achieved;

Henceforth, we neglect beamstrahlung since quantitative calculations of this are unavailable.

The rms spread in $\sqrt{s}$ (denoted by $\sigma_{\sqrt{s}}$) prior to including bremsstrahlung is given by

$$\sigma_{\sqrt{s}} = R\sqrt{s}/\sqrt{2}\,, \tag{2.53}$$

where R is the resolution in the energy of each beam. A convenient formula for $\sigma_{\sqrt{s}}$ is

$$\sigma_{\sqrt{s}} = (7\text{ MeV})\left(\frac{R}{0.01\%}\right)\left(\frac{\sqrt{s}}{100\text{ GeV}}\right)\,. \tag{2.54}$$

The critical issue is how this resolution compares to the calculated total widths of Higgs bosons when $\sqrt{s} = m_h$. For $R \lesssim 0.01\%$, the energy resolution in Eq. (2.54) is smaller than the Higgs widths in Fig. 2.3 for all but a light SM-like Higgs. We shall demonstrate that the smallest possible R allows the best measurement of a narrow Higgs width, and that the total luminosity required for discovery by energy scanning when $\Gamma_h^{\rm tot} \lesssim \sigma_{\sqrt{s}}$ is minimized by employing the smallest possible R. For a Higgs boson with width larger than $\sigma_{\sqrt{s}}$, results from a fine scan with small R can be combined without any increase in the luminosity required for discovery and width measurement.

The Feynman diagram for s-channel Higgs production is illustrated in Fig. 2.2. The s-channel Higgs resonance cross section is

$$\sigma_h(\sqrt{\hat{s}}) = \frac{4\pi\Gamma(h\to\mu\mu)\,\Gamma(h\to X)}{\left(\hat{s}-m_h^2\right)^2 + m_h^2[\Gamma_h^{\rm tot}]^2}\,, \tag{2.55}$$

where $\hat{s} = (p_{\mu^+} + p_{\mu^-})^2$ is the c. m. energy squared of a given $\mu^+\mu^-$ annihilation, X denotes a final state and $\Gamma_h^{\rm tot}$ is the total width.[1] The sharpness of the resonance peak is determined by $\Gamma_h^{\rm tot}$. Neglecting bremsstrahlung for the moment, the effective signal cross section is obtained by convoluting $\sigma_h(\hat{s})$ with the Gaussian distribution in $\sqrt{\hat{s}}$ centered at $\sqrt{\hat{s}} = \sqrt{s}$:

$$\overline{\sigma}_h(\sqrt{s}) = \int \sigma_h(\sqrt{\hat{s}})\, \frac{\exp\left[-(\sqrt{\hat{s}} - \sqrt{s})^2/(2\sigma^2_{\sqrt{s}})\right]}{\sqrt{2\pi}\sigma_{\sqrt{s}}}\, d\sqrt{\hat{s}}\,. \tag{2.56}$$

Figure 2.4 illustrates the effective cross section, $\overline{\sigma}_h(\sqrt{s})$, as a function of $\sqrt{s}$ for $m_h = 110$ GeV and beam energy resolutions of $R = 0.01\%$, $R = 0.06\%$, and $R = 0.1\%$. Results are given for the cases: h_{SM}, h^0 with $\tan\beta = 10$, and h^0 with $\tan\beta = 20$. All channels X are summed over.

In the case where the Higgs width is much smaller than the Gaussian width $\sigma_{\sqrt{s}}$, the effective signal cross section result for $\sqrt{s} = m_h$, denoted by $\overline{\sigma}_h$, is

$$\overline{\sigma}_h = \frac{2\pi^2\Gamma(h \to \mu\mu)\, BF(h \to X)}{m_h^2} \times \frac{1}{\sigma_{\sqrt{s}}\sqrt{2\pi}} \qquad (\Gamma_h^{\rm tot} \ll \sigma_{\sqrt{s}})\,. \tag{2.57}$$

Henceforth, we adopt the shorthand notation

$$G(X) = \Gamma(H \to \mu\mu)\, BF(h \to X) \tag{2.58}$$

for the numerator of Eq. (2.57). The increase of $\overline{\sigma}_h(\sqrt{s} = m_h)$ with decreasing $\sigma_{\sqrt{s}}$ when $\Gamma_h^{\rm tot} \ll \sigma_{\sqrt{s}}$ is apparent from the h_{SM} curves of Fig. 2.4. In the other extreme where the Higgs width is much broader than $\sigma_{\sqrt{s}}$, then at $\sqrt{s} = m_h$ we obtain

$$\overline{\sigma}_h = \frac{4\pi BF(h \to \mu\mu) BF(h \to X)}{m_h^2} \qquad (\Gamma_h^{\rm tot} \gg \sigma_{\sqrt{s}})\,. \tag{2.59}$$

Note that this equation implies that if there is a large contribution to the Higgs width from some channel other than $\mu\mu$, we will get a correspondingly smaller total event rate due to the small size of $BF(h \to \mu\mu)$. That $\overline{\sigma}_h(\sqrt{s} = m_h)$ is independent of the value of $\sigma_{\sqrt{s}}$ when $\Gamma_h^{\rm tot} \gg \sigma_{\sqrt{s}}$ is illustrated by the $\tan\beta = 20$ curves for the h^0 in Fig. 2.4. Raw signal rates (*i.e.* before applying cuts and including other efficiency factors) are computed by multiplying $\overline{\sigma}_h$ by the total integrated luminosity L.

[1] Effects arising from implementing an energy-dependent generalization of the $m_h\Gamma_h^{\rm tot}$ denominator component of this simple resonance form are of negligible importance for our studies, especially for a Higgs boson with $\Gamma_h^{\rm tot} \ll m_h$.

The basic results of Eqs. (2.57) and (2.59) are modified by the effects of photon bremsstrahlung from the colliding muon beams. In the case of a narrow Higgs boson, the primary modification for $\sqrt{s} = m_h$ is due to the fact that not all of the integrated luminosity remains in the central Gaussian peak. These modifications are discussed in sec. 2.12.1; to a good approximation, the resulting signal rate is obtained by multiplying $\overline{\sigma}_h$ of Eq. (2.57) by the total luminosity L times the fraction f of the peak luminosity in the Gaussian after including bremsstrahlung relative to that before (typically $f \approx 0.6$). For a broad Higgs resonance, the lower energy tail in the luminosity distribution due to bremsstrahlung makes some contribution as well. In the results to follow, we avoid any approximation and numerically convolute the full effective luminosity distribution (including bremsstrahlung) with the Higgs cross section of Eq. (2.55). In performing this convolution, we require that the effective $\mu^+\mu^-$ c.m. energy be within 10 GeV of the nominal value. Such a requirement can be implemented by reconstructing the mass of the final state as seen in the detector; planned detectors would have the necessary resolution to impose the above fairly loose limit. This invariant mass selection is imposed in order to reduce continuum (non-resonant) backgrounds that would otherwise accumulate from the entire low-energy bremsstrahlung tail of the luminosity distribution.

As is apparent from Fig. 2.4, discovery and study of a Higgs boson with a very narrow width at the $\mu^+\mu^-$ collider will require that the machine energy $\sqrt{s}$ be within $\sigma_{\sqrt{s}}$ of m_h. The amount of scanning required to find the correct $\sqrt{s}$ depends upon R. From Fig. 2.4 it is apparent that the larger R is, the less the accuracy with which the machine energy needs to be set at each scan point and the fewer the number of scan points needed. But, small R results in much greater event rate for $\sqrt{s} \simeq m_h$. *If $\sqrt{s}$ can be rapidly changed with an accuracy that is a small fraction of R*, then we shall find that smaller R implies that less total time (and, hence, luminosity) will be required for the scan. Further, we find that $R \sim 0.01\%$ and the ability to set $\sqrt{s}$ with an accuracy of order 1 part in 10^6 are both required if we are to be able to measure the Higgs width with sufficient precision to distinguish between the SM h_{SM} and the MSSM h^0 when the latter is SM-like. Thus, for a $\mu^+\mu^-$ collider to reach its full potential, it should be designed so that $R \sim 0.01\%$ and so that it is possible to vary $\sqrt{s}$ rapidly and with great precision. These are not insurmountable tasks [61], but careful planning is certainly required. For Higgs bosons with a large width, the design demands upon the $\mu^+\mu^-$ collider are clearly less.

Due to the bremsstrahlung tail, it is also possible to search for a Higgs boson by running

the $\mu^+\mu^-$ collider at an energy well above the mass of the Higgs boson itself. In some collisions, one (or both) of the muons will have radiated enough of its initial energy that the effective $\sqrt{\hat{s}}$ of the collision is much lower than $\sqrt{s}$. In this circumstance, detection of the Higgs boson requires reconstruction with good resolution of the effective $\sqrt{\hat{s}}$ of each collision from the final state momenta. For a final state mass bin centered at $\sqrt{\hat{s}} = m_h$, if $d\mathcal{L}/d\sqrt{\hat{s}}$ is slowly varying in the vicinity of $\sqrt{\hat{s}} = m_h$ over an interval several times the Higgs total width $\Gamma_h^{\rm tot}$, the effective cross section is

$$\overline{\sigma}_h = \frac{2\pi^2 \Gamma(h \to \mu\mu)\, BF(h \to X)}{m_h^2} \times \left.\frac{d\mathcal{L}}{d\sqrt{\hat{s}}}\right|_{\sqrt{\hat{s}}=m_h} . \tag{2.60}$$

In exploring the possible utility of this bremsstrahlung tail for Higgs detection, we have performed our explicit calculations using the spectrum obtained for $R = 0.1\%$. However, we note that the bremsstrahlung tail well away from the central Gaussian peak is essentially independent of the beam energy resolution R. If a mass resolution in the final state of ± 5 GeV is possible in the $b\overline{b}$ final state, then even when running the FMC at full nominal energy of $\sqrt{s} = 500$ GeV we find that it will be possible to detect a Higgs boson with m_h in a broad range below $\sqrt{s}$ (but not near m_Z) provided that the $h \to \mu^+\mu^-$ coupling is significantly enhanced with respect to the SM $h_{SM} \to \mu^+\mu^-$ coupling. The total integrated luminosity required for Higgs discovery using the bremsstrahlung tail will be compared to that needed for discovery by scanning using a large number of $\sqrt{s}$ machine energy settings.

Highly polarized beams may be possible since the muons are naturally polarized from $\pi^\pm$ ($K^\pm$) decays in the parent rest-frame. However, the luminosity for polarized beams may be significantly reduced during the cooling and acceleration process. If a degree of polarization P is possible for *both* beams, then, relative to the unpolarized case, the s-channel Higgs signal is enhanced by the factor $(1 + P^2)$ while the background is suppressed by $(1 - P^2)$. High polarization P of both beams would be useful if the luminosity reduction is less than a factor of $(1 + P^2)^2 / (1 - P^2)$, *i.e.* the factor which would leave the significance of the signal unchanged. For example, $P = 0.84$ would compensate a factor of 10 reduction in luminosity [63]. We mainly present our results without assuming high polarization beams, but we comment on improvements with beam polarization.

With this introduction, we now proceed with a detailed description of the capability of a $\mu^+\mu^-$ collider to detect and study different types of Higgs bosons. In the next section, we begin with SM-like Higgs bosons. The following section explores the non-SM-like Higgs bosons of the MSSM. The final section gives our conclusions.

2.3.2 A SM-like Higgs Boson

We first review the prospects for discovering and studying a SM-like Higgs boson without s-channel production at a $\mu^+\mu^-$ collider. We then turn to the role of s-channel $\mu^+\mu^- \to h$ production, emphasizing the prospects for precision studies of the Higgs mass and width.

Discovery and Study Without s-Channel Production

Neutral Higgs bosons that are coupled to ZZ with roughly SM-like strength can be discovered via $Z^\star \to Zh$ production for $m_h \lesssim 0.7\sqrt{s}$ at either an e^+e^- collider or a $\mu^+\mu^-$ collider [64]. This discovery reach applies to both the h_{SM} and to the h^0 of the MSSM in the large-m_{A^0} portion of parameter space where it is SM-like in its couplings. The stringent upper bound on m_{h^0}, Eq. (2.49), in the MSSM implies that even a $\sqrt{s} = 300$ GeV machine is guaranteed to find the h^0 if it exists.

As described in the Introduction, we can also consider adding extra singlets to the MSSM two-doublet Higgs sector. In the MNMSSM model, containing one singlet Higgs field, we noted that even if the lightest Higgs boson has small ZZ coupling, there is always a CP-even Higgs boson with substantial ZZ coupling and modest mass. Refs. [50] demonstrate that at least one of the CP-even Higgs bosons of the MNMSSM model will be detected in the Zh mode at a machine with c.m. energy $\sqrt{s} = 500$ GeV. Since it appears that this result may generalize to the case of more than one additional singlet, we regard it as relatively certain that any supersymmetric theory in the SUSY GUT context will contain at least one CP-even Higgs boson that will be discovered in the Zh mode at a machine with $\sqrt{s} = 500$ GeV, and its mass will be in the intermediate mass range ($\lesssim 2m_W$).

Assuming that a SM-like h is discovered in the Zh mode, an important question for s-channel production and study of the h in $\mu^+\mu^-$ collisions is the accuracy with which its mass can be measured á priori via Zh production. The better this accuracy, the easier it will be to set $\sqrt{s}$ of the $\mu^+\mu^-$ collider to a value centered on m_h within the rms spread $\sigma_{\sqrt{s}}$. Another critical question bearing on the importance of the s-channel $\mu^+\mu^- \to h$ production mode is whether the Zh mode is useful for measurement of the h width. We find that it is not.

Generally speaking, the accuracy of the Higgs boson mass measurements depends on the detector performance and the signal statistics. As a general guide, we consider two examples for the uncertainty on m_h in the mass range $m_h < 2m_W$ (*i.e.* below where W-pair decays

become important)

$$\Delta m_h \simeq 4.0 \text{ GeV}/\sqrt{N} \quad \text{(SLD)}, \tag{2.61}$$

$$\simeq 0.3 \text{ GeV}/\sqrt{N} \quad \text{(super} - \text{LC)}. \tag{2.62}$$

where our notation will always be that ΔX represents the absolute magnitude of the 1σ error on the quantity X; that is the 1σ limits on X are $X \pm \Delta X$. Equation (2.61) results for performance typified by the SLD detector [65], where 4 GeV is the single event resolution and N is the number of events in the $Z(\to q\overline{q})h(\to b\overline{b})$, $Z(\to q\overline{q})h(\to \tau\overline{\tau})$, plus $Z(\to \ell^+\ell^-)h(\to$ any) modes. For a SM-like Higgs, these modes have an effective final state branching fraction that varies between about 70% and 50% as m_h varies from low masses up to 140 GeV. We plot Δm_h in Fig. 2.1 according to Eqs. (2.61) and (2.62), with $N = \epsilon L\sigma(Zh)BF(\text{effective})$, assuming detection efficiencies of $\epsilon = 0.9$ [$\epsilon = 0.5$] for the $Z(\to \ell^+\ell^-)h(\to$ any) [$Z(\to q\overline{q})h(\to b\overline{b})$, $Z(\to q\overline{q})h(\to \tau\overline{\tau})$] modes and assuming a fixed $\sqrt{s} = 500$ GeV. For SLD detector performance, results for luminosities of $L = 1$, 10, and 50 fb^{-1} are shown; with these integrated luminosities, m_h (for $m_h \lesssim 150$ GeV) will be determined to an accuracy of at least 1.4, 0.5, 0.21 GeV (respectively).

Equation (2.62) is applicable for a "super" performance Linear Collider detector (hereafter referred to as the super-LC detector) [66, 67], the special features of which include excellent momentum resolutions and high b-tagging efficiency. For this detector, the best determination of $m_{h_{SM}}$ is obtained by examining the recoil mass peak in Zh_{SM} production. For $Z \to \ell^+\ell^-$ events, the resolution for the recoil mass is expected to be of order 0.3 GeV per event. A measurement of $m_{h_{SM}}$ to ± 0.3 GeV$/\sqrt{N} \sim \pm 20$ MeV would be possible for $m_{h_{SM}} \lesssim 140$ GeV and $L = 50$ fb^{-1}, as illustrated in Fig. 2.1, assuming detection efficiency of $\epsilon = 0.9$ for the $Z(\to \ell^+\ell^-)h(\to$ any) mode. The total width $\Gamma^{\rm tot}_{h_{SM}}$ could also be measured down to $\sim$200 MeV using the Zh_{SM} recoil mass distribution. However, this latter sensitivity is not likely to be useful since $\Gamma_{h_{SM}} \lesssim 10$ MeV for $m_{h_{SM}} \lesssim 140$ GeV (see Fig. 2.3).

It could happen that there is no e^+e^- collider at the time the $\mu^+\mu^-$ collider is built but that the LHC has been operational for several years. One of the primary modes for discovery of a SM-like Higgs boson at the LHC is the $\gamma\gamma$ mode. Simulations by the LHC collaborations indicate that this mode is detectable for $50 \lesssim m_h \lesssim 150$ GeV. For $m_h \gtrsim 130$ GeV, discovery will be possible in the 4ℓ mode. Both modes, but especially the $\gamma\gamma$ mode, offer the possibility of a very accurate determination of the Higgs mass. Resolution will be 1% or better in the $\gamma\gamma$ mode, and probably not much worse than 1% in the 4ℓ mode. Thus, even in the absence of an

e^+e^- collider, the LHC can reasonably be expected to provide us with a $\lesssim 1\%$ determination of m_h in the mass region where the Higgs total width is small.

s-Channel Production of a SM-like *h*

Once a SM-like Higgs boson is found in the Zh mode at either an e^+e^- collider or the $\mu^+\mu^-$ collider itself,[2] or at the LHC, it will generally be easy to also produce and detect it via direct s-channel production at a $\mu^+\mu^-$ collider [60] if $m_h \lesssim 2m_W$. Should there be no e^+e^- collider in operation, an important question at a $\mu^+\mu^-$ collider will then be whether to concentrate subsequent running on s-channel production or on Zh production, as the best means for studying the properties of the h in detail. Generally speaking, these two different processes provide complementary information and it would be very valuable to accumulate substantial integrated luminosity in both modes.

The potential importance of s-channel production of a SM-like h is illustrated by two facts pertaining to distinguishing between the MSSM h^0 and the SM h_{SM}.

(1) Expected experimental errors imply that the ability to discriminate between the SM h_{SM} and the MSSM h^0 on the basis of the branching fractions and production rates that can be measured in the Zh channel is limited to m_{A^0} values below about 300 GeV [41].

(2) Both the total width and the production rate (proportional to $\Gamma(h \to \mu^+\mu^-)$) of a SM-like h could be measured at a muon collider with sufficient accuracy so as to distinguish the h^0 from the h_{SM} in the large-m_{A^0} region 300 GeV $\lesssim m_A \lesssim$ 600 GeV where the h^0 is approximately SM-like.

A quantitative discussion of the MSSM parameter space region for which deviations of the total width and production rate from SM expectations are measurable will be given later. For now we emphasize that (2) requires the excellent $R = 0.01\%$ beam energy resolution.

Choosing the right $\sqrt{s}$ Our proposed strategy is to first discover the SM-like h via $\ell^+\ell^- \to Zh$ or in hadron collisions in order to determine the $\sqrt{s}$ region in which $\mu^+\mu^- \to h$ s-channel production should be explored. If $\Gamma_h^{\rm tot}$ is smaller than the rms spread $\sigma_{\sqrt{s}}$ in $\sqrt{s}$

[2] While discovery at a $\mu^+\mu^-$ collider is also possible by scanning in s, the Zh mode is more luminosity efficient for discovery.

(as is the case for the SM when $m_{h_{SM}} \lesssim 140$ GeV), then to obtain the maximum $\mu^+\mu^- \to h$ production rate it is necessary to set $\sqrt{s}$ equal to m_h within $\lesssim \sigma_{\sqrt{s}}$. The ability to do this is assessed by comparing the errors on m_h from Zh production to both the $\sqrt{s}$ spread $\sigma_{\sqrt{s}}$ at a $\mu^+\mu^-$ collider and to $\Gamma_h^{\rm tot}$. As an illustration, consider $h = h_{SM}$. With the super-LC $L = 50$ fb^{-1} determination of $m_{h_{SM}}$ to ± 20 MeV, $\sigma_{\sqrt{s}}$ for $R = 0.01\%$ will be at worst a factor of 2 or 3 smaller than the uncertainty in $m_{h_{SM}}$ and only two or three tries will be needed to set the $\mu^+\mu^-$ collider energy to a value equal to $m_{h_{SM}}$ within the rms spread in $\sqrt{s}$. If the SLD $L = 50$ fb^{-1} determination of $m_{h_{SM}}$ to 210 MeV is all that is available, then for $m_{h_{SM}} \lesssim 2m_W$ two or three tries would be adequate to set $\sqrt{s} \simeq m_{h_{SM}}$ within $\sigma_{\sqrt{s}}$ only if $R = 0.06\%$. The number of settings required in the case of $R = 0.01\%$ would be a factor of 6 larger. If only SLD performance and $L = 1$ fb^{-1} is available in the Zh_{SM} mode, or if only a $\sim 1\%$ determination of $m_{h_{SM}}$ from the LHC is provided, both of which imply errors on $m_{h_{SM}}$ that are $\gtrsim 1$ GeV, then even with $R = 0.06\%$ one must scan over 10 to 20 $\sqrt{s}$ values to determine the central $\sqrt{s} \simeq m_{h_{SM}}$ value within the rms $\sqrt{s}$ error, $\sigma_{\sqrt{s}}$. Later, we will compute the amount of luminosity that must be invested at each $\sqrt{s} = m_h$ choice in order to detect a SM-like Higgs signal.

In contrast to the above narrow width situation, for $m_{h_{SM}} \gtrsim 200$ GeV one finds $\Gamma_{h_{SM}}^{\rm tot} \gtrsim \sigma_{\sqrt{s}}$ for $R \leq 0.06\%$. Then, even if $m_{h_{SM}}$ is only known to within $\Gamma_{h_{SM}}^{\rm tot}$, we can immediately set $\sqrt{s}$ for the $\mu^+\mu^-$ collider to be within the Higgs peak. Unfortunately, we find that the event rate in s-channel collisions is too low to allow detection of the h_{SM} in this case. This situation does not arise in the case of the h^0 of the MSSM, which is guaranteed to have $m_{h^0} \lesssim 130$ GeV.

Detecting a SM-like h in the s-channel The effective cross section, $\overline{\sigma}_{h_{SM}}(\sqrt{s} = m_{h_{SM}})$ for inclusive SM Higgs production is given in Fig. 2.3.2 versus $\sqrt{s} = m_{h_{SM}}$ for resolutions of $R = 0.01\%$, 0.06%, 0.1% and 0.6%. These results include Gaussian and bremsstrahlung smearing effects. For comparison, the $\mu^+\mu^- \to Z^\star \to Zh_{SM}$ cross section is also shown, evaluated at the energy $\sqrt{s} = m_Z + \sqrt{2}m_{h_{SM}}$ for which it is a maximum. The s-channel $\mu^+\mu^- \to h_{SM}$ cross sections for small R and $m_{h_{SM}} \lesssim 2m_W$ are much larger than the corresponding Zh_{SM} cross section. The increase in the $\mu^+\mu^- \to h_{SM}$ cross section that results if bremsstrahlung smearing is removed is illustrated in the most sensitive case ($R = 0.01\%$).

For a SM-like Higgs boson, the only potentially useful final state modes X are $b\overline{b}$, $WW^{(\star)}$

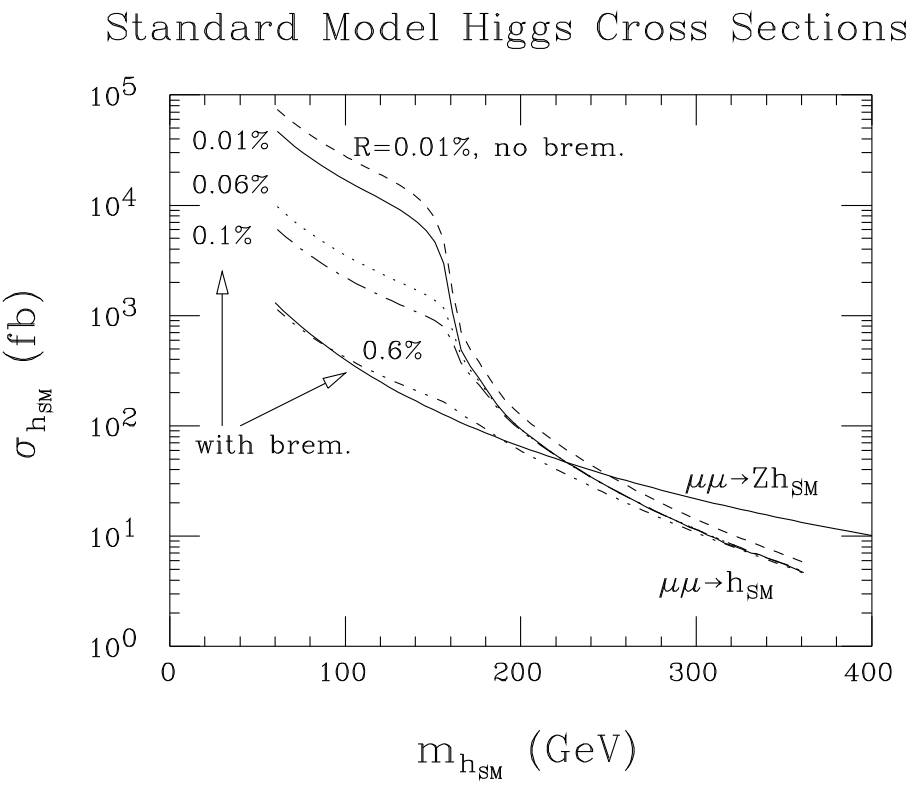

Figure 2.20: Cross sections vs $m_{h_{SM}}$ for inclusive SM Higgs production: (i) the s-channel $\overline{\sigma}_h$ for $\mu^+\mu^- \to h_{SM}$ with $R = 0.01\%$, 0.06%, 0.1% and 0.6%, and (ii) $\sigma(\mu^+\mu^- \to Zh_{SM})$ at $\sqrt{s} = m_Z + \sqrt{2}m_{h_{SM}}$. Also shown is the result for $R = 0.01\%$ if bremsstrahlung effects are not included.

and $ZZ^{(\star)}$, where the $^{(\star)}$ indicates the possibility that the weak boson is virtual. The $t\bar{t}$ channel does not give a viable signal for the range of luminosity that we consider. All these channels have irreducible backgrounds from $\mu^+\mu^-$ continuum production processes. We note that

(a) The light-quark backgrounds to the $b\bar{b}$ channel can be rejected using b-tagging. We assume a 50% efficiency for isolating the $2b$ final state (via tagging one of the b's); this efficiency is to include cuts and detector efficiencies.

(b) For the $b\bar{b}$ final state, we have checked that interference between the s-channel signal and the backgrounds is never of importance. This is because the Higgs signal contributes to RR and LL helicity amplitudes for the incoming muons, whereas the

backgrounds come almost entirely from RL and LR helicity combinations (the RR and LL background contributions are suppressed by a factor of m_μ/E at the amplitude level).

(c) For the $WW^{(\star)}$ and $ZZ^{(\star)}$ final states the useful channels depend upon whether or not the $W^{(\star)}$ or $Z^{(\star)}$ is virtual. We shall find that discovery in these channels is only possible for $m_h \lesssim 2m_W$, in which case the final states of interest are $WW^\star \to \ell\nu 2j$ with $BF^{\rm eff}_{WW} \sim 0.3$ and $ZZ^\star \to 2\ell 2j, 2\nu 2j, 4\ell, 2\ell 2\nu$ with $BF^{\rm eff}_{ZZ} \sim 0.42$, $4j$ final states having too large a QCD background and mass reconstruction of the real W or Z being impossible in the $2\ell 2\nu$ or 4ν final states, respectively. (Here, we consider only $\ell = e$ or μ.) In our analysis, we assume an overall efficiency of 50% for isolating these channels. For the $ZZ^\star$, a cut requiring that $M^\star$ (the invariant mass of the virtual $Z^\star$) be greater than a given value $M^{\star\,\rm min}$ is imposed. Full details regarding our procedures in the $WW^{(\star)}$ and $ZZ^{(\star)}$ channels are presented in sec. 2.12.2.

The h_{SM} signal and background cross sections, $\epsilon\overline{\sigma}BF(X)$, for $X = b\overline{b}$, and the above $WW^{(\star)}$ and $ZZ^{(\star)}$ final states are presented in Fig. 2.3.2 (including a channel-isolation efficiency of $\epsilon = 0.5$) as a function of $m_{h_{SM}}$ for SM Higgs s-channel production with resolution $R = 0.01\%$ and $R = 0.06\%$. For both resolutions, we also plot the luminosity required for a $S/\sqrt{B} = 5\sigma$ signal in the $b\overline{b}$, $WW^{(\star)}$ and $ZZ^{(\star)}$ channels. In the case of the $WW^{(\star)}$ final state, we give event rates only for the mixed leptonic/hadronic final state modes; in the case of the $ZZ^{(\star)}$ final state we include the mixed hadronic/leptonic and (visible) purely leptonic final state modes listed earlier.

From Fig. 2.3.2 we see that:

- $R = 0.01\%$, $L = 0.1$ fb^{-1} would yield a detectable s-channel Higgs signal for all $m_{h_{SM}}$ values between the current LEP I limit of 63 GeV and $2m_W$ except in the region of the Z peak; a luminosity $L \sim 1$ fb^{-1} at $\sqrt{s} = m_{h_{SM}}$ is needed for $m_{h_{SM}} \sim m_Z$.
- For $R = 0.06\%$, 5σ signals typically require about 20–30 times the luminosity needed for $R = 0.01\%$; $L = 30$ fb^{-1} would be required for a 5σ signal if $m_{h_{SM}} \sim m_Z$.

This argues for a $\mu^+\mu^-$ collider design with R near the 0.01% level. A search for the h_{SM} (or any Higgs with width smaller than the achievable resolution) by scanning would be most efficient for the smallest possible R. For a specific illustration, let us consider $m_{h_{SM}} \sim 110$ GeV and assume that just $L = 1$ fb^{-1} has been accumulated in the Zh_{SM} mode

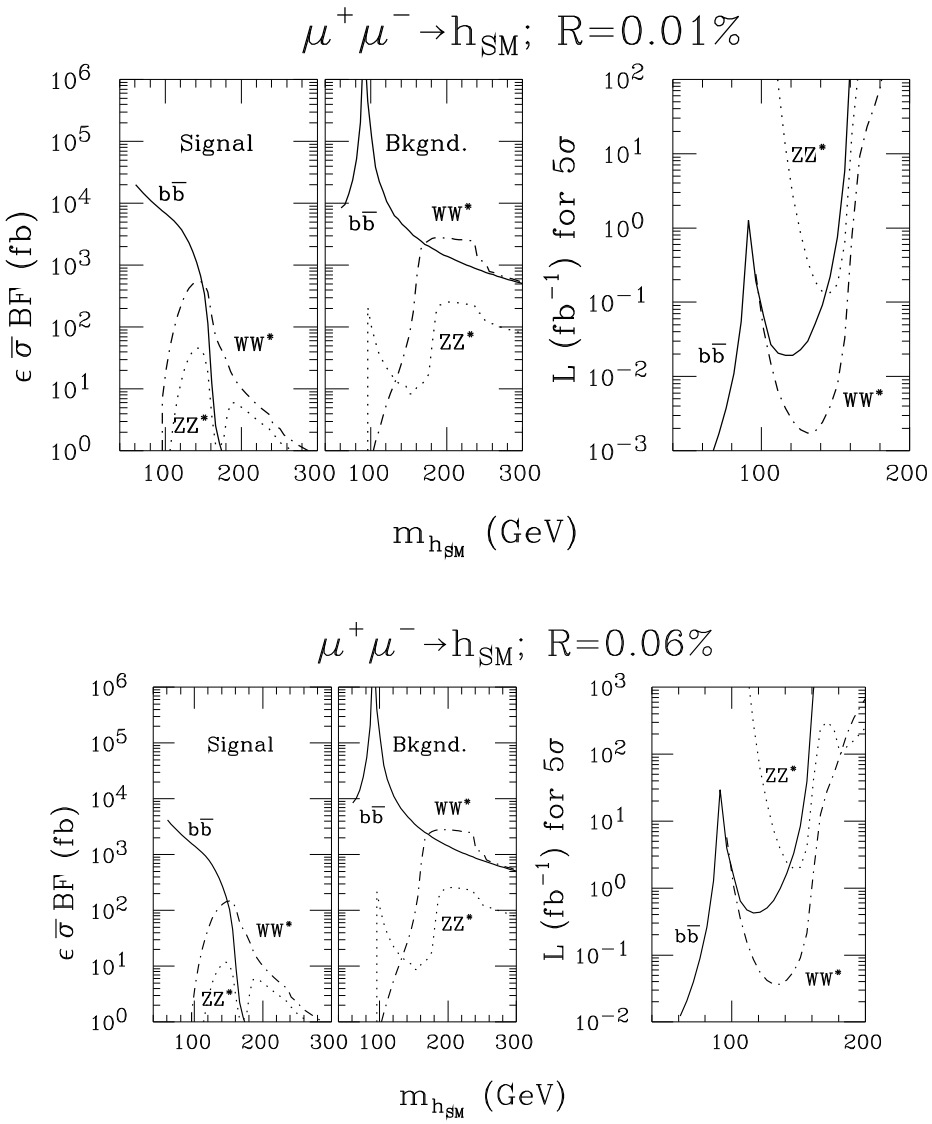

Figure 2.21: The (a) h_{SM} signal and (b) background cross sections, $\epsilon\bar{\sigma}BF(X)$, for $X = b\bar{b}$, and useful (reconstructable, non-$4j$) $WW^{(\star)}$ and $ZZ^{(\star)}$ final states (including a channel-isolation efficiency of $\epsilon = 0.5$) versus $m_{h_{SM}}$ for SM Higgs s-channel production. Also shown: (c) the corresponding luminosity required for a $S/\sqrt{B} = 5$ standard deviations signal in each of the three channels. Results for $R = 0.01\%$ and $R = 0.06\%$ are given.

(at either an e^+e^- collider or at the $\mu^+\mu^-$ collider itself). Fig. 2.1 shows that the error in the determination of $m_{h_{SM}}$ will be of order ± 0.8 GeV (assuming an SLD-type detector). How much luminosity will be required to observe the h_{SM} in the s-channel by zeroing in on $m_{h_{SM}}$ within the rms resolution $\sigma_{\sqrt{s}}$? The number of scan points required to cover the 1.6 GeV mass zone at intervals of $\sigma_{\sqrt{s}}$, the luminosity required to observe (or exclude) the Higgs at each point, and the total luminosity required to zero-in on the Higgs using the scan is given in Eq. (2.63), for resolutions of $R = 0.01\%$ and 0.06%.

R	$\sigma_{\sqrt{s}}$	#points	L/point	$L_{\rm tot}$
0.01%	7 MeV	230	0.01 fb^{-1}	2.3 fb^{-1}
0.06%	45 MeV	34	0.3 fb^{-1}	10.2 fb^{-1}

(2.63)

More generally, the L required at each scan point decreases as (roughly) $R^{1.7}$, whereas the number of scan points only grows like $1/R$, implying that the total L required for the scan decreases as $\sim R^{0.7}$. Thus, the $\mu^+\mu^-$ collider should be constructed with the smallest possible R value. (Note that if the Higgs resonance is broad, using small R, although not necessary, is not harmful since the data from a fine scan can be rebinned to test for its presence.) In the case of a narrow Higgs, a by-product of the above zeroing-in scan will be to ascertain if the Higgs width is in the $\lesssim \sigma_{\sqrt{s}}$ range. However, the large number of $\sqrt{s}$ settings required when conducting a scan with small R implies that it must be possible to quickly and precisely adjust the energy of the $\mu^+\mu^-$ collider. For example, if the machine can deliver 50 fb^{-1} per year and $R = 0.01\%$, so that only $L \sim 0.01$ fb^{-1} should be devoted to each point, we must be able to step the machine energy in units of ~ 7 MeV once every hour or so.

Let us compare the above procedure, where the Zh mode at low luminosity is used to find the SM-like h and then s-channel collisions are used to zero-in on m_h, to the possibility of searching directly for the h by s-channel scanning without the benefit of Zh data. The latter would be a possible alternative if the $\mu^+\mu^-$ collider were to be built before the light Higgs boson is observed at either the LHC or an e^+e^- collider. The question is whether it is most useful to employ the Zh mode or direct s-channel production for initial discovery. We shall suppose that precision radiative corrections pin down the mass of the SM-like Higgs boson to a 20 GeV interval, although this may be way too optimistic. Let us again focus on $m_h = 110$ GeV. The number of scan points required to cover the 20 GeV mass zone at intervals of $\sigma_{\sqrt{s}}$, the luminosity required to observe (or exclude) the Higgs at each point, and

the total luminosity required to zero-in on the Higgs using the scan is given in Eq. (2.64), for resolutions of $R = 0.01\%$ and 0.06%.

R	$\sigma_{\sqrt{s}}$	#points	L/point	$L_{\rm tot}$
0.01%	7 MeV	2857	0.01 fb^{-1}	29 fb^{-1}
0.06%	45 MeV	426	0.3 fb^{-1}	128 fb^{-1}

(2.64)

Thus, much greater luminosity would be required (not to mention the much greater demands upon the machine for performing efficiently such a broad scan) than if the Zh mode is employed for the initial h discovery. Note that it is not useful to expend more than $L \sim 1$ fb^{-1} in the Zh mode simply to pin down the mass; however, precision studies with $L = 50$ fb^{-1} in this mode would be useful for determining $\sigma(Zh) \times BF(h \to X)$ for various different final states, X [41].

For $m_{h_{SM}}$ above $2m_W$, $\Gamma^{\rm tot}_{h_{SM}}$ rises dramatically, $BF(h_{SM} \to \mu^+\mu^-)$ falls rapidly and, thus [see Eq. (2.59) and Fig. 2.3.2], $\overline{\sigma}_h$ declines precipitously. Even after combining all channels, the luminosity requirements in the double-on-shell WW and ZZ final states are such that Higgs detection in s-channel production will be difficult. How severe a drawback is this? One of the unique and most important features of s-channel Higgs production is the ability to scan with sufficient statistics to determine the width of a narrow Higgs boson. In the case of the h_{SM}, only below WW threshold is the Higgs so narrow that this is the only possible measurement technique. The h_{SM} can be detected straightforwardly in the standard Zh_{SM} mode and, at the super-LC detector, its width can be measured down to 0.2 GeV via the recoil mass spectrum in Zh_{SM} events with $Z \to \ell^+\ell^-$. Since $\Gamma^{\rm tot}_{h_{SM}} \gtrsim 0.2$ GeV for $m_{h_{SM}} \gtrsim 2m_W$, this Zh_{SM} technique becomes viable just as s-channel detection becomes difficult. Without the super-LC detector there could, however, be a gap between the $m_{h_{SM}} \lesssim 2m_W$ region where s-channel measurement of $\Gamma^{\rm tot}_{h_{SM}}$ will be possible at a muon collider and the region $m_{h_{SM}} \gtrsim 200$ GeV where $\Gamma^{\rm tot}_{h_{SM}}$ becomes comparable to the event by event mass resolution of ~ 4 GeV (see earlier discussion and Fig. 2.3) and would become measurable at a linear e^+e^- collider. The high resolution for lepton momenta of the super-LC detector could thus prove critical in avoiding a gap in the region between about 150 GeV and 200 GeV where $\Gamma^{\rm tot}_{h_{SM}}$ measurement might not be possible using either s-channel scanning or the Zh_{SM} mode.

The most important conclusions of this subsection are two:

(1) Excellent beam energy resolution is absolutely critical to guaranteeing success in detecting a SM-like h in $\mu^+\mu^- \to h$ s-channel collisions and to our ability to perform

detailed studies once the Higgs boson mass is known. Every effort should therefore be made to achieve excellent resolution. (It is only if $m_h > 2m_W$ where the SM-like Higgs boson begins to become broad that the advantage of having small R declines. But, for such masses s-channel discovery of the SM Higgs will be very difficult in any case, as we have discussed.)

(2) The scanning required when R is small implies that the machine design must be such that $\sqrt{s}$ can be *quickly* reset with a precision that is a small fraction of $\sigma_{\sqrt{s}}$.

Precision Measurements: m_h and $\Gamma_h^{\rm tot}$

Once the machine is set to the central value of $\sqrt{s} = m_h$, one can proceed to precisely measure the mass m_h and the total width $\Gamma_h^{\rm tot}$. A precision determination of the total width $\Gamma_h^{\rm tot}$ is of particular interest to differentiate between the h_{SM} and the h^0 of the MSSM. Knowledge of the total width will also allow extraction of the partial width (and associated Higgs couplings) for any channel in which the Higgs can be observed.

A precise measurement of the Higgs mass is possible via s-channel collisions. We initially focus our discussion on $m_{h_{SM}} \lesssim 2m_W$, for which $\Gamma_{h_{SM}}^{\rm tot}$ is quite likely to be smaller, perhaps much smaller, than the rms $\sqrt{s}$ resolution, $\sigma_{\sqrt{s}}$. Despite this, a highly accurate determination of $m_{h_{SM}}$ is still possible via a straightforward scan in the vicinity of $\sqrt{s} = m_{h_{SM}}$. In Fig. 2.3.2 we illustrate sample data points (statistically fluctuated) in the case of $m_{h_{SM}} = 110$ GeV, assuming $L = 0.5$ fb^{-1} is accumulated at each $\sqrt{s}$ setting. A resolution of $R = 0.01\%$ is assumed. The solid curve is the theoretical prediction. A visual inspection reveals that $m_{h_{SM}}$ can be pinned down to within about 4 MeV using seven scan points centered around $\sqrt{s} = m_{h_{SM}}$ (involving a combined luminosity of 3.5 fb^{-1}). Using somewhat more sophisticated techniques, to be described shortly, we will find that with this same total luminosity we can do better. These latter techniques are those needed for a direct measurement of the total Higgs width $\Gamma_{h_{SM}}^{\rm tot}$.

If the partial widths for $h_{SM} \to \mu^+\mu^-$ and $h_{SM} \to b\overline{b}$ are regarded as theoretically computable with no systematic uncertainties (not a valid assumption in the case of the MSSM h^0), then determination of $\Gamma_{h_{SM}}^{\rm tot}$ is straightforward based on Eq. (2.57). We have plotted the theoretical predictions for $m_{h_{SM}} = 110$ GeV in Fig. 2.3.2 corresponding to keeping the above partial widths constant while varying only $\Gamma_{h_{SM}}^{\rm tot}$ by $\pm 10\%$. Assuming that the background can be absolutely normalized by a combination of theory and experiment, the height of the

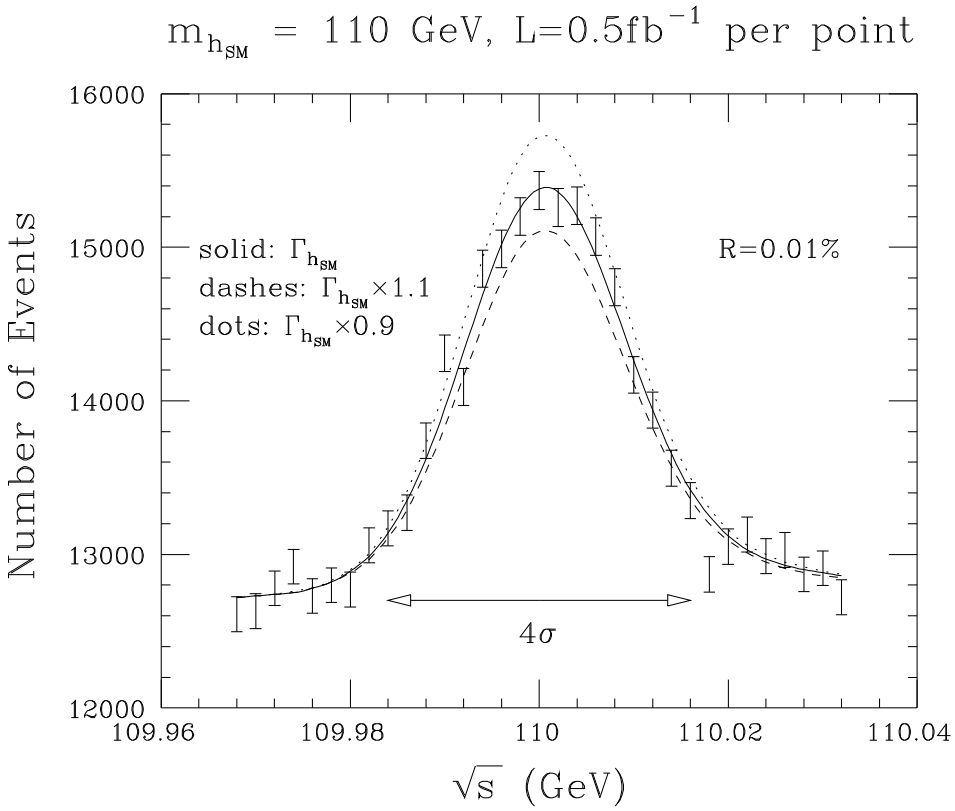

Figure 2.22: Number of events and statistical errors in the $b\bar{b}$ final state as a function of $\sqrt{s}$ in the vicinity of $m_{h_{SM}} = 110$ GeV, assuming $R = 0.01\%$, and $L = 0.5$ fb^{-1} at each data point. The precise theoretical prediction is given by the solid line. The dotted (dashed) curve is the theoretical prediction if $\Gamma^{\rm tot}_{h_{SM}}$ is decreased (increased) by 10%, *keeping the* $\Gamma(h_{SM} \to \mu^+\mu^-)$ *and* $\Gamma(h_{SM} \to b\bar{b})$ *partial widths fixed at the predicted SM value.*

peak is a measure of $\Gamma^{\rm tot}_{h_{SM}}$. The seven central points would determine $\Gamma^{\rm tot}_{h_{SM}}$ to better than 10%.

Since in practice we are not able to accurately pre-determine the partial widths, a *model-independent* technique for discriminating between the total width of the SM h_{SM} and that of some other SM-like h must be devised that does not involve a theoretical computation of the partial widths. Such a determination of the total width requires measurements sensitive to the breadth of the spectrum illustrated in Fig. 2.3.2. We outline below a procedure by which roughly $L \sim 3$ fb^{-1} of total luminosity will allow a $\pm 33\%$ determination of $\Gamma^{\rm tot}_{h_{SM}}$ (for

$m_{h_{SM}} = 110$ GeV) without any assumption regarding the partial widths.

The key observation is that if one adjusts the partial widths so that the normalization of the theoretical curve at $\sqrt{s} = m_{h_{SM}}$ agrees with experiment, then the normalization of the wings of the theoretical curve will be correspondingly increased or decreased in the case that $\Gamma_h^{\rm tot}$ is larger or smaller, respectively. Experimental measurements of sufficient precision both at a central $\sqrt{s}$ value and on the wings would thus allow a direct measurement of $\Gamma_{h_{SM}}^{\rm tot}$ via the ratio of the central peak cross section to the cross sections on the wings (the partial widths cancel out in the ratio). With this in mind, we define the quantity

$$d \equiv |\sqrt{s} - m_{h_{SM}}|/\sigma_{\sqrt{s}} \tag{2.65}$$

and propose the following procedure:

(1) Perform a rough scan to determine $m_{h_{SM}}$ to a precision $\sigma_{\sqrt{s}} d$, with $d \lesssim 0.3$; d will not be known ahead of time, but the value of d, and hence of $m_{h_{SM}}$ will be determined by the procedure.

(2) Then perform three measurements. At $\sqrt{s}_1 = m_{h_{SM}} + \sigma_{\sqrt{s}} d$ we employ a luminosity of L_1 and measure the total rate $N_1 = S_1 + B_1$. Then perform two additional measurements at

$$\sqrt{s}_2 = \sqrt{s}_1 - n_{\sigma_{\sqrt{s}}} \sigma_{\sqrt{s}} \tag{2.66}$$

and one at

$$\sqrt{s}_3 = \sqrt{s}_1 + n_{\sigma_{\sqrt{s}}} \sigma_{\sqrt{s}} \tag{2.67}$$

yielding $N_2 = S_2 + B_2$ and $N_3 = S_3 + B_3$ events, respectively, employing luminosities of $L_2 = \rho_2 L_1$ and $L_3 = \rho_3 L_1$. We find that $n_{\sigma_{\sqrt{s}}} \sim 2$ and $\rho_2 = \rho_3 \sim 2.5$ are optimal for maximizing sensitivity and minimizing the error in determining d (*i.e.* $m_{h_{SM}}$) and $\Gamma_{h_{SM}}^{\rm tot}$.

(3) To determine $m_{h_{SM}}$ and $\Gamma_{h_{SM}}^{\rm tot}$ consider the ratios

$$\begin{aligned} r_2 &\equiv (S_2/\rho_2)/S_1 \quad = (S_2/L_2)/(S_1/L_1) \\ r_3 &\equiv (S_3/\rho_3)/S_1 \quad = (S_3/L_3)/(S_1/L_1)\,. \end{aligned} \tag{2.68}$$

The ratios r_2 and r_3 are governed by d and $\Gamma_{h_{SM}}^{\rm tot}$. Conversely, we have implicitly $d = d(r_2, r_3)$ and $\Gamma_{h_{SM}}^{\rm tot} = \Gamma_{h_{SM}}^{\rm tot}(r_2, r_3)$. Determining the statistical errors $\Delta m_{h_{SM}}$ and

$\Delta\Gamma^{\rm tot}_{h_{SM}}$ is then simply a matter of computing the partial derivatives of d and $\Gamma^{\rm tot}_{h_{SM}}$ with respect to the $r_{2,3}$ (we do this numerically) and using errors on the ratios $r_{2,3}$ implied by statistics. The procedure is detailed in sec. 2.12.3, as is the cross check on its accuracy that we have used.

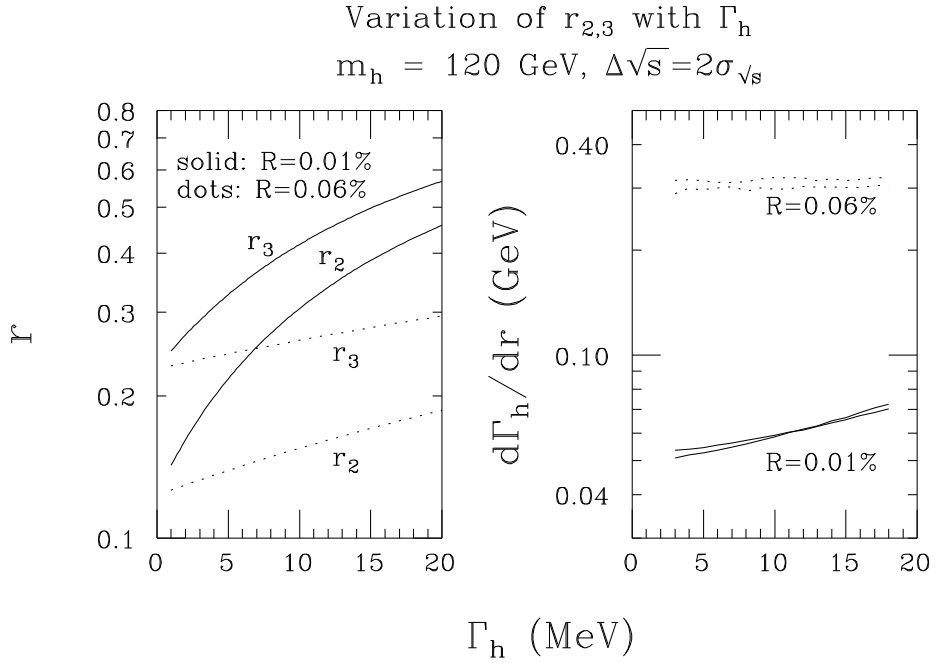

Figure 2.23: We plot r_2 and r_3 as a function of Higgs width, $\Gamma^{\rm tot}_h$, for resolutions of $R = 0.01\%$ and $R = 0.06\%$, assuming that $\sqrt{s} = m_h = 120$ GeV. Also shown are the derivatives $d\Gamma^{\rm tot}_h/dr$ as a function of $\Gamma^{\rm tot}_h$. We have taken $n_{\sigma_{\sqrt{s}}} = 2$ corresponding to a shift in $\sqrt{s}$ of $\mp 2\sigma_{\sqrt{s}}$ in computing r_2 and r_3, respectively.

The utility of the ratios r_2 and r_3 is basically governed by how rapidly they vary as d and $\Gamma^{\rm tot}_h$ are varied in the ranges of interest. Since we are most interested in $\Gamma^{\rm tot}_h$ here, we illustrate the sensitivity of $r_{2,3}$ to $\Gamma^{\rm tot}_h$ in Fig. 2.3.2 taking $\sqrt{s} = m_h = 120$ GeV. For this figure we employ $n_{\sigma_{\sqrt{s}}} = 2$ for computing r_2 and r_3, respectively. Results are shown for resolutions $R = 0.01\%$ and $R = 0.06\%$. Because of the bremsstrahlung tail, r_2 is substantially larger than r_3. Nonetheless, both r_2 and r_3 show rapid variation as $\Gamma^{\rm tot}_h$ varies in the vicinity of $\Gamma^{\rm tot}_{h_{SM}}$ in the case of $R = 0.01\%$, but much less variation if $R = 0.06\%$. The error in the determination of $\Gamma^{\rm tot}_h$ is basically determined by $d\Gamma^{\rm tot}_h/dr_{2,3}$. Figure 2.3.2 shows that these

derivatives are almost the same and quite small for $R = 0.01\%$. The much larger values of these derivatives for $R = 0.06\%$ imply that determining $\Gamma_h^{\rm tot}$ accurately would be very difficult in this case.

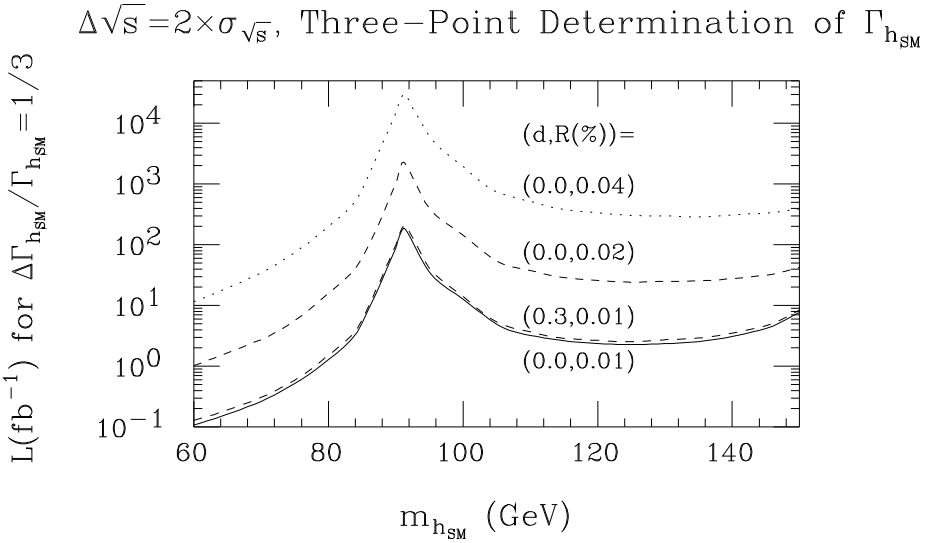

Figure 2.24: Luminosity required for a $\Delta\Gamma^{\rm tot}_{h_{SM}}/\Gamma^{\rm tot}_{h_{SM}} = 1/3$ measurement in the $b\overline{b}$ final state using the three point technique described in the text. Results for resolutions of $R = 0.01\%$, 0.02% and 0.04% are shown for $d = 0$, where $d = |\sqrt{s} - m_{h_{SM}}|/\sigma_{\sqrt{s}}$. The result for $d = 0.3$ and $R = 0.01\%$ is also shown.

In Fig. 2.3.2, we plot the total luminosity $L = L_1 + L_2 + L_3 = 6L_1$ required to achieve $\Delta\Gamma^{\rm tot}_{h_{SM}}/\Gamma^{\rm tot}_{h_{SM}} = 1/3$ in the $b\overline{b}$ final state as a function of $m_{h_{SM}}$ for several beam resolutions. (The error scales statistically; *e.g.* to achieve a 10% measurement would require $(10/3)^2$ as much luminosity.) We also illustrate the fact that the total luminosity required is rather insensitive to the initial choice of d for $d \lesssim 0.3$; $d = 0.3$ results in no more than a 20% increase in the luminosity needed relative to $d = 0$.

In Fig. 2.3.2, we plot the 1σ error $\Delta m_{h_{SM}}$ that results using our three-point technique after accumulating the luminosity required for a $\Delta\Gamma^{\rm tot}_{h_{SM}}/\Gamma^{\rm tot}_{h_{SM}} = 1/3$ measurement in the $b\overline{b}$ final state. The specific result plotted is for $R = 0.01\%$ and $d = 0$, but is essentially independent of R and d given the stated luminosity. Also shown, for comparison, is $\Gamma^{\rm tot}_{h_{SM}}$ itself. We see that $\Delta m_{h_{SM}}$ is of order 1.5–2 times $\Gamma^{\rm tot}_{h_{SM}}/10$, *i.e.* a fraction of an MeV for $m_{h_{SM}} \lesssim 130$ GeV. (Again, $\Delta m_{h_{SM}}$ scales as $1/\sqrt{L}$.)

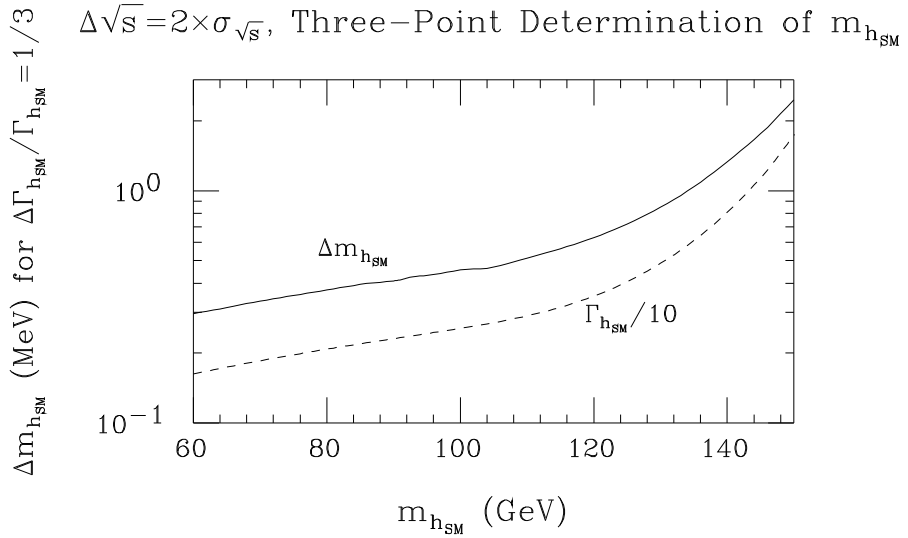

Figure 2.25: We plot the 1σ error, $\Delta m_{h_{SM}}$, in the determination of $m_{h_{SM}}$ using the three point technique described in the text with $R = 0.01\%$ and $d = 0$. The error given is that achieved for the luminosity that allows a $\Delta\Gamma^{\rm tot}_{h_{SM}}/\Gamma^{\rm tot}_{h_{SM}} = 1/3$ measurement in the $b\bar{b}$ final state. For such luminosity, $\Delta m_{h_{SM}}$ is essentially independent of R and d. Also shown, for comparison, is $\Gamma^{\rm tot}_{h_{SM}}/10$.

It should be stressed that the ability to precisely set the energy of the machine when the three measurements are taken is crucial for the success of the three-point technique. A misdetermination of the spacing of the measurements in Eqs. (2.66) and (2.67) by just 3% (*i.e.* $\sqrt{s}$ uncertainty of order 0.25 MeV for any one setting near $m_{h_{SM}} \sim 120$ GeV) would result in an error in $\Gamma^{\rm tot}_{h_{SM}}$ of 30%. For a measurement of $\Gamma^{\rm tot}_{h_{SM}}$ at the 10% level the $\sqrt{s}$ settings must be precise at a level of better than one part in 10^6. This is possible [61] provided the beam can be partially polarized so that the precession of the spin of the muon as it circulates in the final storage ring can be measured. From the precession and the rotation rate the energy can be determined. The ability to perform this critical measurement needed for the determination of the total width of a narrow Higgs must be incorporated in the machine design.

Precision Measurements: $\Gamma(h \to \mu^+\mu^-) \times BF(h \to X)$

Assuming that the Higgs width is much narrower than the rms uncertainty in $\sqrt{s}$,

Eq. (2.57) shows that the event rate in a given channel measures $G(X) = \Gamma(h \to \mu^+\mu^-) \times BF(h \to X)$. If the background can be determined precisely (either by off-resonance measurements or theory plus Monte Carlo calculation), the error in the determination of this product is $\sqrt{N}/S$, where $N = S + B$ and S, B are the number of signal, background events, respectively. The results for $\sqrt{N}/S$ in the case of $P = 0$ and $L = 50$ fb^{-1} in the $b\bar{b}$, $WW^{(\star)}$ and $ZZ^{(\star)}$ modes are shown in Fig. 2.3.2 for $h = h_{SM}$. For each final state, the efficiencies and procedures employed are precisely those discussed with regard to Fig. 2.3.2. Good accuracy in this measurement is possible for $m_{h_{SM}} \lesssim 2m_W$ even if $m_{h_{SM}}$ is near m_Z.

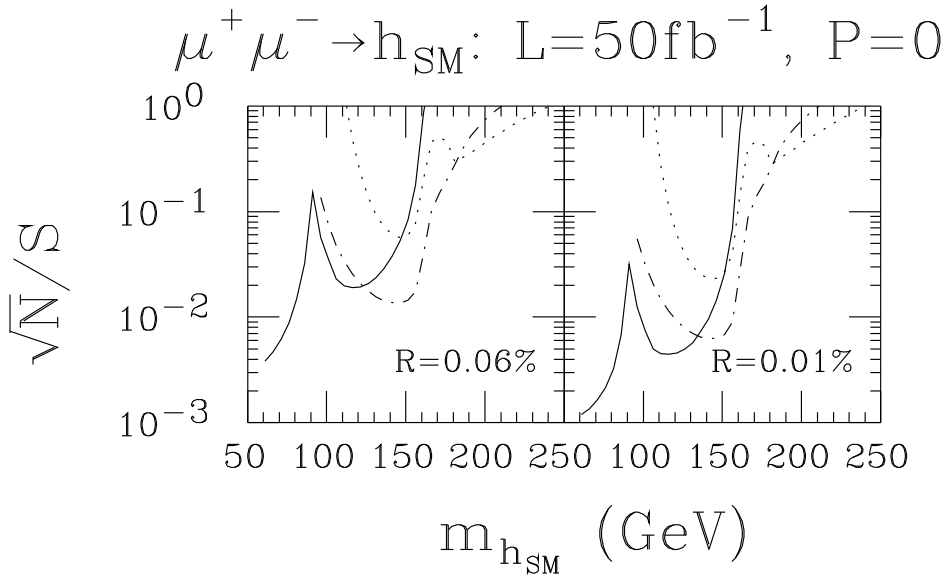

Figure 2.26: Fractional error in determining $\Gamma(h_{SM} \to \mu\mu) \times BF(h_{SM} \to X)$ for $X = b\bar{b}$ (solid), $WW^{(\star)}$ (dotdash) and $ZZ^{(\star)}$ (dots), assuming $L = 50$ fb^{-1}. (See text for $WW^\star$ and $ZZ^\star$ final states employed.)

h^0 or h_{SM}?

We now discuss the possibility of distinguishing the MSSM h^0 from the SM h_{SM} using precision measurements of $\Gamma_h^{\rm tot}$ and $G(b\bar{b}) \equiv \Gamma(h \to \mu\mu) \times BF(h \to b\bar{b})$. The accuracy to which $\Gamma_h^{\rm tot}$ and $G(b\bar{b})$ need to be determined can be gauged by the ratio of the h^0 predictions to the h_{SM} predictions for these quantities at $m_{h^0} = m_{h_{SM}}$. Contours for various fixed values of these ratios are plotted in Fig. 2.3.2 in the standard $(m_{A^0}, \tan\beta)$ parameter space [68]. In computing results for $\Gamma_h^{\rm tot}$ and $G(b\bar{b})$ for h^0 we have taken $m_{\tilde{t}} = 1$ TeV, $m_t = 175$ GeV,

and included two-loop/RGE-improved radiative corrections to the Higgs masses, mixing angles and self-couplings, neglecting squark mixing. The ratios for both $\Gamma_h^{\rm tot}$ and $G(b\overline{b})$ are substantially bigger than 1, even out to fairly large m_{A^0} values. This is because the h^0 retains somewhat enhanced $b\overline{b}$, $\tau^+\tau^-$ and $\mu^+\mu^-$ couplings until quite large m_{A^0} values. Two facts are of particular importance:

- $\Gamma_{h^0}^{\rm tot}$ is enhanced relative to $\Gamma_{h_{SM}}^{\rm tot}$ by virtue of the enhanced partial widths into its dominant decay channels, $b\overline{b}$ and $\tau^+\tau^-$.
- The enhancement in $G(b\overline{b})$ derives mainly from $\Gamma(h \to \mu\mu)$, as can be deduced by comparing Fig. 2.3.2(b) and 2.3.2(c).

This latter point is also apparent in Fig. hltohsmratios(d), where we observe that the MSSM to SM ratio of $BF(h \to b\overline{b})$'s is very close to 1 along the 1.1 contour of the MSSM/SM $G(b\overline{b})$. This is because the enhanced $b\overline{b}$ partial width in the numerator of $BF(h \to b\overline{b})$ is largely compensated by the extra contribution to the total width from this same channel. Thus, in comparing the MSSM to the SM, a measurement of $G(b\overline{b})$ is most sensitive to deviations of $\Gamma(h \to \mu\mu)$ from SM expectations. As seen numerically in Fig. 2.3.2(e), $\Gamma(h \to \mu\mu)$ grows rapidly at lower m_{A^0} or higher $\tan\beta$. For small squark mixing, a deviation in $G(b\overline{b})$ from the SM value implies almost the same percentage deviation of $\Gamma(h \to \mu\mu)$ from its SM value. However, when squark mixing is large, this equality breaks down. In general, one must separately determine $\Gamma(h \to \mu\mu)$ in order to probe MSSM vs. SM differences. The procedure for this will be discussed shortly.

The measured value of m_h provides a further constraint. For example, suppose that a Higgs boson is observed with $m_h = 110$ GeV. A fixed value for m_h implies that the parameters which determine the radiative corrections to m_{h^0} must change as m_{A^0} and $\tan\beta$ are varied. For example, if squark mixing is neglected, then the appropriate value of $m_{\tilde{t}}$ is a function of m_{A^0} and $\tan\beta$. Given the assumption of no squark mixing and the fixed value of $m_h = 110$ GeV, results for the same ratios as plotted in Fig. 2.3.2 are given in Fig. 2.3.2. Also shown are contours of fixed $\Gamma(h^0 \to \mu\mu)$ and contours of fixed $m_{\tilde{t}}$ (as required to achieve $m_{h^0} = 110$ GeV). The vertical nature of the $\mu\mu$ ratio and partial width contours implies that a measurement of any of these quantities could provide a determination of m_{A^0} (but would yield little information about $\tan\beta$).

Contours for other mixing assumptions, can also be plotted. The only contours that remain essentially unaltered as the amount of squark mixing is varied (keeping $m_h = 110$ GeV)

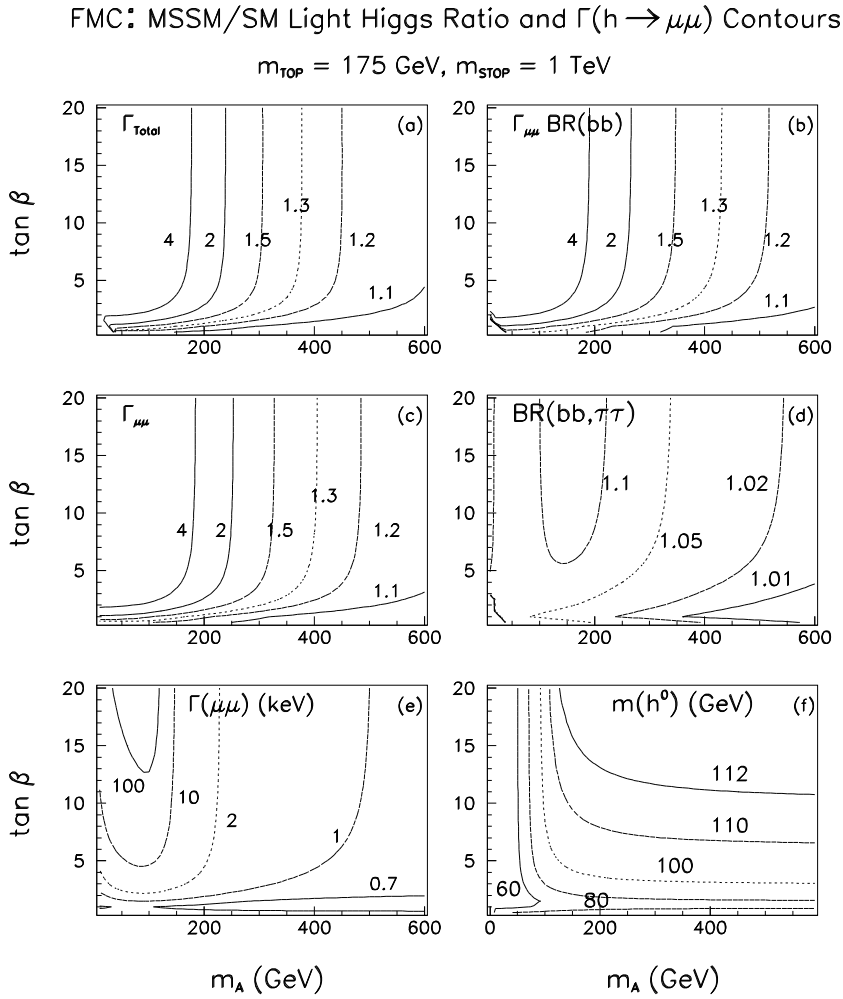

Figure 2.27: Contours of constant MSSM/SM ratios for $\Gamma_h^{\rm tot}$, $\Gamma(h \to \mu\mu) \times BF(h \to b\bar{b})$, $\Gamma(h \to \mu\mu)$ and $BF(h \to b\bar{b}, \tau\tau)$ in $(m_{A^0}, \tan\beta)$ parameter space. We have taken $m_t = 175$ GeV, $m_{\tilde{t}} = 1$ TeV, and included two-loop/RGE-improved radiative corrections, neglecting squark mixing, for Higgs masses, mixing angles and self-couplings. Also shown are contours for fixed values of $\Gamma(h^0 \to \mu\mu)$ using units of keV, and contours of fixed m_{h^0}. This graph was obtained using the programs developed for the work of Ref. [68].

are those for the ratio $\Gamma(h^0 \to \mu\mu)/\Gamma(h_{SM} \to \mu\mu)$ and for the $\Gamma(h^0 \to \mu\mu)$ partial width itself. Once $m_{h^0} \lesssim 100$ GeV, even these contours show substantial variation as a function

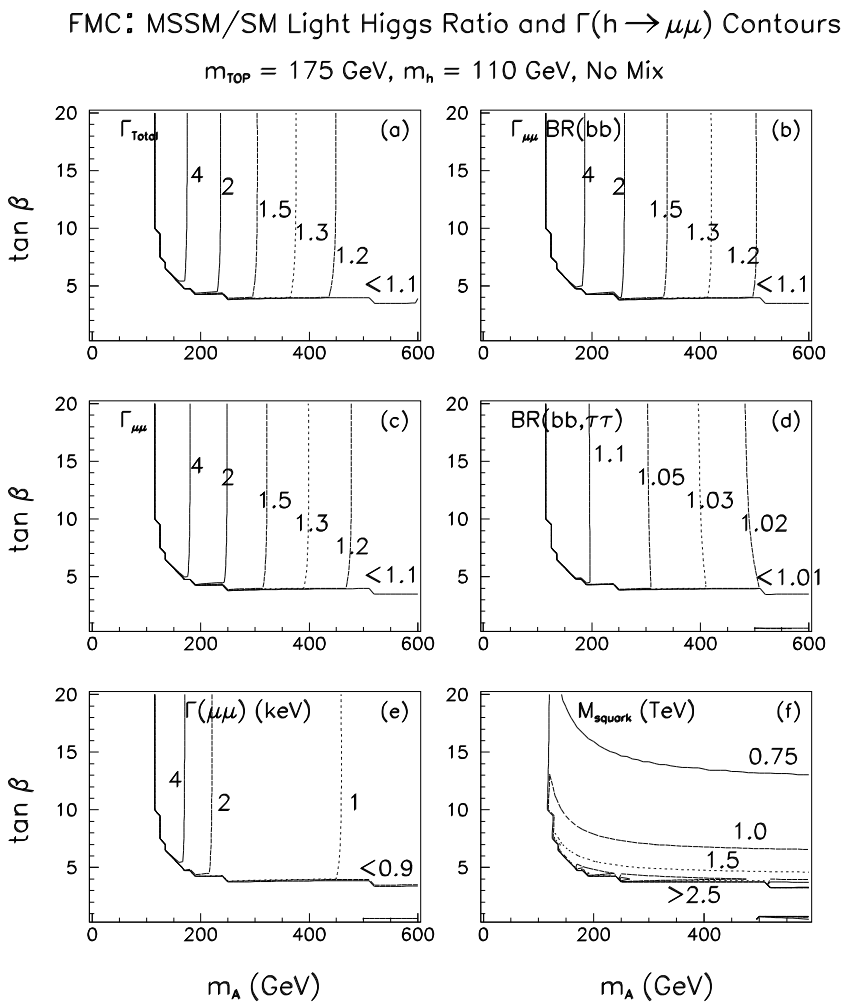

Figure 2.28: Contours of constant MSSM/SM ratios for $\Gamma_h^{\rm tot}$, $\Gamma(h \to \mu\mu) \times BF(h \to b\overline{b})$, $\Gamma(h \to \mu\mu)$ and $BF(h \to b\overline{b}, \tau\tau)$ in $(m_{A^0}, \tan\beta)$ parameter space. We have taken $m_t = 175$ GeV, and we adjust $m_{\tilde{t}}$ so as to keep a fixed value of $m_{h^0} = 110$ GeV after including two-loop/RGE-improved radiative corrections for Higgs masses, mixing angles and self-couplings, neglecting squark mixing. Also shown are contours for fixed values of $\Gamma(h^0 \to \mu\mu)$ in keV units, and contours for fixed values of $m_{\tilde{t}}$ in TeV units. This graph was obtained using the programs developed for the work of Ref. [68].

of the squark mixing parameters. However, it remains true that a determination of the $\mu\mu$ partial width or partial width ratio provides at least a rough determination of m_{A^0}.

In order to assess the observability of the differences between predictions for $\Gamma_h^{\rm tot}$, $G(b\overline{b})$, and $\Gamma(\mu\mu)$ for the h^0 compared to the h_{SM}, we must examine more closely the error in the experimental determination of these quantities, and consider the theoretical uncertainties in our predictions for them.

Interpreting a measurement of $\boldsymbol{\Gamma_h^{\rm tot}}$ Consider first the total width measurement. Here, the experimental error is the key issue. The h^0 may have a mass of order 110 GeV in the large-m_{A^0} region where it is SM-like, provided $\tan\beta$ is not near 1 (see Fig. 2.17). According to Fig. 2.3.2, $L \sim 3$ fb^{-1} is required to measure $\Gamma_h^{\rm tot}$ to $\pm 33\%$, provided $R = 0.01\%$. A $\pm 10\%$ measurement would require $L \sim 33$ fb^{-1} (using $\Delta\Gamma_{h_{SM}}^{\rm tot} \propto 1/\sqrt{L}$). As seen most clearly from Fig. 2.3.2, this accuracy would probe MSSM/SM differences at the 3σ level for $m_{A^0} \lesssim 400$ GeV if squark mixing is small.

Detecting a difference between the h^0 and h_{SM} using $\Gamma_h^{\rm tot}$ could prove either somewhat easier or much more difficult than outlined above, because the $\tan\beta$, $m_{\tilde{t}}$ values and the degree of squark mixing could very well be different from those assumed above. For example, if $m_{h^0} = 110$ GeV, $\tan\beta \gtrsim 5$ and squark mixing is large, m_{A^0} values above 400 GeV would be probed at the 3σ level by a 10% measurement of $\Gamma_h^{\rm tot}$. On the other hand, the radiative corrections could yield a smaller m_{h^0} value, *e.g.* $m_{h^0} \lesssim 100$ GeV is quite likely if $\tan\beta$ is near 1 or $m_{\tilde{t}}$ is small. In this range, predicted deviations from predictions for the h_{SM} with $m_{h_{SM}} = m_{h^0}$ are not dissimilar to those obtained discussed above. However, a luminosity $L \gtrsim 100$ fb^{-1} would be required for a $\pm 10\%$ measurement of $\Gamma_h^{\rm tot}$ for 80 GeV $\lesssim m_{h^0} \lesssim$ 100 GeV.

Other theoretical uncertainties include: i) extra contributions to $\Gamma_{h^0}^{\rm tot}$ in the MSSM model from SUSY decay modes; ii) the gg decay width of the h^0 could be altered by the presence of light colored sparticles; iii) the h_{SM} could have enhanced gg decay width due to heavy colored fermions (*e.g.* from a fourth family).

Nonetheless, a $\mu^+\mu^-$ collider determination of $\Gamma_h^{\rm tot}$ will be a crucial component in a model-independent determination of all the properties of a SM-like h, and could provide the first circumstantial evidence for a MSSM Higgs sector prior to direct discovery of the non-SM-like MSSM Higgs bosons.

Interpreting a measurement of $\Gamma(h \to \mu\mu) \times BF(h \to b\bar{b})$ How does the h^0–h_{SM} discrimination power of the total width measurement compare to that associated with a measurement of $G(b\bar{b}) \equiv \Gamma(h \to \mu\mu) \times BF(h \to b\bar{b})$? Figure 2.3.2 shows that $\pm 0.4\%$ accuracy in the determination of $G(b\bar{b})$ is possible for $L = 50$ fb^{-1} and $R = 0.01\%$ in the $m_{h^0} \sim 110$–115 GeV mass range predicted for $m_{A^0} \gtrsim 2m_Z$ and larger $\tan\beta$ values, assuming $m_{\widetilde{t}} \gtrsim 0.75$ TeV and no squark mixing.

An uncertainty in $BF(h \to b\bar{b})$ arises from $\Gamma(h \to b\bar{b}) \propto m_b^2$ due to the uncertainty in m_b. Writing $BF(h \to b\bar{b}) = \Gamma_b/(\Gamma_b + \Gamma_{\rm non-}{}_b)$, the error in $BF(h \to b\bar{b})$ is given by

$$\Delta BF(h \to b\bar{b}) = \frac{2\Delta m_b}{m_b} BF(h \to b\bar{b}) BF(h \to \text{non} - b) \; . \tag{2.69}$$

Since $BF(h \to$ non-$b)$ is not very large (0.1 to 0.2 in the mass range in question for either the h_{SM} or h^0), even a 10% uncertainty in m_b only leads to $\Delta BF(h \to b\bar{b}) \lesssim 0.05$. Eventually m_b may be known to the 5% level, leading to $\lesssim 2.5\%$ uncertainty in the branching fraction. Comparison to Fig. 2.3.2 shows that a 2.5% uncertainty from m_b, in combination with a still smaller statistical error, has the potential for h^0–h_{SM} discrimination at the 3σ statistical level out to large m_{A^0} for $m_h = 110$ GeV, if squark mixing is small. However, as squark mixing is increased, it turns out that the maximum m_{A^0} that can potentially be probed decreases if $\tan\beta$ is large.

$BF(h \to b\bar{b})$ is also subject to an uncertainty from the total width. For example, in the MSSM $BF(h^0 \to b\bar{b})$ could be smaller than the SM prediction if $\Gamma^{\rm tot}_{h^0}$ is enhanced due to channels other than the $b\bar{b}$ channel itself (*e.g.* by supersymmetric decay modes, or a larger than expected gg decay width due to loops containing supersymmetric colored sparticle or heavy colored fermions). Thus, a measurement of $G(b\bar{b})$ alone is not subject to unambiguous interpretation.

We note that the $L = 50$ fb^{-1} $\mu^+\mu^-$ collider measurement of $G(b\bar{b})$ is substantially more powerful than a $L = 50$ fb^{-1} precision measurement of $\sigma(e^+e^- \to Zh) \times BF(h \to b\bar{b})$ at an e^+e^- collider [41]. The ratio of the h^0 prediction to the h_{SM} prediction is essentially equal to the h^0 to h_{SM} $BF(h \to b\bar{b})$ ratio and is predicted to be within 1% (2%) of unity along a contour very close to the 1.1 (1.2) contour of $\Gamma(h \to \mu^+\mu^-)BF(h \to b\bar{b})$; see panels (b) and (d) in Figs. 2.3.2 and 2.3.2. Since at best 5% deviations in $G(b\bar{b})$ and $BF(h \to b\bar{b})$ can be detected at the 1σ level (after combining a possibly small statistical error with a large theoretical error), we see from the 1.05 ratio contour for $BF(h \to b\bar{b})$ in Figs. 2.3.2 and 2.3.2 that the $\sigma(Zh)BF(h \to b\bar{b})$ and $BF(h \to b\bar{b})$ ratios, that can be determined experimentally

at an e^+e^- collider, only probe as far as $m_{A^0} \lesssim 250$–300 GeV at the 1σ significance level, with even less reach at the 3σ level.

We must again caution that if m_h is close to m_Z, there could be substantially worse experimental uncertainty in the $G(b\overline{b})$ measurement than taken above. Pre-knowledge of m_h is necessary to determine the level of precision that could be expected for this measurement.

Combining measurements We now discuss how the independent measurements of $\Gamma_h^{\rm tot}$ and $G(b\overline{b})$ can be combined with one another and other experimental inputs to provide a model-independent determination of the properties of the h. We consider three complementary approaches.

(1) A model-independent determination of $\Gamma(h \to \mu\mu)$ can be made by combining the s-channel $\mu^+\mu^-$ collider measurement of $G(b\overline{b})$ with the value of $BF(h \to b\overline{b})$ measured in the Zh mode at an e^+e^- collider or the $\mu^+\mu^-$ collider. With $L = 50$ fb^{-1} of luminosity, $BF(h \to b\overline{b})$ can potentially be measured to $\pm 7\%$ [41]. From our earlier discussion, the error on $G(b\overline{b})$ will be much smaller than this if $m_h \gtrsim 100$ GeV, and $\Gamma(h \to \mu\mu)$ would be determined to roughly ± 8–10%. Figures 2.3.2 and 2.3.2 show that this procedure would probe the h^0 versus h_{SM} differences at the 3σ level out to $m_{A^0} \sim 400$ GeV if $\tan\beta$ is not close to 1 (see the 1.3 ratio contour in the figures). This is a far superior reach to that possible at the 3σ level at either the LHC, NLC and/or $\gamma\gamma$ collider. Further, we note that the $\mu\mu$ partial width at fixed $m_h \gtrsim 100$ GeV is relatively independent of the squark mixing scenario and provides a rather precise determination of m_{A^0} [41].

(2) A model-independent determination of $\Gamma(h \to b\overline{b})$ is possible by computing $\Gamma_h^{\rm tot} BF(h \to b\overline{b})$ using the value of $\Gamma_h^{\rm tot}$ measured at the $\mu^+\mu^-$ collider and the value of $BF(h \to b\overline{b})$ measured in the Zh mode. Taking 10% accuracy for the former and 7% accuracy for the latter, we see that the error on $\Gamma(h \to b\overline{b})$ would be of order 12%. The ratio contours for $\Gamma(h \to b\overline{b})$ are the same as the ratio contours for $\Gamma(h \to \mu\mu)$. Thus, ignoring systematics, this measurement could also probe out to $m_{A^0} \gtrsim 400$ GeV at the 3σ level if $m_h \sim 110$ GeV, see Fig. 2.3.2. However, the $2\Delta m_b/m_b$ systematic uncertainty in the partial width is also of order 10% for 5% uncertainty in m_b, implying a total statistical plus theoretical error of order 16%. This would restrict 3σ sensitivity to h^0 vs. h_{SM} differences to $m_{A^0} \lesssim 300$ GeV.

(3) A third approach uses only the $\mu^+\mu^-$ collider measurements. We note that

$$W \equiv \Gamma(h \to \mu\mu)\Gamma(h \to b\overline{b}) = [\Gamma_h^{\rm tot}] \times [\Gamma(h \to \mu\mu) BF(h \to b\overline{b})]\,. \tag{2.70}$$

In the MSSM (or any other type-II two-Higgs-doublet model) the $\mu\mu$ and $b\bar{b}$ squared couplings have exactly the same factor, call it f, multiplying the square of the SM coupling strength. Thus,

$$W = \Gamma(h \to \mu\mu)\Gamma(h \to b\bar{b}) \propto f^2 \left(\frac{g}{2m_W}\right)^4 m_\mu^2 m_b^2 \,. \tag{2.71}$$

Following our earlier discussion, in the MSSM f^2 would be $(1.3)^2 \sim 1.7$ along the 1.3 ratio contours for $\Gamma(h \to \mu\mu)$ in Figs. 2.3.2 and 2.3.2. For $m_h \gtrsim 100$ GeV, experimental errors in W of Eq. (2.70) would be dominated by the $\pm 10\%$ error on $\Gamma_h^{\rm tot}$. The dominant systematic error would be that from not knowing the value of m_b: $\Delta W/W = 2\Delta m_b/m_b$. Thus, a combined statistical and theoretical 1σ error for W below 20% is entirely possible for $m_h \gtrsim 100$ GeV, in which case deviations in f^2 from unity can be probed at the 3σ level for m_{A^0} values at least as large as $m_{A^0} \sim 400$ GeV. Since both $\Gamma(h^0 \to \mu\mu)$ and $\Gamma(h^0 \to b\bar{b})$ are relatively independent of the squark mixing scenario for fixed m_{h^0} and fixed m_{A^0}, a fairly reliable value of m_{A^0} would result from the determination of f^2.

By combining the strategies just discussed, one can do even better. Thus, a $\mu^+\mu^-$ collider has great promise for allowing us to measure the crucial $b\bar{b}$ and $\mu^+\mu^-$ couplings of a SM-like h, provided m_h is not within 10 GeV of m_Z (nor $\gtrsim 2m_W$) and that $m_A \lesssim 400$ GeV. In particular, for such masses we can distinguish the h^0 from the h_{SM} in a model-independent fashion out to larger m_{A^0} than at any other accelerator or combination of accelerators.

The $WW^\star$ and $ZZ^\star$ channels Precision measurements of $\Gamma(h \to \mu^+\mu^-)BF(h \to X)$ are also possible for $X = WW^\star$ and, to a lesser extent, $ZZ^\star$, see Fig. 2.3.2. Once again, $\Gamma(h \to \mu^+\mu^-)$ can be determined in a model-independent fashion using $BF(h \to X)$ measured in the Zh mode, and $\Gamma(h \to X)$ can be computed in a model-independent fashion as the product $BF(h \to X)\Gamma_h^{\rm tot}$. We will not go through the error analysis in detail for these cases, but clearly determination of both the WW and ZZ couplings will be possible at a reasonable statistical level. Unfortunately, the h^0WW, h^0ZZ couplings are very close to the SM values for $m_{A^0} \gtrsim 2m_W$ and the expected statistical errors would not allow h^0 vs. h_{SM} discrimination.

2.3.3 Non-SM-like Higgs Bosons in the MSSM

In what follows, we shall demonstrate that it is possible to observe the H^0 and A^0 in s-channel Higgs production for $m_{A^0} \sim m_{H^0} > \sqrt{s}/2$ over much of $(m_{A^0}, \tan\beta)$ parameter

space. It is this fact that again sets the $\mu^+\mu^-$ collider apart from other machines.

1. The LHC can only detect the H^0 and A^0 for masses above 200–250 GeV if $\tan\beta$ is either large or $\lesssim$ 3–5; a wedge of unobservability develops beginning at $m_{A^0} \gtrsim 200$ GeV, covering an increasingly wide range of $\tan\beta$ as m_{A^0} increases [69]. This is illustrated in Fig. 2.3.3 from Ref. [70].

2. At an e^+e^- collider, $Z^\star \to ZA^0, ZH^0$ production will be negligible when $m_{A^0} > 2m_Z$.

3. $e^+e^- \to Z^\star \to A^0H^0$ could easily be kinematically disallowed, especially for e^+e^- machine energies in the $\sqrt{s} \sim 500$ GeV range — GUT scenarios often give $m_{A^0} \sim m_{H^0} \gtrsim 300$ GeV.

4. If an e^+e^- collider is run in the photon-photon collider mode, discovery of the H^0 and A^0 in the $m_{A^0}, m_{H^0} \gtrsim 200$ GeV region via $\gamma\gamma \to A^0, H^0$ requires extremely high luminosity ($\gtrsim 200$ fb^{-1}) [71].

5. s-channel production of the A^0 and H^0 will not be significant in e^+e^- collisions due to the small size of the electron mass.

A $\mu^+\mu^-$ collider can overcome the limitations 3 and 5 of an e^+e^- collider, though not simultaneously. If the $\mu^+\mu^-$ collider is run at energies of $\sqrt{s} = m_{A^0} \sim m_{H^0}$, then we shall find that s-channel production will allow discovery of the A^0 and H^0 if $\tan\beta \gtrsim 3-4$. Here, the kinematical Higgs mass reach is limited only by the maximum $\sqrt{s}$ of the machine. Alternatively, the $\mu^+\mu^-$ collider can be designed to have $\sqrt{s} \sim 4$ TeV in which case $m_{A^0} \sim m_{H^0}$ values up to nearly 2 TeV can be probed via the $Z^\star \to A^0H^0$ process, a mass range that encompasses all natural GUT scenarios. We focus in this report on s-channel production and detection. In our analysis, we will assume that more or less full luminosity can be maintained for all $\sqrt{s}$ values over the mass range of interest (using multiple storage rings, as discussed in the introduction).

MSSM Higgs Bosons in the s-Channel: $\sqrt{s} = m_h$

Here we investigate the potential of a $\mu^+\mu^-$ collider for probing those Higgs bosons whose couplings to ZZ, WW are either suppressed or absent at tree-level — that is the A^0, the H^0 (at larger m_{A^0}), or the h^0 (at small m_{A^0}). The $WW^{(\star)}$ and $ZZ^{(\star)}$ final states in s-channel production are then not relevant. We consider first the $b\bar{b}$ and $t\bar{t}$ decay modes, although

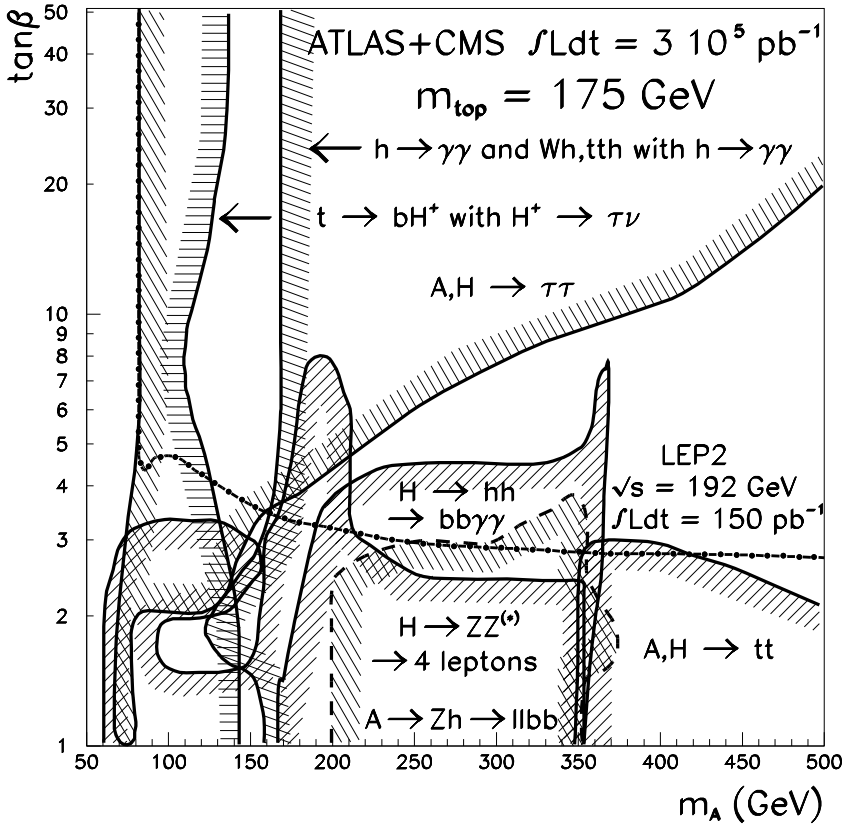

Figure 2.29: MSSM Higgs discovery contours (5σ) in the parameter space of the minimal supersymmetric model for ATLAS+CMS at the LHC: $L =$ 300 fb^{-1} per detector. Figure from Ref. [70]. Two-loop/RGE-improved radiative corrections are included for m_{h^0} and m_{H^0} assuming $m_{\tilde{t}} = 1$ TeV and no squark mixing.

we shall later demonstrate that the relatively background free $H^0 \to h^0 h^0$ or $A^0 A^0 \to b\bar{b}b\bar{b}$, $H^0 \to ZA^0 \to Zb\bar{b}$ and $A^0 \to Zh^0 \to Zb\bar{b}$ modes might also be useful.

Figure 2.3.3 shows the dominant branching fractions to $b\bar{b}$ and $t\bar{t}$ of Higgs bosons of mass $m_{A^0} = 400$ GeV $\approx m_{H^0}$ versus $\tan\beta$, taking $m_t = 170$ GeV. The $b\bar{b}$ decay mode is dominant for $\tan\beta > 5$, which is the region where observable signal rates are most easily obtained. From the figure we see that $BF(H^0, A^0 \to b\bar{b})$ grows rapidly with increasing $\tan\beta$ for $\tan\beta \lesssim 5$, while $BF(H^0, A^0 \to t\bar{t})$ falls slowly.

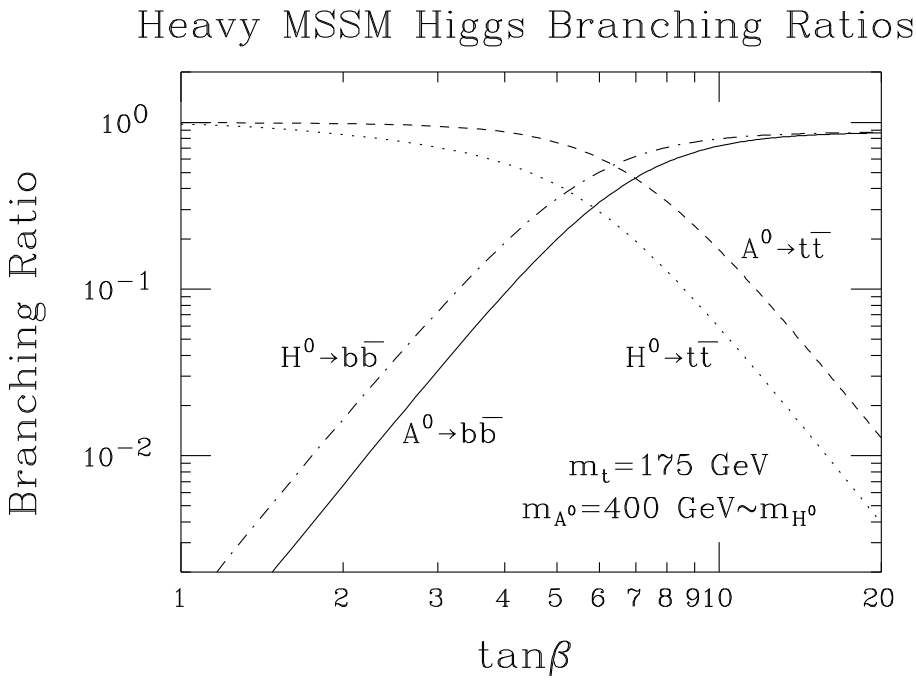

Figure 2.30: Dependence of the $b\bar{b}$ and $t\bar{t}$ branching fractions of the heavy supersymmetric Higgs bosons on $\tan\beta$. Results are for $m_t = 175$ GeV and include two-loop/RGE-improved radiative corrections to Higgs masses, mixing angles, and self-couplings, computed with $m_{\tilde{t}} = 1$ TeV neglecting squark mixing.

Resolution compared to Higgs widths

The first critical question is how the resolution in $\sqrt{s}$ compares to the H^0 and A^0 total widths. The calculated H^0 and A^0 widths are shown in Fig. 2.3 versus m_{H^0}, m_{A^0} for $\tan\beta = 2$ and 20. In Fig. 2.3.3 we give contours of constant total widths for the H^0 and A^0 in the $(m_{A^0}, \tan\beta)$ parameter space. For $m_{A^0}, m_{H^0} \lesssim 500$ GeV, the H^0 and A^0 are typically moderately narrow resonances ($\Gamma_{H^0,A^0} \sim 0.1$ to 6 GeV), unless $\tan\beta$ is larger than 20. For a machine energy resolution of $R = 0.06\%$, and Higgs masses in the 100 GeV to 1 TeV range, the resolution $\sigma_{\sqrt{s}}$ in $\sqrt{s}$ will range from roughly 0.04 GeV to to 0.4 GeV, see Eq. (2.54). Thus, Figs. 2.3 and 2.3.3 indicate that the H^0 and A^0 widths are likely to be somewhat larger than this resolution in $\sqrt{s}$. For $R = 0.01\%$, this is always the dominant situation.

When the $\sqrt{s}$ resolution is smaller than the Higgs width, then Eq. (2.55), with $\sqrt{s} \sim m_h$ shows that the cross section will behave as the product of the $\mu\mu$ and final state branching

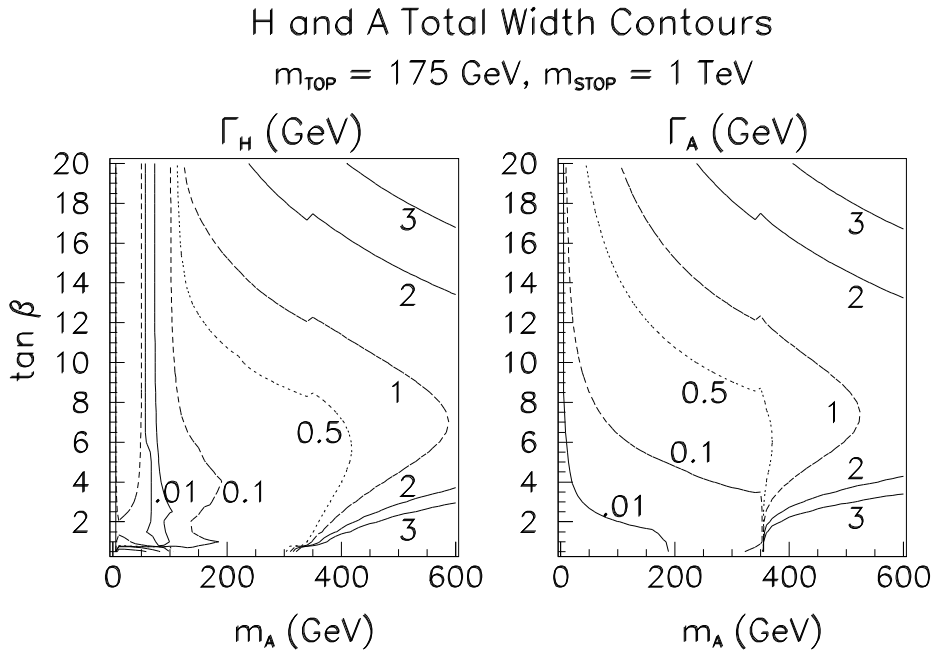

Figure 2.31: Contours of H^0 and A^0 total widths (in GeV) in the $(m_{A^0}, \tan\beta)$ parameter space. We have taken $m_t = 175$ GeV and included two-loop/RGE-improved radiative corrections using $m_{\tilde{t}} = 1$ TeV and neglecting squark mixing. SUSY decay channels are assumed to be absent.

fractions. For low to moderate $\tan\beta$ values, $BF(H^0, A^0 \to \mu\mu)$ and $BF(H^0, A^0 \to b\bar{b})$ grow with increasing $\tan\beta$, while $BF(H^0, A^0 \to t\bar{t})$ falls slowly. Thus, the number of H^0 and A^0 events in both the $b\bar{b}$ and $t\bar{t}$ channels increases with increasing $\tan\beta$. It is this growth with $\tan\beta$ that makes H^0, A^0 discovery possible for relatively modest values of $\tan\beta$ larger than 1. For higher $\tan\beta$ values, the $\mu\mu$ and $b\bar{b}$ branching fractions asymptote to constant values, while that for $t\bar{t}$ falls as $1/(\tan\beta)^4$. Thus, observability in the $t\bar{t}$ channel does not survive to large $\tan\beta$ values.

Overlapping Higgs resonances

The Higgs widths are a factor in the observability of a signal in that approximate Higgs mass degeneracies are not unlikely. For larger m_{A^0}, $m_{A^0} \sim m_{H^0}$, while at smaller m_{A^0} values, $m_{h^0} \sim m_{A^0}$ at larger $\tan\beta$, as illustrated in Fig. 2.3.3, where the plotted mass difference should be compared to the Higgs widths in Figs. 2.3 and 2.3.3. At large m_{A^0} and $\tan\beta$, there can be significant overlap of the A^0 and H^0 resonances. To illustrate the possibilities, we show

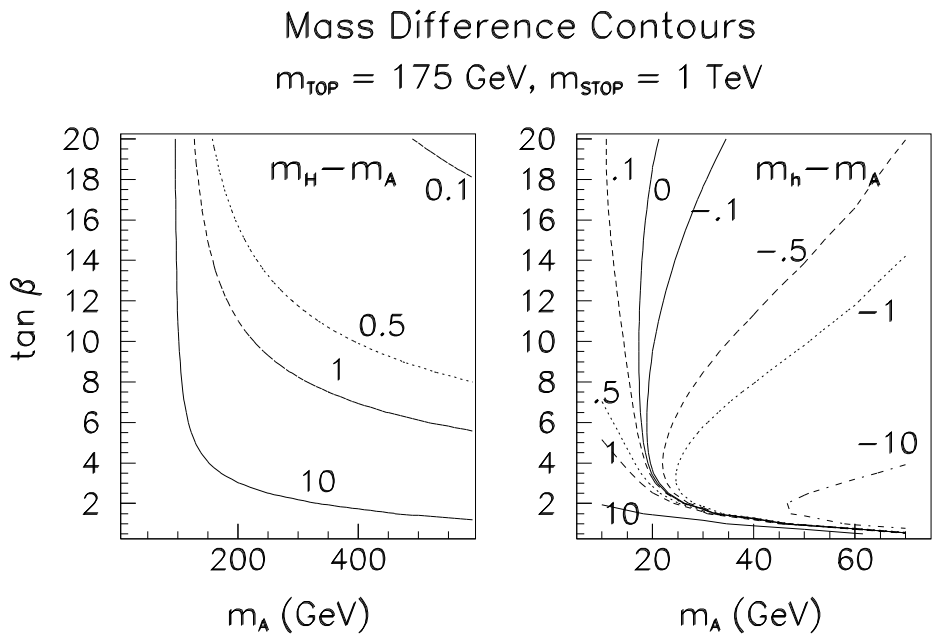

Figure 2.32: Contours of $m_{H^0} - m_{A^0}$ (in GeV) in the $(m_{A^0}, \tan\beta)$ parameter space. Two-loop/RGE-improved radiative corrections are included taking $m_t = 175$ GeV, $m_{\tilde{t}} = 1$ TeV, and neglecting squark mixing.

in Fig. 2.3.3 the event rate in the $b\bar{b}$ channel as a function of $\sqrt{s}$ (assuming $L = 0.01$ fb^{-1} and event detection/isolation efficiency $\epsilon = 0.5$) taking $m_{A^0} = 350$ GeV in the cases $\tan\beta = 5$ and 10. Continuum $b\bar{b}$ background is included. Results are plotted for the two different resolutions, $R = 0.01\%$ and $R = 0.06\%$. For $R = 0.01\%$, at $\tan\beta = 5$ the resonances are clearly separated and quite narrow, whereas at $\tan\beta = 10$ the resonances have become much broader and much more degenerate, resulting in substantial overlap; but, distinct resonance peaks are still visible. For $R = 0.06\%$, at $\tan\beta = 5$ the resonances are still separated, but have been somewhat smeared out, while at $\tan\beta = 10$ the H^0 and A^0 peaks are no longer separately visible. The $R = 0.06\%$ smearing does not greatly affect the observation of a signal, but would clearly make separation of the H^0 and A^0 peaks and precise determination of their individual widths much more difficult.

In the following section, we perform our signal calculations by centering $\sqrt{s}$ on m_{A^0}, but including any H^0 signal tail, and vice versa. At small m_{A^0}, there is generally only small overlap between the A^0 and h^0 since their widths are small, but we follow a similar procedure there. We also mainly employ the optimistic $R = 0.01\%$ resolution that is highly

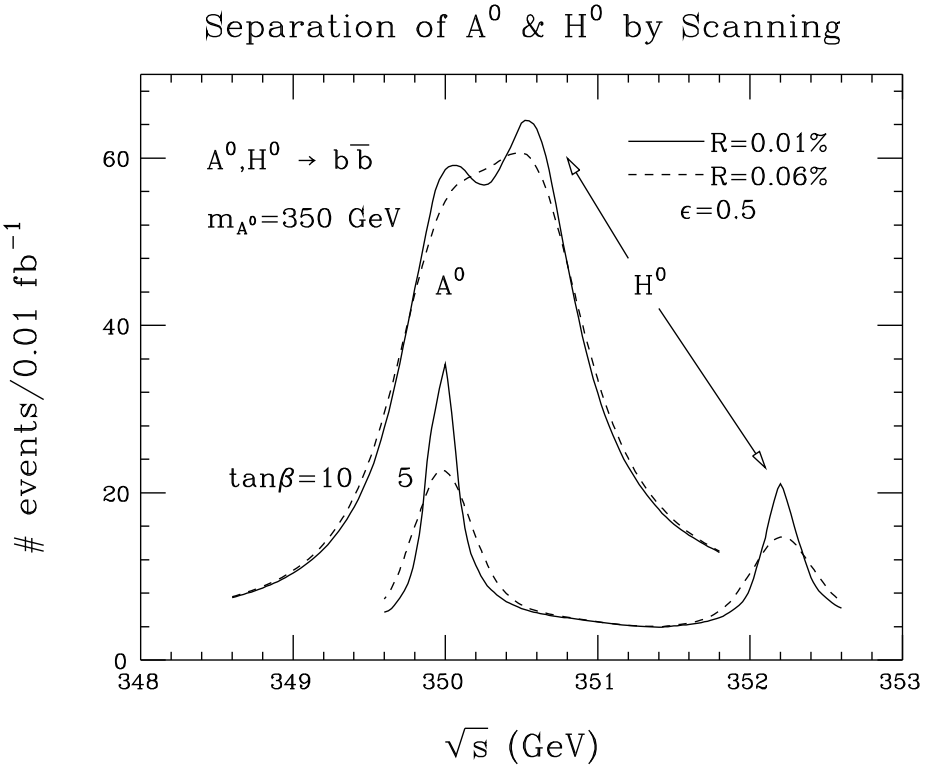

Figure 2.33: Plot of $b\overline{b}$ final state event rate as a function of $\sqrt{s}$ for $m_{A^0} = 350$ GeV, in the cases $\tan\beta = 5$ and 10, resulting from the H^0, A^0 resonances and the $b\overline{b}$ continuum background. We have taken $L = 0.01$ fb^{-1} (at any given $\sqrt{s}$), $\epsilon = 0.5$, $m_t = 175$ GeV, and included two-loop/RGE-improved radiative corrections to Higgs masses, mixing angles and self-couplings using $m_{\tilde{t}} = 1$ TeV and neglecting squark mixing. SUSY decays are assumed to be absent. Curves are given for two resolution choices: $R = 0.01\%$ and $R = 0.06\%$

preferred for a SM-like Higgs boson. Since the MSSM Higgs bosons do not have especially small widths, results for $R = 0.06\%$ are generally quite similar.

Observability for h^0, H^0 and A^0

We first consider fixed $\tan\beta$ values of 2, 5, and 20, and compute $\epsilon\overline{\sigma}_h BF(h \to b\overline{b}, t\overline{t})$ for $h = h^0, H^0, A^0$ as a function of m_{A^0}. (The corresponding h^0 and H^0 masses can be found in Fig. 2.17.) Our results for $R = 0.01\%$ appear in Figs. 2.3.3, 2.3.3, and 2.3.3. Also shown

in these figures are the corresponding $S/\sqrt{B}$ values assuming an integrated luminosity of $L = 0.1$ fb^{-1}; results for other L possibilities are easily obtained by using $S/\sqrt{B} \propto 1/\sqrt{L}$. These figures also include (dot-dashed) curves for $R = 0.06\%$ in the $b\bar{b}$ channel at $\tan\beta = 2$.

Figure 2.3.3 shows that the h^0 can be detected at the 5σ statistical level with just $L = 0.1$ fb^{-1} for essentially all of parameter space, if $R = 0.01\%$. Only for $\tan\beta \lesssim 2$ is m_{h^0} sufficiently near m_Z at large m_{A^0} (for which its $\mu^+\mu^-$ coupling is not enhanced) that more luminosity may be required. At low m_{A^0}, the h^0 is not SM-like and has highly enhanced $\mu^+\mu^-$ and $b\bar{b}$ couplings. It is also no longer extremely narrow, and is produced with a very high rate implying that high statistics studies of its properties would be possible. The $R = 0.06\%$ $\tan\beta = 2$ curve illustrates the large loss in observability that occurs for non-optimal resolution when the h^0 is SM-like at large m_{A^0} and has a very small width.

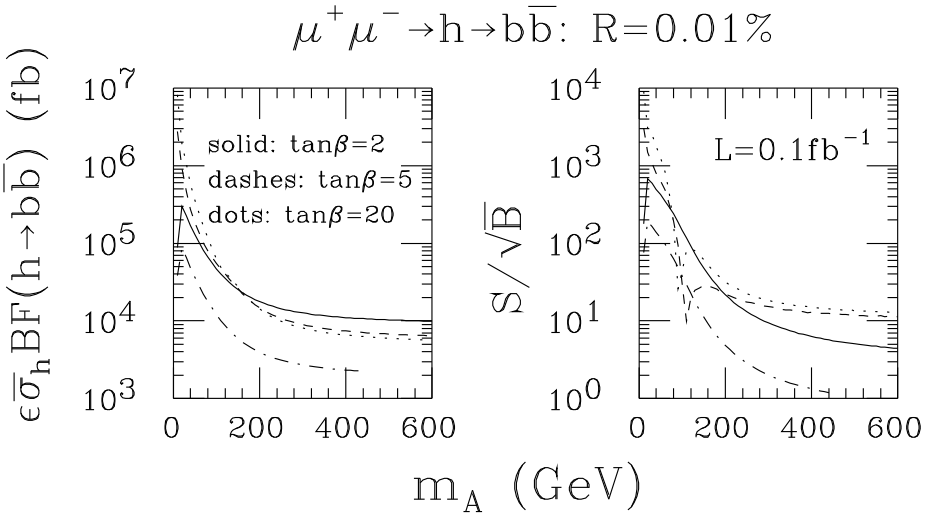

Figure 2.34: Plot of $\epsilon\overline{\sigma}_{h^0}BF(h^0 \to b\bar{b})$ vs m_{A^0} for $\tan\beta = 2$, 5 and 20. Also shown is the corresponding $S/\sqrt{B}$ for $L = 0.1$ fb^{-1}. We have taken $R = 0.01\%$, $\epsilon = 0.5$, $m_t = 175$ GeV, and included two-loop/RGE-improved radiative corrections to Higgs masses, mixing angles and self-couplings using $m_{\widetilde{t}} = 1$ TeV and neglecting squark mixing. SUSY decays are assumed to be absent in computing BF. Also shown as the dot-dashed curve are the $R = 0.06\%$ results at $\tan\beta = 2$ in the $b\bar{b}$ channel.

Results for $\epsilon\overline{\sigma}_h BF(h \to b\bar{b}, t\bar{t})$ for $h = H^0$ and $h = A^0$ are displayed in Figs. 2.3.3 and 2.3.3, respectively, along with the corresponding $L = 0.1$ fb^{-1} $S/\sqrt{B}$ values. For a luminosity

of $L = 0.01$ fb^{-1}, the $S/\sqrt{B}$ values of the figures should be reduced by a factor of 0.32. For $L = 0.3$, multiply by 1.7. This range of luminosities will be that which arises when we consider searching for the H^0 and A^0 by scanning in $\sqrt{s}$. The dot-dashed curves illustrate the fact that $R = 0.06\%$ resolution does not cause a large loss in observability relative to $R = 0.01\%$ in the case of the A^0 and, especially, the H^0; the largest effect is for the $\tan\beta = 2$ case in the $b\bar{b}$ channel. For $\tan\beta = 5$ and 20, and for all $t\bar{t}$ curves, the results for $R = 0.06\%$ are virtually indistinguishable from those for $R = 0.01\%$.

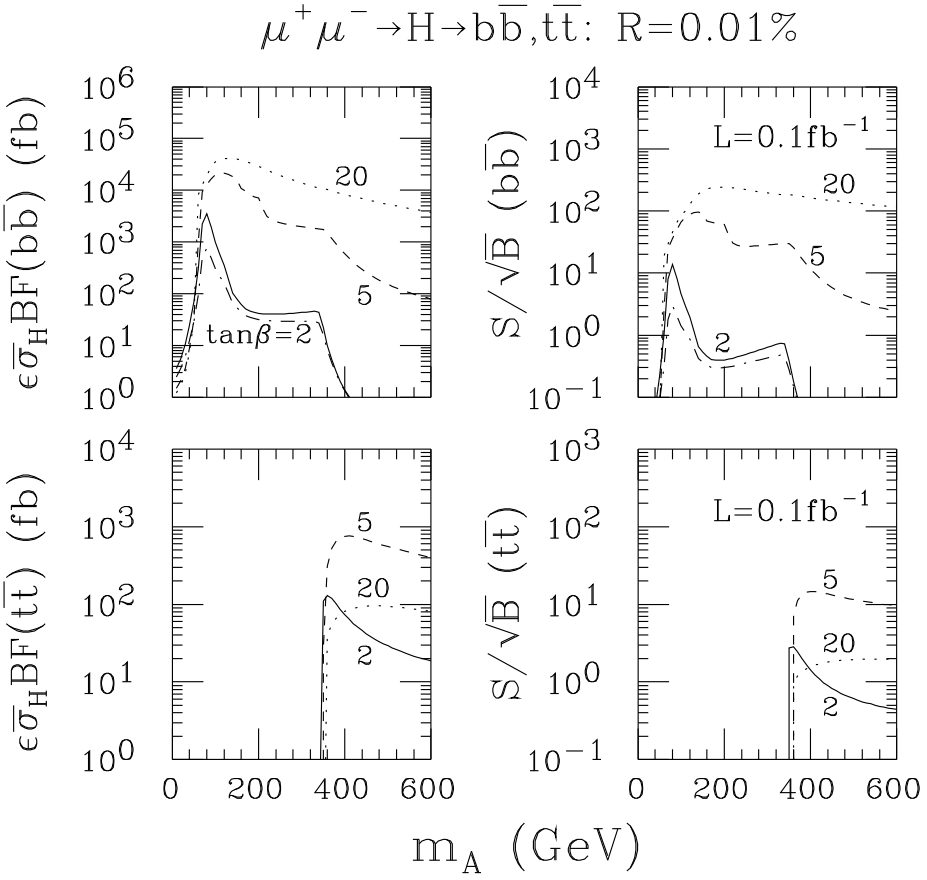

Figure 2.35: Plot of $\epsilon\overline{\sigma}_{H^0}BF(H^0 \to b\bar{b}, t\bar{t})$ vs m_{A^0} for $\tan\beta = 2$, 5 and 20. Also shown are the corresponding $S/\sqrt{B}$ values for $L = 0.1$ fb^{-1}. The inputs are specified in the caption of Fig. 2.3.3. Also shown as the dot-dashed curve are the $R = 0.06\%$ results at $\tan\beta = 2$ in the $b\bar{b}$ channel.

An alternative picture that is especially useful for assessing the parameter space region over which h^0, A^0 and/or H^0 discovery will be possible at the $\mu^+\mu^-$ collider is that given

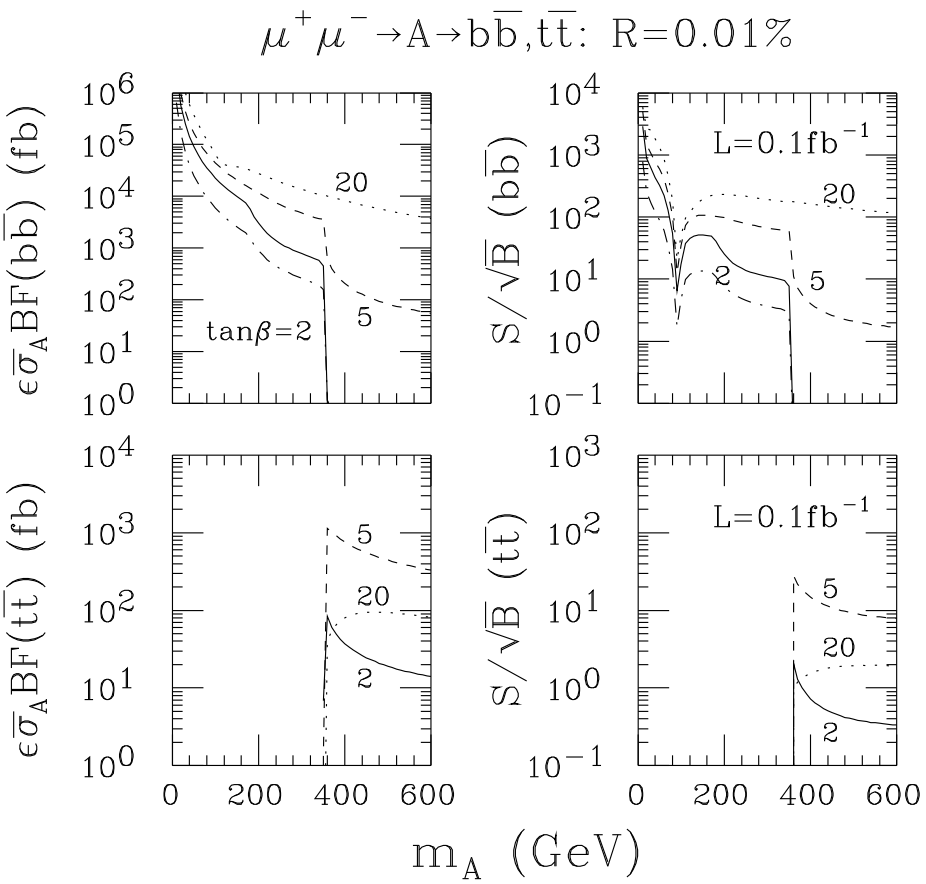

Figure 2.36: Plot of $\epsilon\overline{\sigma}_{A^0} BF(A^0 \to b\bar{b}, t\bar{t})$ vs m_{A^0} for $\tan\beta = 2$, 5 and 20. Also shown are the corresponding $S/\sqrt{B}$ values for $L = 0.1$ fb^{-1}. The inputs are specified in the caption of Fig. 2.3.3. Also shown as the dot-dashed curve are the $R = 0.06\%$ results at $\tan\beta = 2$ in the $b\bar{b}$ channel.

in Fig. 2.3.3, for which we have taken $R = 0.06\%$. The contours in $(m_{A^0}, \tan\beta)$ parameter space denote the luminosity required for a 5σ signal when $\sqrt{s}$ is taken equal to the Higgs mass in question. For the window labelled $H^0 \to b\bar{b}$ we take $\sqrt{s} = m_{H^0}$, for the $h^0 \to b\bar{b}$ window we take $\sqrt{s} = m_{h^0}$, while $\sqrt{s} = m_{A^0}$ for the $A^0 \to b\bar{b}$ and $A^0 \to t\bar{t}$ contours. The 5σ contours are for luminosities of $L = 0.001$, 0.01, 0.1, 1, and 10 fb^{-1}. The larger the L the larger the discovery region. In the case of $A^0 \to t\bar{t}$, 5σ is only achieved for the four luminosities $L = 0.01, 0.1, 1, 10$ fb^{-1}. In the case of the h^0, $L = 10$ fb^{-1} always yields a 5σ signal within the parameter space region shown.

With regard to the h^0, Fig. 2.3.3 shows that for $R = 0.06\%$ and luminosities somewhat

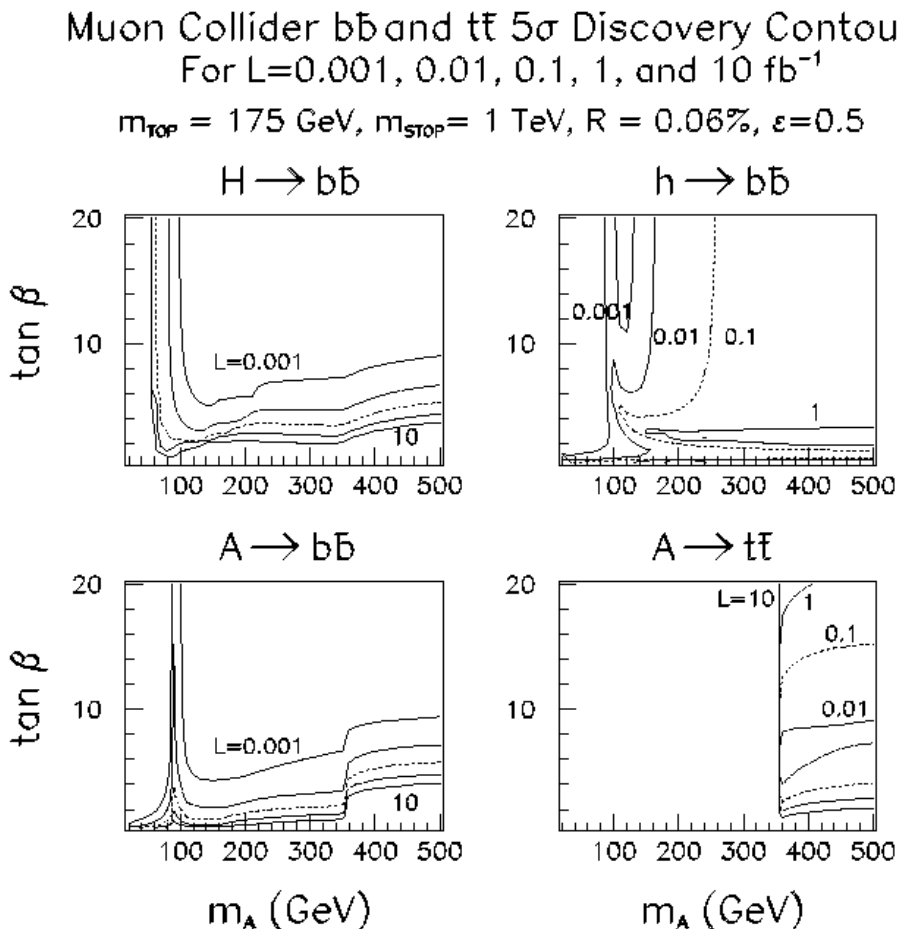

Figure 2.37: Contours in $(m_{A^0}, \tan\beta)$ parameter space of the luminosity required for 5σ Higgs signals. Contours for $L = 0.001$, 0.01, 0.1, 1, and 10 fb^{-1} are given. For $A^0 \to t\bar{t}$, $L = 0.001$ fb^{-1} does not yield a 5σ signal and no corresponding contour appears. For $h^0 \to b\bar{b}$, $L = 10$ fb^{-1} yields a 5σ signal for all of parameter space, and so only $L = 0.001 - 1$ fb^{-1} contours appear. The inputs are specified in the caption of Fig. 2.3.3.

less than 1 fb^{-1}, h^0 could only be detected in the $b\bar{b}$ mode at large m_{A^0} if $\tan\beta$ is sufficiently far from 1 that m_{h^0} is not near m_Z. In contrast, when m_{A^0} is sufficiently small that m_{h^0} is small and the h^0 is no longer SM-like, and has enhanced $\mu\mu$ and $b\bar{b}$ couplings, rather modest luminosity is required for a 5σ signal at $\sqrt{s} = m_{h^0}$; for instance, $L \lesssim 0.001$ fb^{-1} will allow detection of a signal from the h^0 (and the possibly overlapping A^0) over most of the $m_{A^0} \lesssim 100$ GeV portion of parameter space even for $R = 0.06\%$. However, we have noted

that it is theoretically quite likely that m_{A^0} is large and that the h^0 is SM-like. Detection of the H^0 and A^0 then becomes of paramount interest.

Detecting the H^0 and A^0 by scanning in $\sqrt{s}$

In order to discover the H^0 or A^0 in the $\gtrsim 250$ GeV region, we must scan over $\sqrt{s}$ values between 250 GeV and 500 GeV (the presumed upper limit for the FMC). The separation between scan points is determined by the larger of the expected widths and the $\sqrt{s}$ resolution, $\sigma_{\sqrt{s}}$. If $\tan\beta \gtrsim 2$, then for m_{H^0} and m_{A^0} near 250 GeV, the A^0 and H^0 widths are of order $0.05 - 0.1$ GeV. For masses near 500 GeV, their widths are at least 1 GeV (cf. Fig. 2.3.3). Meanwhile, for $R = 0.01\%$ ($R = 0.06\%$), $\sigma_{\sqrt{s}}$ ranges from ~ 0.018 GeV (~ 0.11 GeV) to ~ 0.035 GeV ($\sim .21$ GeV) as $\sqrt{s}$ ranges from 250 GeV to 500 GeV. Thus, it is reasonable to imagine using scan points separated by 0.1 GeV for $m_{A^0} \sim m_{H^0}$ near 250 GeV, rising to 1 GeV by $\sqrt{s} = 500$ GeV. It will also be important to note that the luminosity required per point for detection of the A^0 and H^0 is less for masses below $2m_t$ than above. In assessing the detectability of the H^0 and A^0 by scanning we devote

- $L = 0.01$ fb^{-1} to each of 1000 points separated by 0.1 GeV between 250 and 350 GeV,
- $L = 0.1$ fb^{-1} to each of 100 points separated by 0.5 GeV between 350 and 400 GeV,
- and $L = 0.3$ fb^{-1} to each of 100 points separated by 1 GeV between 400 and 500 GeV.

This selection of points more or less ensures that if the H^0 and A^0 are present then one of the scan points would have $\sqrt{s} \sim m_{H^0}, m_{A^0}$ within either the $\sigma_{\sqrt{s}}$ resolution or the Higgs width. The total luminosity required for this scan would be 50 fb^{-1}.

We now employ the 5σ contours of Fig. 2.3.3 to assess the portion of $(m_{A^0}, \tan\beta)$ parameter space over which the above scan will allow us to detect the H^0 and A^0 in the $b\bar{b}$ and $t\bar{t}$ channels. The 5σ luminosity contours of interest will be the curves corresponding to $L = 0.01$ fb^{-1}, $L = 0.1$ fb^{-1} and $L = 1$ fb^{-1}. The 5σ contour for $L = 0.3$ fb^{-1} luminosity per point, as employed in our scan procedure from 400 to 500 GeV, is midway between these last two curves. Fig. 2.3.3 shows that, by performing the scan in the manner outlined earlier, one can detect the H^0, A^0 in the $b\bar{b}$ mode for all $\tan\beta$ values above about $2 - 4$ for $m_{H^0}, m_{A^0} \lesssim 2m_t$ and above about $3 - 5$ for $2m_t \lesssim m_{H^0}, m_{A^0} \lesssim 500$ GeV. Meanwhile, in the $t\bar{t}$ mode, the $A^0 \to t\bar{t}$ signal can be seen for $m_{A^0} \gtrsim 2m_t$ provided $\tan\beta \gtrsim 3$. Together, the $b\bar{b}$ and $t\bar{t}$ signals are viable for a remarkably large portion of parameter space, which

includes, in particular, essentially all of the wedge region where the LHC lacks sensitivity (see Fig. 2.3.3). At worst, there would be a very small $\tan\beta$ window for $m_{A^0} \gtrsim 2m_t$ between $\tan\beta = 3$ and $\tan\beta = 4$, for which the signal might be missed during the above described scan and also no signal seen at the LHC. In practice, it might be desirable to simply devote several years of running to the scan in order to ensure that the A^0 and H^0 are detected if present.

The implementation of the above scan is very demanding upon the machine design because:

- several rings may be needed to have high luminosities over a broad range of $\sqrt{s}$;
- it must be possible *over this broad range of energies* to quickly (for example, once every hour or so in the 250–350 GeV range) reset $\sqrt{s}$ with an accuracy that is a small fraction of the proposed step sizes.

It is too early to say if these demands can both be met.

Finally, we note the obvious conflict between this scan and the desirable $\sqrt{s} = m_{h^0}$, $L = 50$ fb^{-1} study of the SM-like h^0. A multi-year program will be required to accomplish both tasks.

Non-$b\bar{b}$ final state modes for heavy Higgs detection

The reader may note that $\sqrt{s} = m_{H^0}$ does not yield an observable s-channel signal in the $b\bar{b}$ mode for $m_{A^0} \lesssim 100$ GeV. Although the H^0 is SM-like in this parameter region in that it does not have enhanced coupling to $\mu\mu$ and $b\bar{b}$, its decays are dominated by h^0h^0 and, for $m_{A^0} \lesssim 60$ GeV, A^0A^0 pairs; ZA^0 decays also enter for small enough m_{A^0}. This means that the H^0 total width is quite large, in particular much larger than the $\sqrt{s}$ spread. The large total width also implies that $BF(H^0 \to \mu\mu)$ is small. Equation (2.59) then shows that the production rate for the H^0 will be small, and that the rate in the $b\bar{b}$ final state will be further suppressed by the small value of $BF(H^0 \to b\bar{b})$. The only possible channels for observation of the H^0 in the $m_{A^0} \lesssim 100$ GeV region are h^0h^0, A^0A^0, ZA^0. As we discuss below, these could prove to be viable.

The full set of channels to be considered are

$$H^0 \to h^0h^0, \qquad H^0 \to A^0A^0, \qquad H^0 \to ZA^0, \qquad A^0 \to Zh^0. \tag{2.72}$$

The h^0h^0, A^0A^0 final states primarily ($\sim 80\%$ of the time) yield $4b$'s. The ZA^0, Zh^0 final states yield $2j2b$ about 60% of the time. In either case, we can demand that there be two pairs of jets, each pair falling within narrow mass intervals. In addition, two b-tags can be required. Thus, these channels will have small background. To illustrate the size of the signal in these channels, we present in Fig. 2.3.3 the $L = 10$ fb^{-1} signal rates for the above four modes, assuming a net 50% efficiency (including branching fractions and tagging efficiencies, as well as double mass-binning). In the $H^0 \to h^0h^0$ case, at least 50 events are obtained in essentially all but the $m_{A^0} = 60 - 230, \tan\beta \gtrsim 2.5$ region; the 5000 event contour is confined to a narrow region around $m_{A^0} = 65 - 70, \tan\beta \gtrsim 2$ and to the (disjoint) teardrop region labelled; the 50 and 500 event contours are as labelled. At least 500 events are predicted in the $m_{A^0} \lesssim 60$ region for all $\tan\beta$. In the $H^0 \to A^0A^0$ case, at least 500 events are obtained in the $m_{A^0} \lesssim 60$ and $\tan\beta \gtrsim 2$ region. In the $H^0 \to ZA^0$ case, only the 5 event level is achieved over even the small piece of parameter space shown. Finally, in the $A^0 \to Zh^0$ case all contours are easily identified by the labeling. No events are expected for m_{A^0} below about 200 GeV, where the $A^0 \to Zh^0$ decay mode is no longer kinematically allowed. It is kinematics that also dictates the rather restricted regions at low m_{A^0} for which $H^0 \to A^0A^0$ and $H^0 \to ZA^0$ events occur.

In order to discuss the observability of the above signals, we need to compute the background level, which we do not do in this report. After b-tagging and mass reconstruction we believe that backgrounds should be modest. In the absence of any explicit calculation we can only make the following guesstimates. Based on the event rates of Fig. 2.3.3 it should be possible to study the $H^0 \to h^0h^0$ channel over a significant fraction of parameter space with $L \sim 1$ fb^{-1}. In particular, luminosities at and above this level could open up the $m_{A^0} \lesssim 60$ GeV region for both this mode and the $H^0 \to A^0A^0$ mode. In contrast, it will obviously require very substantial luminosity to detect $H^0 \to ZA^0$, even when not kinematically suppressed. A viable $A^0 \to Zh^0$ signal may be possible, when kinematically allowed, only so long as m_{A^0} and $\tan\beta$ are not large; when m_{A^0} is large the tree-level coupling is suppressed (which suppression occurs most rapidly at large $\tan\beta$) and there are too few events for a useful signal.

Although these modes provide somewhat more challenging signals than the $b\overline{b}$ channel signal, their observation would provide tests of important Higgs couplings. In particular, detection of the $H^0 \to h^0h^0$ and $H^0 \to A^0A^0$ modes would allow a direct probe of these very interesting Higgs boson self-couplings. The procedure will be outlined in a later section. In

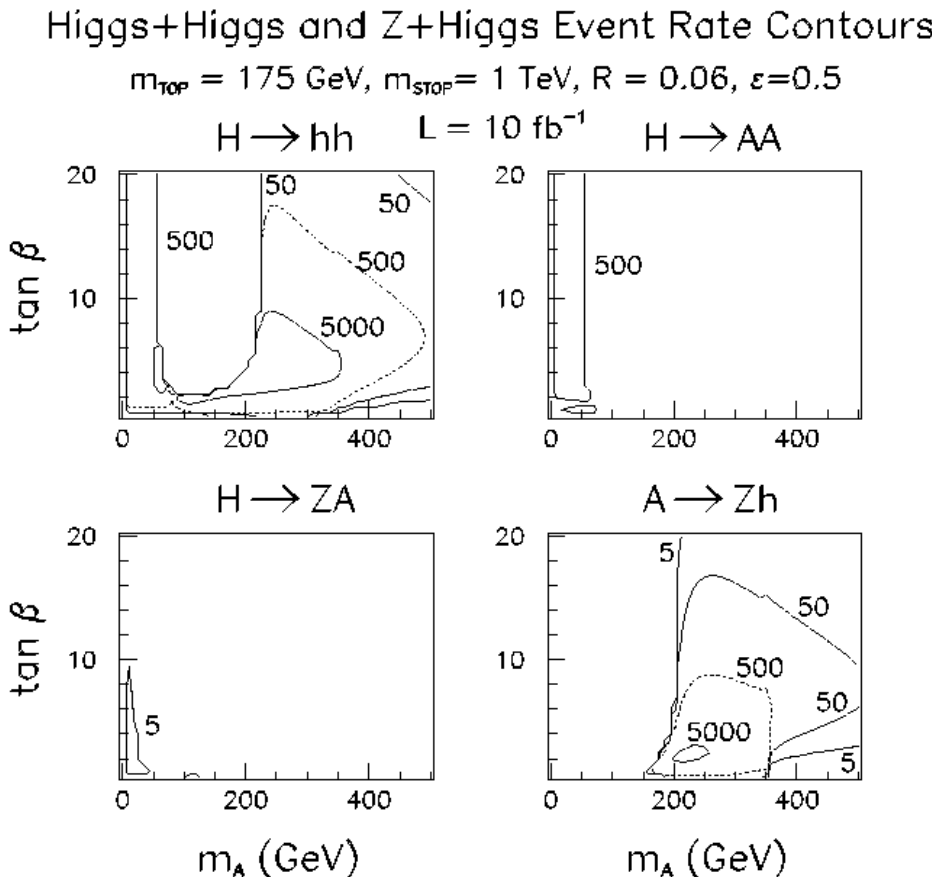

Figure 2.38: Event rate contours for $H^0 \to h^0 h^0$, $H^0 \to A^0 A^0$, $H^0 \to Z A^0$ and $A^0 \to Z h^0$ in $(m_{A^0}, \tan\beta)$ parameter space for integrated luminosity $L = 10$ fb^{-1}. Contours for 5, 50, 500 and 5000 events are shown in the first and last cases. There are 500 or more $H^0 \to A^0 A^0$ events if $m_{A^0} \lesssim 60$ GeV and $\tan\beta \gtrsim 2$, but $H^0 \to Z A^0$ barely reaches the 5 event level. Two-loop/RGE-improved radiative corrections to Higgs masses, mixing angles and self-couplings are included, taking $m_t = 175$ GeV, $m_{\tilde{t}} = 1$ TeV and neglecting squark mixing.

general, determination of the Higgs boson self-couplings is quite difficult at other machines. In particular, even when a relevant branching fraction can be measured, knowledge of the total width is required in order to extract the partial width and coupling. Without a $\mu^+\mu^-$ collider, measurement of the total width is only possible if the width is substantially larger than the resolution implied by final state mass reconstruction at the Higgs mass. This is not

the case for the H^0 and A^0 unless $\tan\beta$ is very large.

MSSM Higgs Boson Detection Using the Bremsstrahlung Tail Spectrum

In this section, we discuss an alternative way of searching for the A^0 and H^0 by running the $\mu^+\mu^-$ collider at full energy but looking for excess events arising from the luminosity on the low-energy end of the bremsstrahlung tail (see sec. 2.12.3). This latter technique proves to be somewhat competitive with the scan technique just described, provided that excellent resolution in reconstructing the $b\bar{b}$ final state mass can be achieved and provided that large total integrated luminosity is devoted to such running. It would have two distinct advantages over the scanning approach.

- It would not require the construction of multiple rings in order to maintain high luminosity over a broad range of $\sqrt{s}$ collision energies.
- A large number of events in the Zh mode for the SM-like h^0 could be simultaneously accumulated.

As for the scan procedure, the bremsstrahlung tail technique is viable only if the $h \to \mu^+\mu^-$ coupling is significantly enhanced relative to the SM $h_{SM} \to \mu^+\mu^-$ coupling; only then is a Higgs boson with mass substantially below $\sqrt{s}$ produced at a large rate by virtue of the bremsstrahlung tail. Of course, once the H^0 and/or A^0 is found using the bremsstrahlung technique, it would then be highly desirable to run the machine with $\sqrt{s} \sim m_{H^0}, m_{A^0}$ in order to study in detail the widths and other properties of the H^0, A^0.

For our study of the bremsstrahlung tail possibility, we shall assume that the $b\bar{b}$ final state mass can be reconstructed to within ± 5 GeV. A full study of this mode of detection should generate events, smear the b jets using expected resolutions, allow for semi-leptonic b decays, and incorporate tagging efficiencies. The reconstructed mass of the $b\bar{b}$ final state for each event should then be binned and one would then look for a peak over the expected background level. We will not perform this detailed simulation here. Instead, we compute as a function of $m_{b\bar{b}}$ (the central value of the $b\bar{b}$ final state mass) the number of events in the interval $[m_{b\bar{b}} - 5\text{ GeV}, m_{b\bar{b}} + 5\text{ GeV}]$. In estimating the significance of any peak seen in the spectrum, we will choose $m_{b\bar{b}}$ at the center of the peak, and compare the excess of events in the above interval (the signal S) to the number of events expected if there is no Higgs boson present (the background B). The statistical significance will be computed as $S/\sqrt{B}$.

In computing the number of events we assume an integrated luminosity of $L = 50$ fb^{-1} and assume an event reconstruction and tagging efficiency of $\epsilon = 0.5$. Correspondingly, only the continuum $b\bar{b}$ final states from $\gamma^\star, Z^\star$ processes will be included in B (using also $\epsilon = 0.5$). These latter assumptions are the same ones employed in our other analysis.

Mass peaks

It will be useful to first display some typical mass peaks. In Fig. 2.3.3, we plot the number of events in the interval $[m_{b\bar{b}}-5 \text{ GeV}, m_{b\bar{b}}+5 \text{ GeV}]$ as a function of $m_{b\bar{b}}$ for three m_{A^0} choices: $m_{A^0} = 120$, 300 and 480 GeV. In each case, results for $\tan\beta = 5$ and 20 are shown. The event enhancements derive from the presence of the H^0 and A^0 Higgs bosons. There would be no visible effect for the choice of $m_{A^0} = 100$ GeV for any $\tan\beta$ value below 20. This is because all the Higgs masses are sitting on the very large Z peak and, in addition, none of the $\mu^+\mu^-$ couplings are fully enhanced. For the three m_{A^0} values considered in Fig. 2.3.3, we observe event excesses for $\tan\beta = 20$ in all cases. For $\tan\beta = 5$, the $m_{A^0} = 300$ GeV peak is clear, while $m_{A^0} = 480$ GeV yields a shoulder of excess events (that is statistically significant); nothing is visible for $m_{A^0} = 120$ GeV. For $\tan\beta \lesssim 2$, no peaks or excesses would be visible for any of the above m_{A^0} choices. Finally, we note that enhancements due to the h^0 resonance would not be visible, regardless of $\tan\beta$, for $m_{A^0} \gtrsim 100$ GeV.

Significance of signals

We will now proceed to survey the $S/\sqrt{B}$ expectations. We do this as a function of location in the $(m_{A^0}, \tan\beta)$ parameter space as follows. For each choice of $(m_{A^0}, \tan\beta)$ we determine m_{h^0} and m_{H^0}. We then compute $S/\sqrt{B}$ for the three locations $m_{b\bar{b}} = m_{h^0}$, $m_{b\bar{b}} = m_{H^0}$ and $m_{b\bar{b}} = m_{A^0}$, where S and B are computed by counting events in the $m_{b\bar{b}} \pm 5$ GeV window. Effects from overlapping Higgs resonances are included. The 5σ discovery contours for each of these three window locations are plotted in $(m_{A^0}, \tan\beta)$ parameter space for integrated luminosities of $L = 0.5$, 5, 50 and 200 fb^{-1} in Fig. 2.3.3, taking $\sqrt{s} = 500$ GeV and $R = 0.1\%$.

As expected from Fig. 2.3.3, the window centered at $m_{b\bar{b}} = m_{h^0}$ only yields a statistically significant excess if $\tan\beta$ is large and m_{h^0} is not near m_Z. (m_{h^0} near m_Z at high $\tan\beta$ corresponds to $m_{A^0} \sim 95$ GeV.) Since the Zh^0 mode will yield an observable signal regardless of the $(m_{A^0}, \tan\beta)$ values, the bremsstrahlung tail excess would mainly be of interest as a probe of the $\Gamma(h^0 \to \mu^+\mu^-)$ partial width prior to running at $\sqrt{s} = m_{h^0}$.

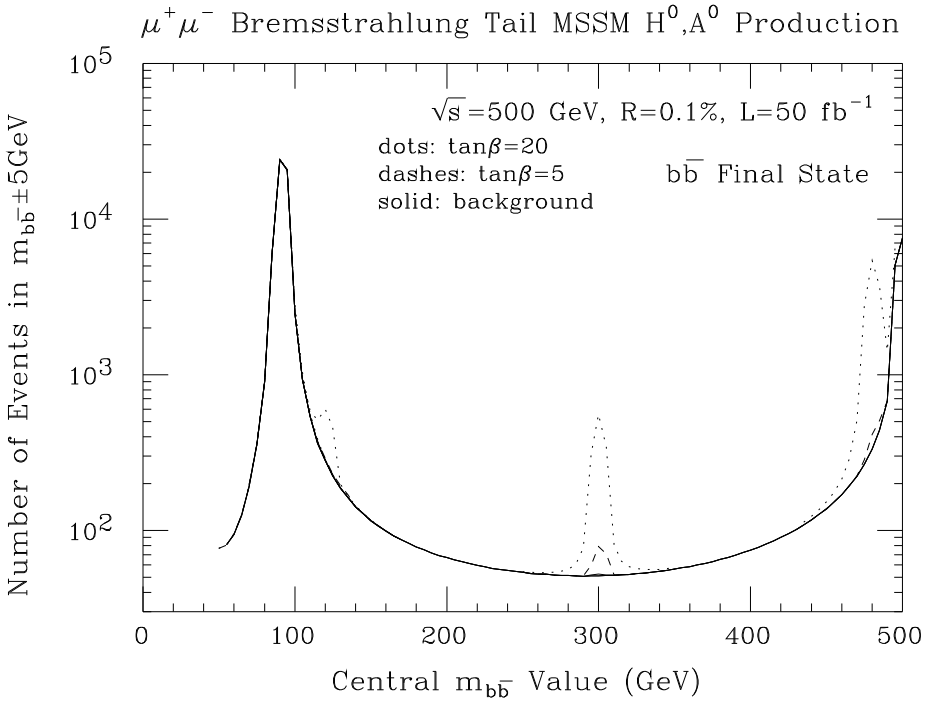

Figure 2.39: Taking $\sqrt{s} = 500$ GeV, integrated luminosity $L = 50$ fb^{-1}, and $R = 0.1\%$, we consider the $b\bar{b}$ final state and plot the number of events in the interval $[m_{b\bar{b}} - 5 \text{ GeV}, m_{b\bar{b}} + 5 \text{ GeV}]$, as a function of the location of the central $m_{b\bar{b}}$ value, resulting from the low $\sqrt{\hat{s}}$ bremsstrahlung tail of the luminosity distribution. MSSM Higgs boson H^0 and A^0 resonances are present for the parameter choices of $m_{A^0} = 120$, 300 and 480 GeV, with $\tan\beta = 5$ and 20 in each case. Enhancements for $m_{A^0} = 120$, 300 and 480 GeV are visible for $\tan\beta = 20$; $\tan\beta = 5$ yields visible enhancements only for $m_{A^0} = 300$ and 480 GeV. Two-loop/RGE-improved radiative corrections are included, taking $m_t = 175$ GeV, $m_{\tilde{t}} = 1$ TeV and neglecting squark mixing. SUSY decay channels are assumed to be absent.

However, the ± 5 GeV intervals centered at $m_{b\bar{b}} = m_{H^0}$ and $m_{b\bar{b}} = m_{A^0}$ (which, include events from the overlapping A^0 and H^0 resonances, respectively) yield 5σ statistical signals for a substantial portion of parameter space if L is large. With $L = 50$ fb^{-1}, a 5 sigma discovery of the H^0 and A^0 using the $\sqrt{s} = 500$ GeV bremsstrahlung tail is viable down to $\tan\beta \gtrsim 6.5$ at $m_{A^0} = 250$ GeV improving to $\tan\beta \gtrsim 5$ at 480 GeV. This is not quite as far down in $\tan\beta$ as can be probed for $250 \lesssim m_{A^0} \lesssim 500$ GeV by the previously described scan

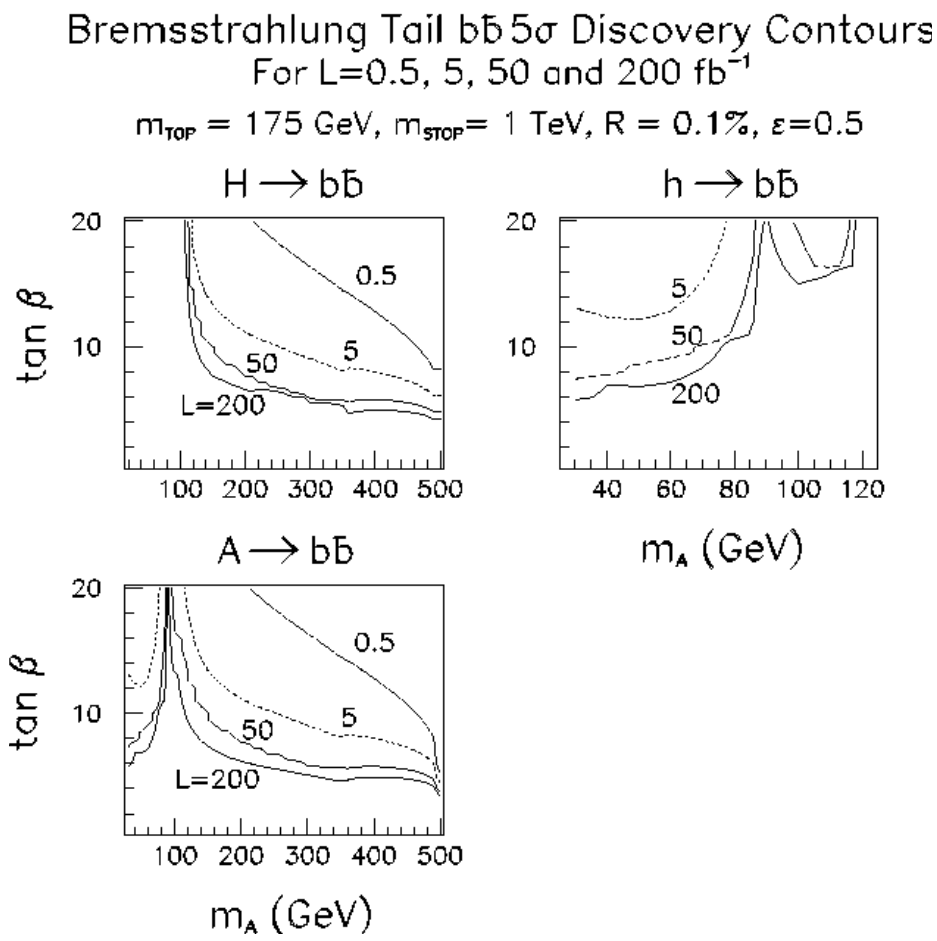

Figure 2.40: Taking $\sqrt{s} = 500$ GeV and $R = 0.1\%$, we consider the $b\bar{b}$ final state and compute the Higgs signal (S) and background (B) rates in the mass interval $[m_{b\bar{b}} - 5 \text{ GeV}, m_{b\bar{b}} + 5 \text{ GeV}]$, with $m_{b\bar{b}} = m_{H^0}$, $m_{b\bar{b}} = m_{h^0}$, and $m_{b\bar{b}} = m_{A^0}$, resulting from the low $\sqrt{\hat{s}}$ bremsstrahlung tail of the luminosity distribution. $S/\sqrt{B} = 5$ contours are shown for integrated luminosities of $L = 0.5$, 5, 50, and 200 fb^{-1}. Two-loop/RGE-improved radiative corrections are included, taking $m_t = 175$ GeV, $m_{\tilde{t}} = 1$ TeV and neglecting squark mixing. SUSY decay channels are assumed to be absent.

over a series of $\sqrt{s}$ values using $0.01 - 0.3$ fb^{-1} of luminosity at each scan point. As m_{H^0}, m_{A^0} move closer to m_Z, the 5σ discovery contours move to much larger $\tan\beta$ values, whereas the scanning technique would yield 5σ signals for $\tan\beta$ values as low as $\tan\beta \sim 3 - 4$ all the way down to $m_{A^0} \gtrsim 60$ GeV.

Strategy: scan vs. maximum energy

If $Z^\star \to H^0A^0$ is not observed at a $\sqrt{s} = 500$ GeV e^+e^- machine and if discovery of the H^0 and A^0 in the $250 - 500$ GeV mass range is the primary goal, at the $\mu^+\mu^-$ collider it would be a close call as to whether it would be better to immediately embark on the $\sqrt{s}$ scan or accumulate luminosity at the maximum machine energy. The $\sqrt{s}$ scan probes $\tan\beta$ values that are lower by only 1 or 2 units than the bremsstrahlung tail search. This statement assumes that a final state mass resolution of order ± 5 GeV can be achieved (even after including all semi-leptonic decay effects and so forth) in the $b\overline{b}$ final state for the latter search. If not, the $\sqrt{s}$ scan is the preferred technique. Thus, resolution and missing energy could become critical issues for the detector(s) in deciding the best approach.

If an e^+e^- collider is not operational at the time a $\mu^+\mu^-$ collider begins running, then the decision as to which approach to choose for H^0 and A^0 discovery becomes even more delicate unless the LHC has clearly ruled out $m_{A^0}, m_{H^0} \lesssim 250$ GeV (which it probably can do — see Fig. 2.3.3). Without a lower bound on m_{A^0}, m_{H^0}, the $\sqrt{s}$ scan would have to be extended to lower $\sqrt{s}$, requiring more luminosity. In contrast, by accumulating $L = 50$ fb^{-1} at full energy, $\sqrt{s} = 500$ GeV, it would be possible to simultaneously either discover or rule out $m_{A^0}, m_{H^0} \lesssim \sqrt{s}/2$ for all $\tan\beta$ and $\sqrt{s}/2 \lesssim m_{H^0}, m_{A^0}, \lesssim \sqrt{s}$ for $\tan\beta \gtrsim 5 - 7$. Note that $m_{A^0}, m_{H^0} \lesssim \sqrt{s}/2 - 20$ GeV can be ruled out in the $Z^\star \to H^0h$ mode with perhaps as little as $5 - 10$ fb^{-1}. For luminosities of order 10 fb^{-1} the bremsstrahlung tail technique would probe $\tan\beta \gtrsim 11$ for $m_{A^0} \sim 250$ GeV improving to $\tan\beta \gtrsim 6$ for $m_{A^0} \sim 500$ GeV. After accumulating the $L = 5 - 10$ fb^{-1}, the $\mu^+\mu^-$ collider could then be switched to the scan mode of operation if no signal has been found.

Detailed Studies of the $\boldsymbol{H^0}$ and $\boldsymbol{A^0}$

However the H^0 and A^0 are first detected, one will wish to measure the total and partial widths of the H^0 and A^0. Once again, the $\mu^+\mu^-$ collider can play a crucial role. We will not give detailed estimates of what can be accomplished, but rather confine ourselves to outlining the procedures and strategies. The time scale and available luminosity for implementing these procedures depends dramatically upon whether or not one must first discover the H^0 and A^0 by scanning or in the bremsstrahlung tail (either of which would require a luminosity expenditure of $L \sim 50$ fb^{-1}), as opposed to observing them at the LHC (typically possible for $\tan\beta \lesssim 3 - 4$ at high m_{A^0}) or at an e^+e^- collider (requiring $m_{A^0}, m_{H^0} \lesssim \sqrt{s}/2$).

One might presume that once a Higgs boson with $\Gamma_h^{\rm tot}$ larger than the rms $\sqrt{s}$ spread is

discovered, direct measurement of the Higgs width would be quite straightforward with a simple scan over several $\sqrt{s}$ settings. This is indeed the case unless there is a second nearby Higgs boson. As it happens, the A^0 and H^0 are sufficiently degenerate in some regions of parameter space (large m_{A^0} and large $\tan\beta$), see Figs. 2.3.3 and 2.3.3, that a measurement of the widths of the A^0 and H^0 separately will require sorting out two overlapping resonance bumps, which, in turn, necessitates an appropriate scan. Two sample possibilities were illustrated earlier in Fig. 2.3.3, where the H^0 and A^0 resonance bumps that would appear as a function of $\sqrt{s}$ are illustrated for $m_{A^0} = 350$ GeV in the cases $\tan\beta = 5$ and 10. As noted earlier, separation of the peaks and precision width measurements are both much easier if we have excellent beam energy resolution; we assume $R = 0.01\%$. At $\tan\beta = 5$, we estimate that by accumulating roughly 0.01 fb^{-1} at each of 3 appropriately placed $\sqrt{s}$ choices near the center and on either side of each of the two separated peaks, the widths of the H^0 and A^0 could be measured to about 33%; 10% width determination would require about 0.1 fb^{-1} per point. At the higher $\tan\beta = 10$ value, one would clearly have to accumulate data in the dip between the overlapping peaks, near both peaks, below the double peak and above the double peak, and perform a fit to the two Higgs resonances simultaneously. A minimum of 5 data points would be required. Again, roughly 0.01 fb^{-1} per point would be needed to determine $\Gamma^{\rm tot}_{H^0}$ and $\Gamma^{\rm tot}_{A^0}$ to the 33% level, or 0.1 fb^{-1} per point for a 10% determination. Very large $\tan\beta$ values yield the worst scenarios since the H^0 and A^0 peaks are, then, simultaneously broad and very degenerate. Determination of the individual widths would become extremely difficult.

The production rate in a given channel is proportional to $BF(h \to \mu^+\mu^-)BF(h \to X)$ (for $\sigma_{\sqrt{s}} \ll \Gamma^{\rm tot}_h$), see Eq. (2.59). We then proceed as follows:

- $BF(h \to \mu^+\mu^-)$ and $BF(h \to b\overline{b})$ can be obtained individually if we use the type-II doublet prejudice that the $\mu^+\mu^-$ and $b\overline{b}$ couplings squared are modified relative to the SM coupling by the same factor, f. (A value of m_b must be specified.)

- Given the individual branching fractions, the partial widths can then be computed:

$$\Gamma(h \to \mu^+\mu^-, b\overline{b}) = \Gamma^{\rm tot}_h BF(h \to \mu^+\mu^-, b\overline{b}) \tag{2.73}$$

- One can use event rates in other observable channels, coupled with the $BF(h \to \mu^+\mu^-)$ determination, to obtain results for $BF(h \to X)$.

- $\Gamma_h^{\rm tot} \times BF(h \to X)$ then yields the partial width and coupling for any observable channel X. For example, if the $H^0 \to h^0 h^0$ channel can be detected we could determine the very interesting associated partial width (and, thence, coupling) via $\Gamma(H^0 \to h^0 h^0) = \Gamma_{H^0}^{\rm tot} BF(H^0 \to h^0 h^0)$ or, equivalently,

$$\Gamma(H^0 \to h^0 h^0) = \frac{[\Gamma_{H^0}^{\rm tot}]^2 BF(H^0 \to \mu\mu) BF(H^0 \to h^0 h^0)}{\Gamma(H^0 \to \mu\mu)} \,. \tag{2.74}$$

Of course, if $\Gamma_h^{\rm tot}$ and $\sigma_{\sqrt{s}}$ are close in size, one must avoid the approximation of Eq. (2.59), but determination of f and the partial widths and branching fractions would nevertheless be straightforward.

Determining a Higgs Boson's CP Properties

A $\mu^+\mu^-$ collider might well prove to be the best machine for directly probing the CP properties of a Higgs boson that can be produced and detected in the s-channel mode. This issue has been explored in Refs. [72, 73] in the case of a general two-Higgs-doublet model.

The first possibility is to measure correlations in the $\tau^+\tau^-$ or $t\bar{t}$ final states. Via such measurements, a $\mu^+\mu^-$ collider is likely to have greater sensitivity to the Higgs boson CP properties for $L = 20$ fb^{-1} than will the e^+e^- collider for $L = 85$ fb^{-1} (using correlation measurements in the Zh production mode) if $\tan\beta \gtrsim 10$ or $2m_W \lesssim m_h \lesssim 2m_t$. Indeed, there is a tendency for the $\mu^+\mu^-$ CP-sensitivity to be best precisely for parameter choices such that CP-sensitivity in the $e^+e^- \to Zh$ mode is worst. Somewhat higher total luminosity ($L \sim 50$ fb^{-1}) is generally needed in order to use these correlations to distinguish a pure CP-odd state from a pure CP-even state.

The second possibility arises if it is possible to transversely polarize the muon beams. Assume that we can have 100% transverse polarization and that the μ^+ transverse polarization is rotated with respect to the μ^- transverse polarization by an angle ϕ. The production cross section for a h with coupling $a + ib\gamma_5$ then behaves as

$$\sigma(\phi) \propto 1 - \frac{a^2 - b^2}{a^2 + b^2} \cos\phi + \frac{2ab}{a^2 + b^2} \sin\phi \,. \tag{2.75}$$

To prove that the h is a CP admixture, use the asymmetry

$$A_1 \equiv \frac{\sigma(\pi/2) - \sigma(-\pi/2)}{\sigma(\pi/2) + \sigma(-\pi/2)} = \frac{2ab}{a^2 + b^2} \,. \tag{2.76}$$

For a pure CP eigenstate, either a or b is zero. For example, in the MSSM the Higgs sector is CP-conserving; $b = 0$ for the CP-even h^0 and H^0, while $a = 0$ for the CP-odd A^0. In such cases, it is necessary to employ a different asymmetry than that discussed in Ref. [73]. The quantity

$$A_2 \equiv \frac{\sigma(\pi) - \sigma(-\pi)}{\sigma(\pi) + \sigma(-\pi)} = \frac{a^2 - b^2}{a^2 + b^2} \tag{2.77}$$

is $+1$ or -1 for a CP-even or CP-odd h, respectively. Background processes in the final states where a Higgs boson can be most easily observed (*e.g.* $b\overline{b}$) can dilute these asymmetries substantially. Whether or not they will prove useful depends even more upon the very uncertain ability to transversely polarize the muon beams, especially while maintaining high luminosity.

Note that longitudinally polarized beams are not useful for studying the CP properties of a Higgs produced in the s-channel. Regardless of the values of a and b in the h coupling, the cross section is simply proportional to $1 - \lambda_{\mu^+}\lambda_{\mu^-}$ (the λ's being the helicities), and is only non-zero for LR or RL transitions, up to corrections of order m_μ^2/m_h^2.

2.3.4 Summary and Conclusion

A $\mu^+\mu^-$ collider would be a remarkably powerful machine for probing Higgs physics using direct s-channel production, and thus ultimately for finding the underlying theory of the scalar sector. In this report we have concentrated on the procedures and machine requirements for direct measurement of the properties of a Higgs boson.

SM-like Higgs Boson

We expect that a SM-like h (which nominally includes the h^0 of the MSSM) will first be detected either at the LHC or in the Zh mode at an e^+e^- collider. If not, it would be most advantageous to expend a small amount of luminosity at full machine energy to discover it in the Zh mode at the $\mu^+\mu^-$ collider. Once m_h is approximately known, a $\mu^+\mu^-$ collider can zero-in on $\sqrt{s} \simeq m_h$ for detailed studies of a SM-like Higgs boson provided $m_h \lesssim 2m_W$ (as is the case for the h^0 of the MSSM). The mass can be measured to a fraction of an MeV for $m_{h_{SM}} \lesssim 130$ GeV.

Crucial to a model-independent determination of all the properties of the Higgs boson at the $\mu^+\mu^-$ collider is the ability to make a direct precision measurement of its total width,

which is very narrow for a SM-like h when $m_h < 2m_W$. The proposed method (described in sec. 2.12.3) relies on measuring the ratio of the central peak cross section to the cross section on the wings of the peak, a ratio that is determined by $\Gamma_h^{\rm tot}$ alone. Once $\Gamma_h^{\rm tot}$ is measured, determinations of the crucial $\mu^+\mu^-$ and $b\overline{b}$ couplings are possible. The precision for $\Gamma_h^{\rm tot}$ and the $\mu^+\mu^-$ and $b\overline{b}$ partial widths/couplings achieved for total integrated luminosity of $L = 50$ fb^{-1} and an excellent beam resolution of $R = 0.01\%$ would be sufficient to distinguish the MSSM h^0 from the SM h_{SM} at the 3σ statistical level for values of the parameter m_{A^0} as large as ~ 400 GeV provided that m_{h^0} is not in the range $80 \lesssim m_{h^0} \lesssim 100$ GeV (*i.e.* near m_Z). No other accelerator or combination of accelerators has the potential of seeing the h^0 vs. h_{SM} differences at this level of precision out to such large m_{A^0} values. For a SM-like Higgs with $m_h \gtrsim 200$ GeV, the event rate is too low for detection in the s-channel.

Machine requirements for the precision studies are:

- High luminosity $\mathcal{L} \gtrsim 2 \times 10^{33}{\rm cm}^{-2}{\rm s}^{-1}$ at $\sqrt{s} \sim m_h$.
- Excellent beam energy resolution of $R = 0.01\%$.
- Ability to adjust the machine energy $\sqrt{s}$ accurately (to one part in a million) and quickly (once an hour in the initial scan to precisely determine m_h) over a $\sqrt{s}$ interval of several GeV.

Non-SM-like Higgs Bosons

For other Higgs bosons with weak WW, ZZ couplings (such as the H^0 and A^0 of the MSSM), but enhanced $\mu^+\mu^-$ and $b\overline{b}$ couplings, discovery in s-channel collisions at the $\mu^+\mu^-$ collider is typically possible. There are three possible techniques. In order to compare these techniques it is reasonable to suppose that the H^0 and A^0 have been excluded for $m_{H^0}, m_{A^0} \lesssim \sqrt{s}/2$ via the $Z^\star \to H^0A^0$ mode at an e^+e^- collider running with $\sqrt{s} \sim 500$ GeV.

a) Scan method
In this approach, a scan for the H^0 and A^0 of the MSSM would be made over a sequence of $\sqrt{s}$ values all the way out to the maximal $\sqrt{s}$ value achievable at the $\mu^+\mu^-$ collider. Assuming that $L = 50$ fb^{-1} is devoted to the scan and that both the e^+e^- and the $\mu^+\mu^-$ colliders have maximal energies of order 500 GeV, discovery via the scan would be robust for $250 \lesssim m_{H^0,A^0} \lesssim 500$ GeV if $\tan\beta \gtrsim 3$ to 4. Fortuitously, the domain

$250 \lesssim m_{H^0}, m_{A^0} \lesssim 500$ GeV, $\tan\beta \lesssim 3$, in which much more luminosity would clearly be required for discovery at the $\mu^+\mu^-$ collider, is a parameter region where the H^0 and A^0 are likely to be accessible at the LHC for accumulated luminosity of 300 fb^{-1} per detector (ATLAS+CMS), as illustrated in Fig. 2.3.3. There is, nonetheless, a small window, $3 \lesssim \tan\beta \lesssim 4$, at large m_{A^0} (between about 400 and 500 GeV) for which the LHC and the $\mu^+\mu^-$ collider might both miss seeing the H^0 and A^0 unless higher luminosities are accumulated.

In order that the required $L = 50$ fb^{-1} can be optimally distributed over the full $250 - 500$ GeV scan range in the course of a year or two of running, it would be necessary to design the storage ring or rings so that it would be possible to adjust $\sqrt{s}$ quickly and accurately (to within a small fraction of the step size, which must be $\lesssim 0.1$ GeV in some mass ranges) while maintaining the full luminosity.

b) Bremsstrahlung tail method

In this technique, the A^0 and H^0 search is made while running the $\mu^+\mu^-$ collider at full energy, looking for excess events arising from the luminosity at the low-energy end of the bremsstrahlung tail. This approach is competitive with the scan technique if the $b\overline{b}$ final state mass can be reconstructed with excellent resolution (roughly ± 5 GeV, including all detector effects and semi-leptonic b decays). The lower $\tan\beta$ limits for 5σ signals are about one to two units higher than for the scan technique in the $m_{A^0} = 250 - 480$ GeV range. Thus the bremsstrahlung search leaves a larger gap between the upper limit in $\tan\beta$ for which H^0, A^0 discovery would be possible at the LHC ($\tan\beta \lesssim 3 - 4$ at high m_{A^0}) and the lower limit for which the H^0, A^0 would be detected at the $\mu^+\mu^-$ collider ($\tan\beta \gtrsim 5 - 7$) than would the scan technique.

The bremsstrahlung technique has the advantage of not requiring that high luminosity be maintained over a broad range of $\sqrt{s}$ collision energies while being able to step quickly and accurately in $\sqrt{s}$, but detector costs associated with the very demanding resolution in the $b\overline{b}$ invariant mass might be high.

c) Pair production

It may well be possible to build a $\mu^+\mu^-$ collider with $\sqrt{s}$ substantially above 500 GeV. If a $\sqrt{s} \geq 1$ TeV machine with high luminosity were built instead of a 500 GeV collider, it could discover the H^0, A^0 for $m_{H^0}, m_{A^0} \geq 500$ GeV in the pair production mode.

If the H^0, A^0 have already been discovered, either

- with $m_{H^0}, m_{A^0} \lesssim 250$ GeV in the $Z^\star \to H^0 A^0$ mode at an e^+e^- collider, or
- with $m_{H^0}, m_{A^0} \lesssim 2$ TeV in the $Z^\star \to H^0 A^0$ mode at a 4 TeV $\mu^+\mu^-$ collider, or
- with $m_{H^0}, m_{A^0} \lesssim 500$ GeV at the LHC (if $\tan\beta \lesssim 3-4$ or $\tan\beta \gtrsim 8-20$),

scanning over a broad energy range would not be necessary at the $\mu^+\mu^-$ collider. By constructing a single appropriate storage ring and devoting full luminosity to accumulating events at $\sqrt{s} \simeq m_{A^0}, m_{H^0}$, detailed studies of the total widths and partial widths of the A^0 and H^0 would then be possible at the $\mu^+\mu^-$ collider *for all* $\tan\beta$ *values above 1.*

Summary of Machine and Detector Requirements

We re-emphasize the crucial machine and detector characteristics for detection and study of both SM-like Higgs bosons and non-SM-like Higgs bosons.

- High luminosity, $\mathcal{L} \gtrsim 2 \times 10^{33}\mathrm{cm}^{-2}\mathrm{s}^{-1}$, is required at any $\sqrt{s}$ where a Higgs boson is known to exist and throughout any range of energy over which we must scan to detect a Higgs boson.
- A machine design such that beamstrahlung is small compared to the effects of bremsstrahlung (included in our studies) is highly desirable for scan searches and precision studies. However, significant beamstrahlung might improve the ability to discover Higgs bosons using the low-energy tail of the luminosity spectrum.
- An extremely precise beam energy, $R \sim 0.01\%$, will be needed for precision studies of a narrow-width SM-like Higgs boson. Such precise resolution is also extremely helpful in the zeroing-in scan for a very narrow SM-like and is not harmful for discovering a Higgs boson with broad width. Precision measurements of the non-SM-like H^0 and A^0 widths and separation of these two resonances when they overlap becomes difficult if R is substantially larger than 0.01%.
- To zero-in on $\sqrt{s} \simeq m_h$ for a narrow-width SM-like Higgs boson requires being able to rapidly set $\sqrt{s}$ with an accuracy that is small compared to the beam resolution R, for $\sqrt{s}$ values within about a few GeV of the (approximately known) value of m_h. To

discover the H^0 and A^0 by scanning requires being able to rapidly set $\sqrt{s}$ with an accuracy that is small compared to their widths over a $\sqrt{s}$ interval of order several hundred GeV.

- To measure $\Gamma_h^{\rm tot}$ for a SM-like h to $\pm 10\%$, it must be possible to set $\sqrt{s}$ with an accuracy of order 1 part in 10^6 over $\sqrt{s}$ values in an interval several times Rm_h, *i.e.* over an interval of tens of MeV. This (and the accuracy for the mass measurements) requires a machine design that allows quick spin rotation measurements of a polarized muon in the storage ring.

- If both muon beams can be polarized and the polarization (P) maintained through the cooling and acceleration process, the significance of the s-channel Higgs signal can be significantly enhanced provided the factor by which the luminosity is decreased is less than $(1+P^2)/(1-P^2)$.

- To detect non-SM-like Higgs bosons with enhanced $\mu^+\mu^-$ couplings in the bremsstrahlung luminosity tail when the machine is run at full energy, one needs excellent mass resolution ($\sim \pm 5$ GeV) in the $b\overline{b}$ final state mass as reconstructed in the detector.

In conclusion, if a Higgs bosons is discovered at the LHC and/or an e^+e^- collider, construction of a $\mu^+\mu^-$ collider with $\sqrt{s}$ covering the range of masses observed will become almost mandatory purely on the basis of s-channel Higgs physics. There are many other motivations for building a $\mu^+\mu^-$ collider, especially one with $\sqrt{s} \gtrsim 2$ TeV, based on other types of new physics that could be probed. The physics motivations for a high-energy $\mu^+\mu^-$ collider will be treated elsewhere [74].

Bibliography

[1] *Proceedings of the First Workshop on the Physics Potential and Development of $\mu^+\mu^-$ Colliders*, Napa, California (1992), Nucl. Instru. and Meth. **A350**, 24 (1994).

[2] *Proceedings of the Second Workshop on the Physics Potential and Development of $\mu^+\mu^-$ Colliders*, Sausalito, California (1994), ed. by D. Cline, American Institute of Physics Conference Proceedings 352.

[3] *Proceedings of the 9th Advanced ICFA Beam Dynamics Workshop*, Ed. J. C. Gallardo, AIP Conference Proceedings 372, 1996.

[4] *Proceedings of the Symposium on Physics Potential and Development of $\mu^+\mu^-$ Colliders*, San Francisco, CA (1995); Supplement to Nuclear Physics B. .

[5] R.B. Palmer and A. Tollestrup, unpublished report.

[6] D.V. Neuffer, Ref. [2], p. 22.

[7] D.V. Neuffer and R.B. Palmer, Ref. [2], p. 70.

[8] V. Barger, M.S. Berger, K. Fujii, J.F. Gunion, T. Han, C. Heusch, W. Hong, S.K. Oh, Z. Parsa, S. Rajpoot, R. Thun and B. Willis, *Physics Goals of a $\mu^+\mu^-$ Collider*, appearing in Ref. [2], p. 55, hep-ph/9503258.

[9] V. Barger, M. Berger, J.F. Gunion, T. Han, and R. Phillips, in preparation.

[10] G.P. Jackson and D. Neuffer, private communications.

[11] P. Janot, *Proceedings of the 2nd International Workshop on "Physics and Experiments with Linear e^+e^- Colliders",* eds. F. Harris, S. Olsen, S. Pakvasa and X. Tata, Waikoloa,

HI (1993), World Scientific Publishing, p. 192, and references therein; T. Barklow and D. Burke, private communication.

[12] See "JLC-I", KEK-92-16, December 1992.

[13] K. Kawagoe, *Proceedings of the 2nd International Workshop on "Physics and Experiments with Linear e^+e^- Colliders"*, Eds. F. Harris, S. Olsen, S. Pakvasa and X. Tata, Waikoloa, HI (1993), World Scientific Publishing, p. 660.

[14] J.F. Gunion, A. Stange, and S. Willenbrock, preprint UCD-95-28 (1995), hep-ph/9602238, to be published in *Electroweak Physics and Beyond the Standard Model*, World Scientific Publishing Co., eds. T. Barklow, S. Dawson, H. Haber, and J. Siegrist.

[15] V. Barger, M. Berger, J.F. Gunion, and T. Han, Phys. Rev. Lett. **75**, 1462 (1995).

[16] V. Barger, M. Berger, J.F. Gunion, and T. Han, UCD-96-6, hep-ph/9602415.

[17] R.B. Palmer, private communication.

[18] H. Haber, R. Hempfling and A. Hoang, CERN-TH/95-216.

[19] M. Carena, J.R. Espinosa, M. Quiros and C.E.M. Wagner, Phys. Lett. **B355**, 209 (1995); J.A. Casas, J.R. Espinosa, M. Quiros and A. Riotto, Nucl. Phys. **B436**, 3 (1995).

[20] J.F. Gunion and H.E. Haber, Phys. Rev. **D48**, 5109 (1993).

[21] See, for example, R. Arnowitt and P. Nath, Phys. Rev. **69**, 725 (1992); Phys. Lett. **B289**, 368 (1992); G. G. Ross and R. G. Roberts, Nucl. Phys. **B377**, 571 (1992); S. Kelley, J. L. Lopez, D. V. Nanopoulos, H. Pois, and K. Yuan, Nucl. Phys. **B398**, 3 (1993); M. Drees and M. M. Nojiri, Phys. Rev. **D47**, 376 (1993); M. Olechowski and S. Pokorski, Nucl. Phys. **B404**, 590 (1993); D. J. Castaño, E. J. Piard, and P. Ramond, Phys. Rev. **D49**, 4882 (1994); V. Barger, M.S. Berger, and P. Ohmann, Phys. Rev. **D49**, 4908 (1994); M. Carena, M. Olechowski, S. Pokorski, and C.E.M. Wagner, Nucl. Phys. **B419**, 213 (1994); G. Kane, C. Kolda, and J. Wells, Phys. Rev. **D49**, 6173 (1994); W. de Boer, R. Ehret, and D.I. Kazakov, Z. Phys. **C67**, 647 (1995); M. Carena and C.E.M. Wagner, Nucl. Phys. **B452**, 45 (1995); S.F. King and P. White, Phys. Rev. **D52**, 4183 (1995).

[22] Z. Parsa (unpublished).

[23] S. Dawson, appearing in Ref. [3], hep-ph/9512260.

[24] For discussions of the $t\bar{t}$ threshold behavior at e^+e^- colliders, see V.S. Fadin and V.A. Khoze, JETP Lett. **46** 525 (1987); Sov. J. Nucl. Phys. **48** 309 (1988); M. Peskin and M. Strassler, Phys. Rev. **D43**, 1500 (1991); G. Bagliesi, *et al.*, CERN Orange Book Report CERN-PPE/92-05; Y. Sumino, *et al.*, Phys. Rev. **D47**, 56 (1992); M. Jezabek, J.H. Kühn, T. Teubner, Z. Phys. **C56**, 653 (1992).

[25] M.S. Berger, talk presented at the *Workshop on Particle Theory and Phenomenology: Physics of the Top Quark*, Iowa State University, May 25–26, 1995, hep-ph/9508209.

[26] P. Igo-Kemenes, M. Martinez, R. Miquel and S. Orteu, CERN-PPE/93-200, Contribution to the *Workshop on Physics with Linear e^+e^- Colliders at 500 GeV*, K. Fujii, T. Matsui, and Y. Sumino, Phys. Rev. **D50**, 4341 (1994).

[27] C.P. Yuan, talk presented at *Int. Workshop on Elementary Particle Physics: Present and Future*, Valencia, Spain, June 5–9, 1995, hep-ph/9509209.

[28] B. Grzadkowski and J.F. Gunion, Phys. Lett. **B350**, 218 (1995).

[29] D. Atwood and A. Soni, Phys. Rev. **D52**, 6271 (1995).

[30] A. Pilaftsis, Rutherford preprint RAL-TR/96-021.

[31] D. Atwood, L Reina and A. Soni, Phys. Rev. Lett. **75**, 3800 (1995).

[32] J.F. Gunion, preprint UCD-95-36, hep-ph/9510350, to be published in the Proceedings of the Santa Cruz e^-e^- Workshop, Santa Cruz, CA, Sept. 4-5, 1995.

[33] J.F. Gunion and J. Kelly, Phys. Rev. **D51**, 2101 (1995); and in preparation.

[34] M.S. Chanowitz and M.K. Gaillard, Nucl. Phys. **B261**, 379 (1985).

[35] D. Burke, *Proceedings of the Symposium on Physics Potential and Development of $\mu^+\mu^-$ Colliders*, San Francisco, CA (1995); Supplement to Nuclear Physics B.

[36] J. Bagger, V. Barger, K. Cheung, J.F. Gunion, T. Han, G.A. Ladinsky, R. Rosenfeld, and C.-P. Yuan, Phys. Rev. **D52**, 2878 (1995).

[37] V. Barger, K. Cheung, T. Han, and R.J.N. Phillips, Phys. Rev. **D52**, 3815 (1995).

[38] The constraints on a fourth generation in the context of supergravity models can be found in J.F. Gunion, D.W. McKay, and H. Pois, Phys. Rev. **D53**, 1616 (1996).

[39] For a recent survey, see V. Barger, M.S. Berger, and R.J.N. Phillips, Phys. Rev. **D52**, 1663 (1995).

[40] J.L. Hewett and T.G. Rizzo, Phys. Rep. **183**, 193 (1989).

[41] J.F. Gunion, A. Stange, and S. Willenbrock, Weakly Coupled Higgs Bosons, preprint UCD-95-28, to appear in *Electroweak Symmetry Breaking and New Physics at the TeV Scale*, to be published by World Scientific.

[42] See J.F. Gunion, H.E. Haber, G.L. Kane and S. Dawson, *The Higgs Hunters Guide*, Addison-Wesley Publishing, and references therein.

[43] M. Drees, Int. J. Mod. Phys. **A4**, 3635 (1989); J. Ellis *et al.*, Phys. Rev. **D39**, 844 (1989); L. Durand and J.L. Lopez, Phys. Lett. **B217**, 463 (1989); J.R. Espinosa and M. Quirós, Phys. Lett. **B279**, 92 (1992); P. Binétruy and C.A. Savoy, Phys. Lett. **B277**, 453 (1992); T. Morori and Y. Okada, Phys. Lett. **B295**, 73 (1992); G. Kane, *et al.*, Phys. Rev. Lett. **70**, 2686 (1993); J.R. Espinosa and M. Quirós, Phys. Lett. **B302**, 271 (1993); U. Ellwanger, Phys. Lett. **B303**, 271 (1993); J. Kamoshita, Y. Okada, M. Tanaka *et al.*, Phys. Lett. **B328**, 67 (1994).

[44] V. Barger, *et al.*, Phys. Lett. **B314**, 351 (1993); P. Langacker and N. Polonsky, Phys. Rev. **D50**, 2199 (1994).

[45] H. Haber, R. Hempfling and A. Hoang, **CERN-TH/95-216** (1995).

[46] M. Carena, J.R. Espinosa, M. Quiros and C.E.M. Wagner, Phys. Lett. **B355**, 209 (1995); J.A. Casas, J.R. Espinosa, M. Quiros and A. Riotto, Nucl. Phys. **B436**, 3 (1995).

[47] For a review, see *e. g.*, J.F. Gunion and H.E. Haber, Nucl. Phys. **B272**, 1 (1986).

[48] See, for example, R. Arnowitt and P. Nath, Phys. Rev. **69**, 725 (1992); Phys. Lett. **B289**, 368 (1992); G. G. Ross and R. G. Roberts, Nucl. Phys. **B377**, 571 (1992); S. Kelley, J. L. Lopez, D. V. Nanopoulos, H. Pois, and K. Yuan, Nucl. Phys. **B398**, 3

(1993); M. Drees and M. M. Nojiri, Phys. Rev. **D47**, 376 (1993); M. Olechowski and S. Pokorski, Nucl. Phys. **B404**, 590 (1993); D. J. Castaño, E. J. Piard, and P. Ramond, Phys. Rev. **D49**, 4882 (1994); V. Barger, M.S. Berger, and P. Ohmann, Phys. Rev. **D49**, 4908 (1994); M. Carena, M. Olechowski, S. Pokorski, and C.E.M. Wagner, Nucl. Phys. **B419**, 213 (1994); G. Kane, C. Kolda, and J. Wells, Phys. Rev. **D49**, 6173 (1994); W. de Boer, R. Ehret, and D.I. Kazakov, Z. Phys. **C67**, 647 (1995); M. Carena and C.E.M. Wagner, Nucl. Phys. **B452**, 45 (1995); S.F. King and P. White, Phys. Rev. **D52**, 4183 (1995).

[49] V. Barger, M.S. Berger, R.J.N. Phillips, and A.L. Stange, Phys. Rev. **D45**, 4128 (1992); V. Barger, Kingman Cheung, R.J.N. Phillips, and A.L. Stange, Phys. Rev. **D46**, 4914 (1992).

[50] J. Ellis, J.F. Gunion, H.E. Haber, L. Roszkowski and F. Zwirner, Phys. Rev. **D39**, 844 (1989); B.R. Kim, S.K. Oh and A. Stephan, *Proceedings of the 2nd International Workshop on "Physics and Experiments with Linear e^+e^- Colliders"*, eds. F. Harris, S. Olsen, S. Pakvasa and X. Tata, Waikoloa, HI (1993), World Scientific Publishing, p. 860: J. Kamoshita, Y. Okada and M. Tanaka, Phys. Lett. **B328**, 67 (1994); S.F. King and P.L. White, preprint SHEP-95-27 (1995), hep-ph 9508346; U. Ellwanger, M.R. de Traubenberg and C.A. Savoy, Z. Phys. **C67**, 665 (1995).

[51] *Proceedings of the First Workshop on the Physics Potential and Development of $\mu^+\mu^-$ Colliders*, Napa, California (1992), Nucl. Instru. and Meth. **A350**, 24 (1994).

[52] *Proceedings of the Second Workshop on the Physics Potential and Development of $\mu^+\mu^-$ Colliders*, Sausalito, California (1994), ed. by D. Cline, American Institute of Physics Conference Proceedings 352.

[53] *Proceedings of the 9th Advanced ICFA Beam Dynamics Workshop*, Ed. J. C. Gallardo, AIP Conference Proceedings 372, 1996.

[54] *Proceedings of the Third Workshop on the Physics Potential and Development of $\mu^+\mu^-$ Colliders*, San Francisco, California (1995), ed. by D. Cline, to be published.

[55] V. Barger, M.S. Berger, K. Fujii, J.F. Gunion, T. Han, C. Heusch, W. Hong, S.K. Oh, Z. Parsa, S. Rajpoot, R. Thun and B. Willis, Physics Goals of a $\mu^+\mu^-$ Collider, appearing in Ref. [52], p. 55, hep-ph 9503258.

[56] R.B. Palmer and A. Tollestrup, unpublished report.

[57] D.V. Neuffer, Ref. [52], p. 22.

[58] D.V. Neuffer and R.B. Palmer, Ref. [52], p. 70.

[59] D.J. Miller, Ref. [52], p. 191.

[60] V. Barger, M. Berger, J.F. Gunion, and T. Han, Phys. Rev. Lett. **75**, 1462 (1995).

[61] R.B. Palmer, private communication.

[62] G.P. Jackson and D. Neuffer, private communications.

[63] See, for example, Z. Parsa, $\mu^+\mu^-$ *Collider and Physics Possibilities*, unpublished; K. Hagiwara and D. Zeppenfeld, Nucl. Phys. **B313**, 560 (1989), Appendix B.

[64] For references to in-depth studies of physics at future e^+e^- colliders, see e.g. *Proceedings of the Workshop on Physics and Experiments with Linear Colliders*, ed. F.A. Harris, *et al.*, World Scientific (1993); *Proceedings of the Workshop on Physics and Experiments with Linear* e^+e^- *Colliders*, Waikoloa, Hawaii (April 1993), ed. F. Harris *et al.* (World Scientific, 1993); JLC Group, KEK Report 92-16 (1992); *Proceedings of the Workshop on Physics and Experiments with Linear Colliders*, Saariselkä, Finland (Sept. 1991), ed. R. Orava *et al.*, World Scientific (1992).

[65] P. Janot, *Proceedings of the 2nd International Workshop on "Physics and Experiments with Linear* e^+e^- *Colliders"*, eds. F. Harris, S. Olsen, S. Pakvasa and X. Tata, Waikoloa, HI (1993), World Scientific Publishing, p. 192, and references therein; T. Barklow and D. Burke, private communication.

[66] See "JLC-I", KEK-92-16, December 1992.

[67] K. Kawagoe, *Proceedings of the 2nd International Workshop on "Physics and Experiments with Linear* e^+e^- *Colliders"*, eds. F. Harris, S. Olsen, S. Pakvasa and X. Tata, Waikoloa, HI (1993), World Scientific Publishing, p. 660.

[68] J.F. Gunion and H.E. Haber (unpublished).

[69] Z. Kunszt and F. Zwirner, Nucl. Phys. **B385**, 3 (1992); H. Baer, M. Bisset, C. Kao, and X. Tata, Phys. Rev. **D46**, 1067 (1992); H. Baer, M. Bisset, D. Dicus, C. Kao, and X. Tata, Phys. Rev. **D47**, 1062 (1993); J.F. Gunion *et al.*, Phys. Rev. **D46**, 2040 (1992); J. Gunion and L. Orr, Phys. Rev. **D46**, 2052 (1992); J. Gunion, H. Haber, and C. Kao, Phys. Rev. **D46**, 2907 (1992); V. Barger, K. Cheung, R. Phillips, and A. Stange, Phys. Rev. **D46**, 4914 (1992); J. Dai, J. Gunion, and R. Vega, preprint UCD-95-25 (1995); ATLAS Technical Proposal, CERN/LHCC/94-43, LHCC/P2 (1994); CMS Technical Proposal, CERN/LHCC 94-38, LHCC/P1 (1994); D. Froidevaux, F. Gianotti, and E. Richter-Was, ATLAS Internal Note PHYS-No-64 (1995); F. Gianotti, to appear in the Proceedings of the European Physical Society International Europhysics Conference on High Energy Physics, Brussels, Belgium, July 27 - August 2, 1995.

[70] D. Froidevaux, F. Gianotti, L. Poggioli, E. Richter-Was, D. Cavalli, and S. Resconi, ATLAS Internal Note, PHYS-No-74 (1995).

[71] J.F. Gunion and H.E. Haber, *Proceedings of the 1990 DPF Summer Study on High Energy Physics: "Research Directions for the Decade"*, editor E. Berger, Snowmass (1990), p. 206; Phys. Rev. **D48**, 5109 (1993).

[72] B. Grzadkowski and J.F. Gunion, Phys. Lett. **B350**, 218 (1995).

[73] D. Atwood and A. Soni, Phys. Rev. **D52**, 6271 (1995).

[74] V. Barger, M. Berger, J.F. Gunion, T. Han, and R. Phillips, in preparation.

[75] E.A. Kuraev and V.S. Fadin, Sov. J. Nucl. Phys. **41**, 466 (1985); R.N. Cahn, Phys. Rev. **D36**, 266 (1987); M. Peskin, SLAC Summer Institute: 1989, p. 71.

Contributors

- V. Barger (Univ. of Wisconsin), Editor
- M.S. Berger (Indiana Univ.)
- J.F. Gunion (UC, Davis)
- T. Han (UC, Davis)

List of Figures

List of Tables